THESIS FOR THE DEGREE OF DOCTOR OF PHILOSOPHY

Correlation Effects in Nanostructures

Paata Kakashvili

Department of Applied Physics
Chalmers University of Technology
Göteborg, Sweden 2006

Correlation Effects in Nanostructures
Paata Kakashvili
ISBN 91-7291-776-8

Doktorsavhandlingar vid Chalmers Tekniska Högskola
Ny serie nr 2458
ISSN 0346-718X

Department of Applied Physics
Chalmers University of Technology
SE-412 96 Göteborg
Sweden
Telephone +46 (0)31 - 772 1000

Cover: *upper figure* – Local spectral weight of a Luttinger liquid with an open boundary, analyzed in Chapter 6; *lower figure* – Schematic picture of a setup discussed in Chapter 5: a 1D quantum box side-coupled to a quantum wire via a point contact.

Chalmers Reproservice
Göteborg, Sweden 2006

To the Memory of My Father

Correlation Effects in Nanostructures

Paata Kakashvili
Department of Applied Physics
Chalmers University of Technology
SE-412 96 Göteborg, Sweden

Abstract

In this Ph.D. thesis I present the background and provide further details to the work presented in the appended papers. The background consists of brief overviews of Kondo physics, Luttinger liquid theory, and conformal field theory. My own research is divided into three parts: the first deals with the interplay between Luttinger and Kondo physics (described in **Papers I** and **II**), the second addresses scanning tunneling microscopy (STM) response of a Luttinger liquid with an edge or an impurity (described in **Paper III**), and the third explores the boundary Green's function of 1D electrons in the spin-incoherent regime (described in **Paper IV**).

In **Papers I** and **II** a setup is proposed which allows for a controlled study of Kondo and Luttinger liquid physics. It consists of a quantum box, biased by a gate voltage, and side-coupled to a quantum wire by a point contact. Close to the degeneracy points of the Coulomb blockaded box the setup can be described as a Luttinger liquid interacting with an effective Kondo impurity. Using boundary conformal field theory techniques we predict that for the case of spin-polarized electrons the differential capacitance of the box will exhibit distinctive Luttinger liquid scaling with temperature and gate voltage. In the limit of zero magnetic field the Luttinger liquid behavior gets masked by two-channel Kondo screening, leading to a logarithmic scaling of the differential capacitance with temperature and gate voltage. These effects should be possible to study experimentally, using the recently developed single-electron transistor (SET) electrometer technique.

In **Paper III** the finite-temperature local spectral weight (LSW) of a Luttinger liquid with a hard wall boundary is calculated. Close to the boundary the LSW exhibits characteristic oscillations indicative of spin-charge separation. The line shape of the LSW is also found to have a Fano-like asymmetry, a feature originating from the combined effect of electron-electron interaction and scattering off the boundary. Our results can be used to predict how edges and impurities influence the STM response of one-dimensional electron systems at low temperatures and voltage bias. Applications to STM on single-walled carbon nanotubes are also discussed.

Paper IV, finally, presents a study of the spin-incoherent regime of 1D strongly interacting electrons. For sufficiently low densities the potential energy dominates the kinetic energy, and one can easily reach the spin-incoherent regime where the spin exchange energy is much less than the temperature. We have generalized the description of the spin-incoherent regime to account for the presence of a boundary. By calculating the exact Green's function we find that the charge sector critical exponent is highly sensitive to the boundary, strongly modifying the tunneling of electrons close to it. Our approach also allows for a detailed description of the crossover between boundary and bulk regimes.

Keywords: Strongly correlated electrons, Kondo effect, Luttinger liquid, bosonization, conformal field theory, Coulomb blockade, single-electron transistor, STM, Wigner crystal.

This thesis consists of an introductory text and the following appended research papers, henceforth referred to as **Papers I-IV**:

Paper I:
P. Kakashvili and H. Johannesson, "Measuring Luttinger Liquid Correlations from Charge Fluctuations in a Nanoscale Structure", Phys. Rev. Lett. **91**, 186403 (2003).

Paper II:
P. Kakashvili and H. Johannesson, "Enhanced Two-Channel Kondo Physics in a Quantum Box Device", preprint (2006), ArXiv cond-mat/0602218, submitted for publication.

Paper III:
P. Kakashvili, H. Johannesson and S. Eggert, "Local Spectral Weight of a Luttinger Liquid: Effects from Edges and Impurities", preprint (2006), submitted for publication.

Paper IV:
P. Kakashvili and H. Johannesson, "Boundary Green's Function for Spin-Incoherent Interacting Electrons in 1D", preprint (2006), submitted for publication.

Papers not included in the thesis:

Paper V:
G.I. Japaridze, A.P. Kampf, M. Sekania, P. Kakashvili, and Ph. Brune, "η-Pairing Superconductivity in the Hubbard Chain with Pair Hopping", Phys. Rev. B **65**, 014518 (2002).

Paper VI:
P. Kakashvili and G.I. Japaridze, "Effective Hamiltonian for a Half-filled Hubbard Chain with Alternating On-Site Interactions", J. Phys.: Condens. Matter **16**, 5815 (2004).

Acknowledgments

First of all, I would like to thank my supervisor *Henrik Johannesson* for admitting me to Ph.D. studies. I am indebted to him for his insightful discussions on physics, constant support and endless encouragement. I am thankful to him for carefully proofreading this thesis and for suggesting numerous improvements. I also would like to express my warmest gratitude to my former supervisor *George Japaridze* for being not only an excellent teacher but also a good friend.

I would like to thank all, present and former, members of the Solid State Theory group: *Stellan Östlund*, *Sebastian Eggert*, *Mikael Fogelström*, *Mats Granath*, *Bernhard Mehlig*, *Alex Kleiner*, *Fabrizio Anfuso*, *Juan Alegret*, *Johan Stäring* and *Daniel Larsson* for making the group a nice place to work. Special thanks to our group secretary *Yvonne Steen* without whom I would get lost in the bureaucratic labyrinth. Figures in this thesis would not be as nice if not the help that I got from *Mats Granath*. I would also like to thank all the other members of the former Institute of Theoretical Physics for creating a nice and friendly atmosphere. I am happy to acknowledge all the members of the "Nordic Network on Low-Dimensional Physics" for constant effort to promote "not particularly applied condensed matter physics" which we all find fascinating and beautiful.

My special thanks to my best friends in Göteborg: *Alex Kleiner*, *Jaeuk Kim*, and *Fabrizio Anfuso*. Without them my life in Sweden would not be as enjoyable. It was always fun being in your company, which made me a better person, I hope.

I would like to thank my Scandinavian friends, *Susanne Viefers*, *Fredrik Fälth* and *Caroline Huldt* for all the nice time we spent together.

I am very grateful to *Mikael Tykesson* and *Tove Johansson* for numerous Georgian dinners, with *Khachapuri, Tkemali, Churchkhela* and with many other Georgian dishes, which I was constantly missing in Sweden.

During my stay in Göteborg I was very lucky to meet: *Alex Chakhunashvili* and *Karolina Narmontaite*, *Gio Skhirtladze* and *Linda Segerpalm*, *Anuki Sturua* and *Tukha Gabunia*, *Maia Rodonaia* and *Kjell Karlström*, and *Goga Khabelashvili*. I wish you all the best with your families.

My cordial gratitude to my oldest and best friends *Michael Sekania* and *Irakli Titvinidze* for constantly keeping in touch with me and for all the fun we had together in Georgia, Germany and Sweden.

Finally, I would like to thank my mother and sister for endless support and unconditional love.

Göteborg, May 2006

Paata Kakashvili

Preface

This Ph.D. thesis summarizes the work I have done on correlation effects in nanostructures. The thesis consists of seven chapters. The first four chapters summarize the background while the last three chapters are exclusively devoted to my work.

Chapter 1 presents a brief introduction.

Chapter 2 presents a brief overview of single- and multi-channel Kondo physics and discusses reasons for its revival in mesoscopic and nano systems.

Chapter 3 presents a brief overview of the Luttinger liquid theory and discusses an important theoretical tool - bosonization. Applications of bosonization to boundary problems as well as to systems with strong interactions are also addressed.

Chapter 4 presents a universal framework for describing critical systems in (1+1)D-Conformal Field Theory. A brief overview of conformal invariance and its implications for Conformal Field Theories is discussed.

Chapter 5 presents the work done in **Papers I and II** on Kondo and Luttinger liquid physics in nanostructures. It contains important details which are not presented in the papers due to length limits.

Chapter 6 presents the work done in **Paper III** on STM response of Luttinger liquids with edges and impurities. It summarizes the results obtained in the **Paper III**.

Chapter 7 presents the work done in **Paper IV** on boundary Green's functions in the spin-incoherent regime.

Contents

1

Introduction

"We are the ones who will hear", said Phouchg,
"the answer to the great question of Life ... !"
"The Universe ... !" said Loonquawl.
"And Everything ... !"

Hitchhiker's Guide to the Galaxy,
Douglas Adams

Since prehistoric human beings have looked at the sky and have been amazed by the Yellow Ball, the quest for understanding the Ultimate Truth has come to being. To understand Nature, people followed two different routes – the spiritual and the scientific. While the former defined a relatively easier path, accepting that the Ultimate Truth is impossible to reach and that one should resort to believing in the "High Spirit", the latter never seized to question everything and to search for the Ultimate Answer. Since both spiritual and scientific virtues are present in humans, they have influenced each other and in the course of history the two paths evolved in parallel, modifying each other. Spiritual or philosophical preferences of scientists definitely influenced the evolution of Science, as evidenced by Einstein's famous quote:

"At any rate, I am convinced that He [God] does not play dice".

The science at the present stage follows two distinct strategies. The first is reductionism, where the mysteries of Nature are expected to be answered by studying phenomena on the smallest possible scales. This approach is the driving force for high energy physics and string theory. The second strategy is relevant for modern

condensed matter physics. It is apparent that to use only basic principles for understanding many-particle systems is very difficult, if not impossible (or, if possible, not very useful for applications). As far as the collective behavior of systems is concerned, basic principles governing the dynamics of single particles do not yield much of an insight and there is a need for new principles that operate at the level of the collective dynamics. This is the idea of emergence which has been summarized by P.W. Anderson [1]:

"... at each level of complexity entirely new properties appear, and the understanding of the new behaviors requires research which I think is as fundamental in nature as any other."

Probably thermodynamics was the first branch of physics where emergence of new "effective" fundamental laws and principles became apparent. Even though the microscopic laws are time-reversal invariant, systems with a macroscopic number of particles are not. The time-reversal invariance gets broken and the new fundamental concepts of equilibrium and entropy emerge.

In fact, for low-energy properties of many collective systems, laws governing high-energy and short-distance physics are unimportant. The most striking examples are critical systems, where only the dimensionality of space and the symmetries of the order parameter are important. This observation is at the heart of the renormalization group (RG) method, where high-energy phenomena are gradually integrated out and an effective low-energy description is obtained. Systems where "more is different" include those with broken symmetry such as superconductivity, fractional quantum Hall systems with anyonic and even non-Abelian excitations, classical and quantum critical systems, 1D electronic systems, biological systems, etc. The effective theories describing these systems are very different from the microscopic theories governing few particles.

This thesis is devoted to problems of many-body physics, where "effective" theories predict some very surprising emergent phenomena. More specifically, the thesis is concerned with one-dimensional electron systems with impurities, and with one-dimensional nanostructrues. These systems have unconventional properties, which cannot be understood within a single particle picture (in contrast to most condensed matter systems in higher dimensions where the single-particle picture has proved very successful). Instead, new types of theories have to be used, such as those of the Luttinger liquid and the Kondo effect.

In the subsequent chapters I will give a short description of important aspects of Luttinger liquid and Kondo physics. I will also present the universal framework to understand (1+1)D critical systems - conformal field theory. The remaining chapters will be devoted to my own research.

2

Kondo Physics

2.1 The Kondo Effect

The Kondo effect is a well-known and widely studied phenomenon in condensed matter physics. Already in the 1930's [2, 3, 4] it was found that in many dilute magnetic alloys, the resistivity as a function of temperature shows a minimum at low temperatures. This was in contradiction with the accepted theoretical prediction that impurities give a constant contribution at low temperatures (see Fig. 2.1). This resistivity puzzle was explained only in 1964 [5] by the Japanese theorist J. Kondo.

The effect arises from the interactions between a single magnetic atom and the many electrons in an otherwise non-magnetic metal. Such an impurity typically has an intrinsic angular momentum or spin that interacts with the electrons. As a result, the mathematical description of the system is a difficult many-body problem. However, the Kondo problem is well defined, making it an attractive testing ground for new numerical and analytical tools that have been developed to attack other challenging many-body problems.

The electrical resistivity of a pure metal due to phonons usually drops rapidly ($\sim T^5$) as its temperature is lowered. However, the resistivity saturates as the temperature is lowered below about 10 K due to static defects in the material. The actual value of the low-temperature resistivity depends on the number of defects in the material and is called *residual resistivity*. Adding defects increases the value of the residual resistivity but the character of the temperature dependence remains the same. However, this behavior changes dramatically when magnetic atoms are added. Rather than saturating, the electrical resistivity increases as the temperature is lowered further. The so called *Kondo temperature*, T_K, roughly the temperature at which the resistivity minimum appears, completely determines the low-temperature energy scale of the system.

J. Kondo studied a simple model of a single band of conduction electrons coupled

to a local magnetic moment of spin $S = \frac{1}{2}$, which is called the *Kondo model*:

$$H = \sum_{\boldsymbol{k},\sigma} \epsilon_{\boldsymbol{k}} n_{\boldsymbol{k},\sigma} + J\boldsymbol{S} \cdot \boldsymbol{s}. \tag{2.1}$$

Here $\epsilon_{\boldsymbol{k}}$ is the kinetic energy and $n_{\boldsymbol{k},\sigma}$ is the occupation number of conduction electrons with wave vector $\boldsymbol{k}$ and spin projection σ. The constant J is a coupling between the local moment $\boldsymbol{S}$ of the impurity and the spin $\boldsymbol{s}$ of the conduction electrons at the impurity site. The electrical resistivity is related to the amount of back scattering from defects, which hinders the motion of the electrons through the crystal. In 1964 J. Kondo found that in the perturbative expansion of the resistivity the second term in the calculation could be much larger than the first when $T < T_K$, implying that the resistivity of a metal increases logarithmically when the temperature is lowered. It turns out that Kondo's expansion is correct only above the Kondo temperature.

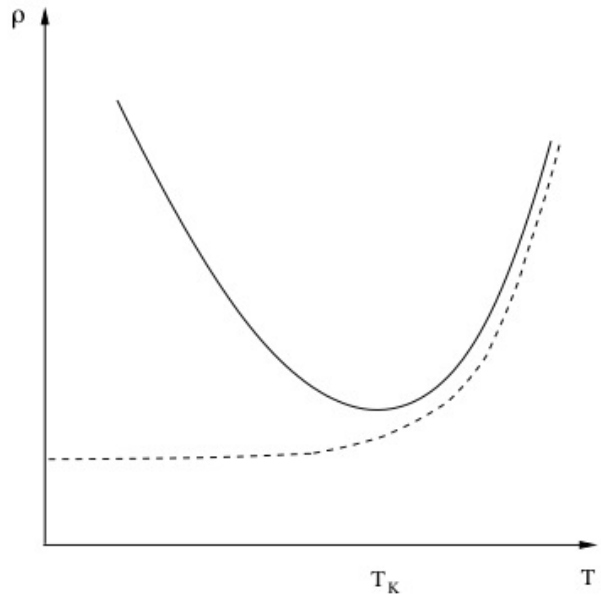

Figure 2.1: Resistivity ρ as a function of temperature T for non-magnetic (dashed line) and magnetic (solid line) impurities.

The theoretical framework for understanding the physics below T_K, which is non-perturbative in nature, emerged from P.W. Anderson's idea of scaling in the Kondo problem already in the late 1960's. Scaling assumes that the low-temperature properties of a real system are adequately represented by a *coarse grained* model. As the temperature is lowered, the model description becomes coarser and the number of degrees of freedom it contains is reduced. The so called *poor man's scaling* approach [6, 7, 8, 9] showed that at low temperatures the impurity interaction was governed by an effective coupling diverging in the low-temperature limit. The divergence of

the effective coupling constant at low energies was the first example of "asymptotic freedom", the concept behind QCD and the Standard Model of particle physics.

Later, in 1974, K. Wilson developed a method known as the *numerical renormalization group* [10] that overcame the shortcomings of conventional perturbation theory, and confirmed the scaling hypothesis. His work proved that at temperatures well below T_K, the magnetic moment of the impurity atom is screened entirely by the spins of the electrons in the metal and a many-body singlet ground state is formed. The resulting *screening cloud* has a size about the Kondo coherence length, $\xi_K = \hbar v_F / k_B T_K$, where v_F is the Fermi velocity (see Fig. 2.2). It was shown by P. Nozières that the excitations around the screening cloud can be described as a local Fermi liquid [11].

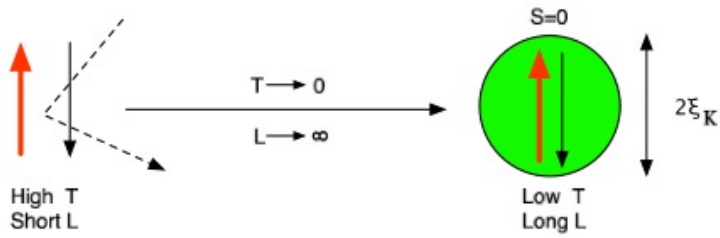

Figure 2.2: Schematic RG flow for the single channel ($S = 1/2$, $m = 1$) Kondo model.

In 1980 an exact solution of the Kondo model was found independently by N. Andrei [12] and P.B. Wiegmann [13]. They used the Bethe Ansatz method after realizing that it is possible to map the 3D Kondo model, which involves only s-wave scattering from the impurity, to a 1D model.

Another important development in 1980 was the introduction of the *multi-channel Kondo model*. The ordinary Kondo model is based on a single band of conduction electrons, which, due to the Pauli principle, allows only a single electron of each spin to interact with the impurity. P. Nozières and A. Blandin [14] introduced a more realistic model, which took into account the nonzero orbital angular momentum of conduction electrons, allowing several degenerate bands of electrons to interact with a local moment of general spin S. This model is known as the multi-channel Kondo model,

$$H = \sum_{\boldsymbol{k},\sigma,i} \epsilon_{\boldsymbol{k}} n_{\boldsymbol{k},\sigma,i} + J\boldsymbol{S} \cdot \sum_i \boldsymbol{s}_i, \tag{2.2}$$

where i is a channel index.

P. Nozières and A. Blandin showed that depending on whether the number of channels, m, is greater than, less than, or equal to twice the size of the impurity spin S, the low-temperature properties are very different. For cases $m < 2S$ (*under-screened*) and $m = 2S$ (*exactly screened*) the low temperature physics is described by a local Fermi liquid picture, as for the ordinary Kondo model. The case $m > 2S$

(*overscreened*) is fundamentally different from the above cases. The electrons here become strongly correlated and they form a collective state together with the impurity spin. The numerical renormalization group approach shows that the coherence length of screening cloud diverges as $1/T$ when $T \to 0$. At each step of the renormalization there is an unscreened spin which couples one electron from each channel and the process is repeated until all electrons form a collective state with an impurity spin (see Fig. 2.3). Due to the strong correlations in this collective state, excitations cannot be described as quasiparticles in the Fermi liquid picture. Instead excitations combine charge and spin in unorthodox ways leading to non-Fermi liquid low-temperature behavior.

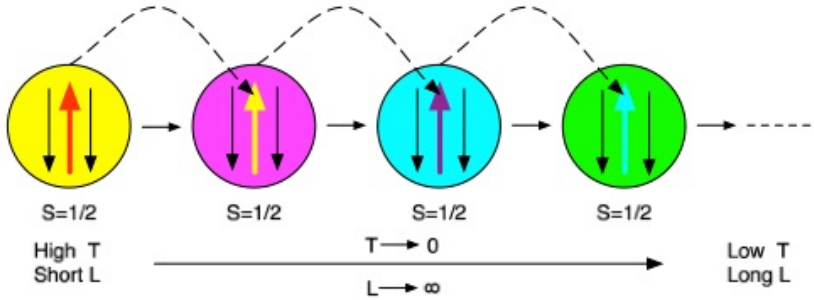

Figure 2.3: Schematic RG flow for the two-channel ($S = 1/2$, $m = 2$) Kondo model.

The overscreened Kondo model was first solved by the Bethe Ansatz method, independently by N. Andrei and C. Destri [15], and A.M. Tsvelik and P.B. Wiegmann [16]. Although exact, the Bethe Ansatz solutions are very complex and not easily open to physical interpretations. A more transparent solution, which is valid for temperatures far below T_K (in contrast to the Bethe Ansatz method, which is exact and valid for all temperatures), was found by I. Affleck and A.W.W. Ludwig [17], using the methods of *non-Abelian bosonization* and *conformal field theory*. The beauty of this method is that it is open to generalizations to other quantum impurity problems.

2.2 Kondo Effect in Mesoscopic Systems

In the previous section we saw that the Kondo effect has been under intensive research. Why would anyone still want to study a physical phenomenon that was discovered in the 1930s, explained in the 1960s and has been the subject of numerous reviews since the 1970s?

The revival of Kondo physics [18] is due to the progress in fabrication technology, making it possible to manufacture [19] small semiconductor devices for investigating fundamental problems in physics. One such device is the quantum dot [20, 21], a tiny semiconductor box that can hold a small number of electrons. Quantum dots

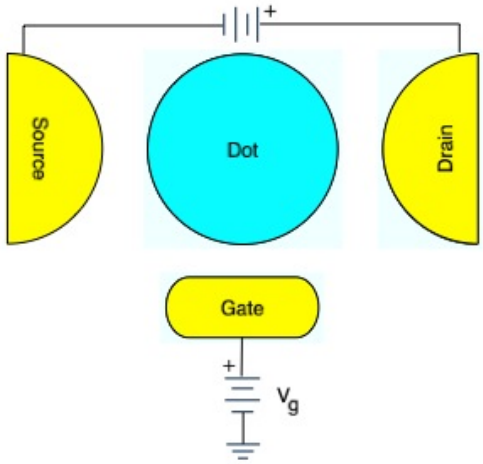

Figure 2.4: A generic setup for observing the Kondo behavior in a quantum dot system. V_g is the gate voltage.

are often called artificial atoms since their electronic properties resemble those of real atoms. However, in contrast to real atoms, the electronic structure of a dot can be easily controlled, e.g. by a gate voltage or an applied magnetic field. A device for observing the Kondo behavior can be realized by embedding a quantum dot between large metallic leads (see Fig. 2.4). A voltage applied to a gate electrode of the device controls the number of electrons, N, that are confined in the dot. If an odd number of electrons is trapped within the dot, the total spin of the dot, S, is necessarily non-zero and has a minimum value of $S = 1/2$. This mimics the impurity-in-metal system where localized spin is embedded in the metallic host and therefor many of the known Kondo phenomena can be expected to occur in these transistor-type devices [22, 23]. One of the main distinctions between a quantum dot and a real metal is related to their different geometries. In a metal, the electron states are plane waves, and scattering from impurities in the metal mixes electron waves with different momenta and consequently increases the resistivity. In a quantum dot, however, all the electrons have to travel through the device, as there is no path for electrons around it. In this case, the *Kondo resonance*, i.e. the enhanced density of states in the vicinity of the Fermi level, makes it easier for states belonging to the two opposite electrodes to mix. The conductance increases due to this mixing. In other words, the Kondo effect produces the opposite behavior in a quantum dot to that of a conventional impurity-in-metal system. Moreover, at very low temperatures, the conductance approaches the quantum limit of conductance $2e^2/h$, where e is the charge of an electron. The low-temperature increase in conductance and the saturation at $2e^2/h$ are somewhat counterintuitive, even though the behavior is in complete agreement with theory. The system initially is highly unfavorable for

electron transport due to a large energy scale of the dot, U, which tries to block electrons from tunneling into or out of it (it is just an electrostatic repulsion, which is the heart of the *Coulomb blockade* [24]). In addition, the electron level of the dot, with energy ϵ_0, is far from the Fermi level, i.e. the system is *off resonance*. However, the *higher-order* spin-flip processes (see Fig. 2.5) that lead to the Kondo effect completely turn the situation around and increase the conductance until it reaches its maximum (Fig. 2.6). Indeed, the fact that the conductance reaches $2e^2/h$ implies that the electrons are transmitted perfectly through the dot, and it becomes completely transparent in the Kondo regime.

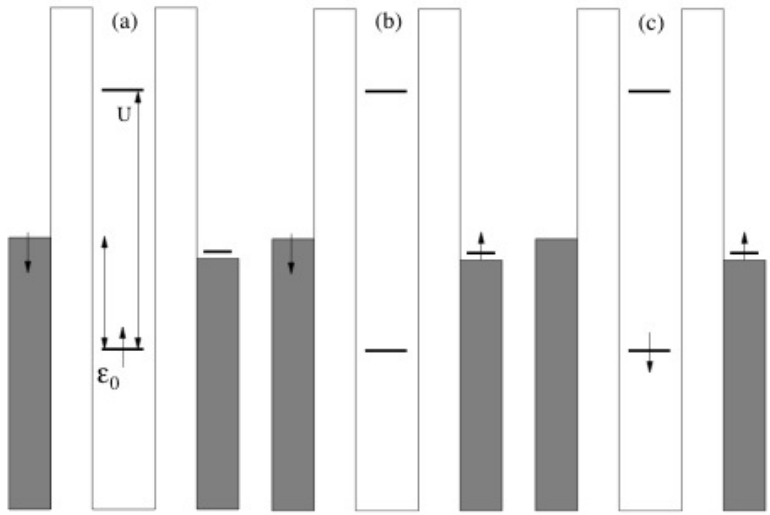

Figure 2.5: Sketch of processes leading to Kondo physics in the lead − quantum dot − lead structure. (a) *Initial state* − level ϵ_0 is occupied by a single spin-up electron. The addition of another electron is prohibited by the Coulomb repulsion energy U. (b) *Virtual state* − electron tunnels out of the dot. (c) *Final state* − electron on the dot is replaced by an electron tunneling from the lead. The combined processes (b) and (c) effectively flip the electron spin on the dot.

The ease of manipulating quantum dots have provided new opportunities to control the Kondo effect experimentally. In many ways the setup described above is similar to the impurity-in-metal system. However, quantum dots can also push research on the Kondo effect in new directions, where artificial structures can be exploited in regimes that are inaccessible with magnetic impurities. An unconventional Kondo effect can occur for quantum dots that have even number of electrons [25]. The spectrum of energy levels in a quantum dot can easily be changed by, for example, applying a magnetic field of order 1T to force a transition between a singlet ($S = 0$) and a triplet ($S = 1$) state. Although the same transition can occur in real atoms, it requires a magnetic field of about 10^6T, which cannot be generated in the lab. At the point of this transition singlet and triplet levels become degenerate and

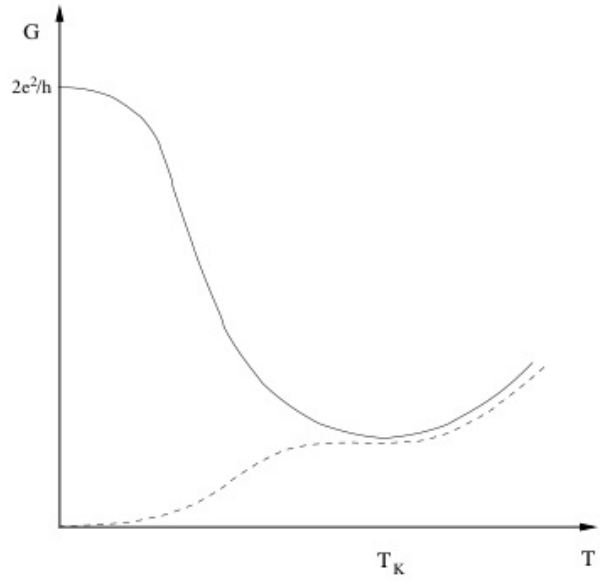

Figure 2.6: Conductance G as a function of temperature T for odd (solid line) and even (dashed line) numbers of electrons in a quantum dot.

an effective two level system is realized. Exchange processes, like those described above, mix the degenerate states. The new many-body effect that arises from the degeneracy and exchange interactions is similar to the conventional Kondo effect. An important difference, however, is that the Kondo effect in this case is induced by a magnetic field.

It may appear that electron spin is essential for the existence of Kondo physics, but in fact it can be found in spinless systems also. Here the so called *Coulomb blockade* plays the essential role. The foundations of Coulomb blockade theory were set by I.O. Kulik and R.I. Shekhter [24]. The prevalence of single-electron charging in semiconductor quantum dots turned the Coulomb blockade concept into an important part of modern semiconductor physics.

In quantum dot structures, in which the charge of the dot, Q, is comparable to the electronic charge e, the relationship between a gate potential V_g and Q must take into account the discrete nature of charge carried by electrons. Although V_g may be varied continuously, the charge in an isolated quantum dot must always be an integer multiple of e, namely $Q = Ne$ (of course coupling to the medium and temperature alters the average charge to noninteger values). As the gate voltage is changed, the actual charge on the dot is the integer multiple of e that comes closest to the quantity of charge that would otherwise reside in the dot if charge were not quantized. Therefore, if V_g is increased continuously, the charge in the dot increases incrementally by e at periodically spaced values of V_g in a stepwise manner (see Fig. 2.7(a)).

Given that the charge in the quantum dot is an integer multiple of e, the electrostatic energy associated with N electrons in the dot reads:

$$H_C(N) = \frac{Q^2}{2C_\Sigma} - V_g Q = \frac{(Ne)^2}{2C_\Sigma} - V_g Ne. \tag{2.3}$$

The first term on the right-hand side of this expression represents the charging

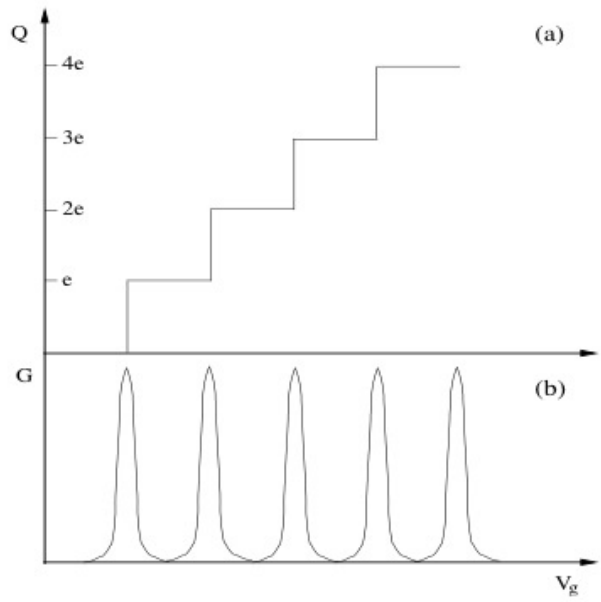

Figure 2.7: (a) Dependence of the charge on the dot Q on the gate voltage V_g – the so called *Coulomb staircase*. (b) Conductance G as a function of the gate voltage V_g.

energy the dot, with C_Σ being the total capacitance of the dot (the capacitance between the quantum dot and the rest of the world). The second term represents the potential energy of the quantum dot. Solving this relation for the integer value of N that minimizes $H_C(N)$ for a given V_g reproduces the staircase relationship. The gate voltages at which the charge on the dot increments by e correspond to situations in which $H_C(N) = H_C(N+1)$. This condition occurs periodically when $V_g = e(N + 1/2)/C_\Sigma$, indicating that if V_g is adjusted to a value at which the electrostatically favored quantity of charge on the dot is a half integer multiple of e, then the actual lowest energy state of the dot is degenerate, corresponding either to N or to $N+1$ electrons, and the dot is energetically free to fluctuate between these two states. Midway between these charge degeneracy points, when $V_g = eN/C_\Sigma$, equation (2.3) indicates that adding (or removing) an additional electron moves the dot away from its lowest energy state by an energy $e^2/2C_\Sigma$. As V_g is swept, this charging energy periodically attains its maximum value of $e^2/2C_\Sigma$ each time V_g is half way between the degeneracy points, and gradually vanishes as the quantum

dot approaches the degeneracy points. This gives periodic conductance peaks as a function of V_g (Fig. 2.7(b)).

At degenerate points, for small tunneling strengths and temperatures (compared to the charging energy $e^2/2C_\Sigma$), the system behaves as a degenerate two-level system which can be mapped onto a *pseudo-spin* $S = 1/2$ Kondo model [26], with pseudo-spin-$\uparrow$ and pseudo-spin-$\downarrow$ states given by N and $N+1$ charge states of the dot. The low-temperature behavior is governed by Kondo physics, although the spin of the electrons only plays the role of a channel index (in the spin-full case).

The advantage of quantum dots is the ease with which the parameters of these artificial atoms can be controlled. External "knobs" allow the discrete energy level structure of the device to be varied, as well as the number of electrons trapped within the dot. Also, the strength of the Kondo coupling (and therefore T_K) can be controlled precisely.

Recent experiments illustrate the generality of the single-channel Kondo effect and its importance to nanoelectronic devices [27, 28, 29, 30]. Whenever a small system with a well defined number of electrons is connected to electrodes, Kondo physics affects the low-temperature electronic properties of the device. It is more tricky to observe the two-channel Kondo effect. The requirement of channel isotropy is hard to meet (in case of the channel anisotropy behavior flows to that of the single channel case [31]). While it is impossible to control this in impurity-in-metal systems, there is possibility to ensure channel isotropy in artificial nanostructures. However, an obstacle for experimentally probing the two-channel physics is the very small Kondo temperature T_K. There exists a number of theoretical proposals of different nanostructures to overcome the above problems [32, 33, 34, 35, 36, 37, 38, 39], but experimental realizations still remain elusive. Recent experimental studies [40] only reveal the crossover regimes with signatures of a two-channel scenario.

3

The Luttinger Liquid

In this chapter I will discuss the physics of 1D strongly correlated electron systems. In section (3.1) I will describe why *Fermi liquid* theory breaks down in a 1D system and introduce the concept of a *Luttinger liquid*. In section (3.2) the analytical tool behind the Luttinger liquid theory – *bosonization* is presented. In sections (3.3), (3.4) and (3.5) I present bosonization schemes for three different cases: 1D electron systems with boundaries, single-wall carbon nanotubes (SWCNTs), and 1D Wigner crystals. The key properties of Luttinger liquids are presented in section (3.6). In section (3.7) I review the experimental evidence for Luttinger liquid behavior in quasi one-dimensional conductors, fractional quantum Hall systems, quantum wires and carbon nanotubes.

3.1 Why 1D is so Different from Higher Dimensions

Landau's Fermi liquid theory [41] successfully explains most $3D$ interacting electron systems. It assumes that as the interaction between electrons is *switched on adiabatically* the eigenstates of the system transform continuously without changing the quantum numbers. From the renormalization group point of view [42] the system renormalizes to a non-interacting fermion system (but with renormalized dynamical parameters), which allows an interpretation of the physics in terms of *quasiparticles*.

This simple picture does not work in one dimension (1D). This can be seen by considering the so called *Lindhard response function* [43]

$$\chi(\mathbf{k}, \omega = 0) = \int \frac{d\mathbf{k}'}{(2\pi)^d} \frac{f_{\mathbf{k}'} - f_{\mathbf{k}'+\mathbf{k}}}{\epsilon_{\mathbf{k}'} - \epsilon_{\mathbf{k}'+\mathbf{k}}}, \tag{3.1}$$

which defines the response of the electron density $\rho(\mathbf{k})$ to a potential $\phi(\mathbf{k})$, which is effectively generated by the electrons in the Fermi gas if these are interacting. If we consider a tiny fluctuation in the electron density, it will change the potential felt by the electrons, which, through the linear response theory, changes the density

according to $\rho(\mathbf{k}) = \chi(\mathbf{k})\phi(\mathbf{k})$. In 2D and 3D the Lindhard response function is nonsingular and the initial density fluctuation will be damped. In the 1D case the Lindhard response function becomes singular and fluctuations are enhanced. This is in contradiction to the main assumption of the Fermi liquid theory that no singularities appear when the interactions are *switched on adiabatically*.

The absence of quasiparticles in 1D can be understood considering the particle-hole spectrum. In marked difference with the 2D (and 3D) case (see Fig. 3.1), in 1D low-energy particle-hole excitations can only be created in the immediate vicinity of $k = 0, 2k_F$ (see Fig. 3.2).

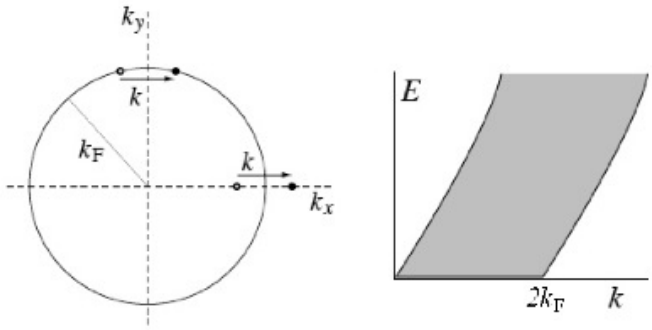

Figure 3.1: Single-electron and particle-hole excitation spectra in 2D. Grey areas represent the allowed excitations. Taken from Ref. [44].

Quasiparticles are usually viewed as electrons "dressed" with particle-hole clouds. Since low-energy particle-hole excitations cannot be created for arbitrary momentum, the quasiparticle description breaks down.

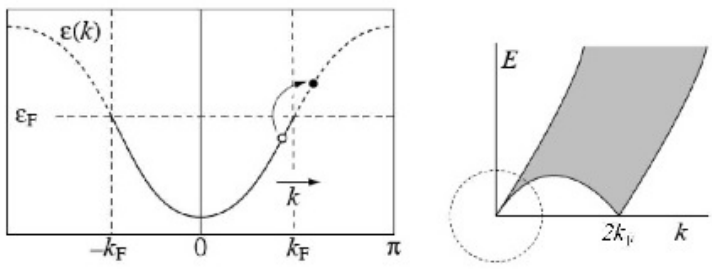

Figure 3.2: Single-electron and particle-hole excitation spectra in 1D. Grey areas represent the allowed excitations. Taken from Ref. [44].

Thus, turning on the interaction between 1D electrons will lead to a new system,

which cannot be described by Fermi liquid theory. In the language of the renormalization group, the interacting electron system flows to a non-Fermi liquid fixed point at low energies, with properties very different from that of a Fermi liquid. As we shall see, all low-lying excitations are collective and separately carry charge and spin. Strong correlations also modify the asymptotic behavior of the correlation functions: at large distances and times they decay with a power law with interaction dependent exponents. This system is known as a *Luttinger liquid* [45].

3.2 Introduction to Bosonization

Here I will review a very useful tool for treating 1D strongly correlated electrons – bosonization. The idea behind the method is to map a strongly correlated electron system to a weakly interacting boson system. One can easily see that the quantum statistics is not well-defined in 1D and there is a room for "transmutation" of statistics. This can be understood by considering the phases of particle wavefunctions. In general there are two independent phases: one coming from the statistics and the other from the interactions. While it is easy to distinguish them in 2D and 3D, it is impossible to do it in 1D, since any interchange of the particles also inevitably involves the interaction (any exchange requires the particles to pass through each other due to the reduced dimensionality). Due to this ambiguity one can absorb part of the interaction in the statistical phase, thus changing the statistics of the new composite object. This idea is behind the *Jordan-Wigner* [46] transformation, which maps a 1D spin-1/2 system onto a spinless fermion system [47]. The new fermion operators are composite operators of the spin-1/2 operators. The beauty of bosonization is that the new system is a noninteracting (or weakly interacting) boson system, which makes the analysis straightforward.

In 1D systems the Fermi surface consists of two points (see Fig. 3.3). At low energies excitations around the Fermi points play an important role. Near the Fermi points $\pm k_F$ we can define a low-energy effective theory by linearizing the spectrum ϵ_k. We also define slow-varying "*right*" ($\psi_{R,\sigma}(x)$) and "*left*" ($\psi_{L,\sigma}(x)$) moving electron fields by expanding the full field $\Psi_\sigma(x)$ operator for a spin σ electron:

$$\Psi_\sigma(x) = e^{ik_F x}\psi_{R,\sigma}(x) + e^{-ik_F x}\psi_{L,\sigma}(x). \tag{3.2}$$

These satisfy the commutation relations

$$\{\psi_{r,\sigma}(x), \psi^\dagger_{r',\sigma'}(x')\} = \delta_{rr'}\delta_{\sigma\sigma'}\delta(x-x'), \tag{3.3}$$

$$\{\psi_{r,\sigma}(x), \psi_{r',\sigma'}(x')\} = 0, \tag{3.4}$$

where r, r' take the values R, L. Then the Hamiltonian of the free theory

$$H_0 = \sum_{k,\sigma} \epsilon_k c^\dagger_{k,\sigma} c_{k,\sigma} \tag{3.5}$$

can be written in the following way

$$H_0 = -iv_F \int dx\ (:\psi^\dagger_{R,\sigma}\partial_x\psi_{R,\sigma}: - :\psi^\dagger_{L,\sigma}\partial_x\psi_{L,\sigma}:), \tag{3.6}$$

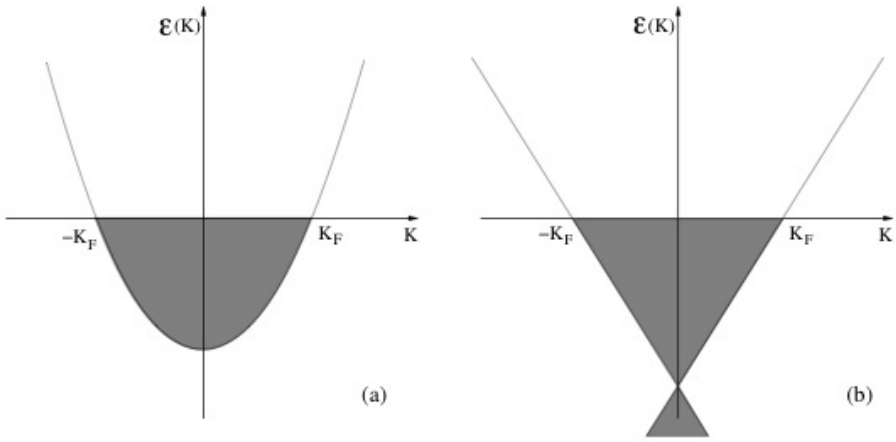

Figure 3.3: (a) Spectrum of a generic one-dimensional system. (b) Spectrum after linearization. The dark region represents the filled states.

which is Dirac's theory for 1D "right" and "left" moving electrons. Here $: \cdots :$ denotes a *normal ordering*, which takes care of divergences coming from the filled Dirac's sea.

The interaction between electrons can be written as

$$H_{int} = \frac{1}{2}\int dxdy\ \Psi^\dagger_\sigma(x)\Psi^\dagger_{\sigma'}(y)U_{\sigma\sigma'}(x-y)\Psi_{\sigma'}(y)\Psi_\sigma(x). \tag{3.7}$$

The range of the interaction $U_{\sigma\sigma'}(x-y)$ is usually *finite* in real 1D systems due to screening provided by nearby gates or the surrounding medium. Since we are interested in the properties in the long-distance (time) limit, we can approximate the finite range interaction to a *local* one. Setting $U_{\sigma\sigma'}(x-y) = U_{\sigma\sigma'}\delta(x-y)$, the interaction Hamiltonian can be expressed as

$$H_{int} = H_1 + H_2^c + H_2^s + H_3 + H_4^c + H_4^s, \tag{3.8}$$

$$H_1 = v_F g_1 \int dx\ :\psi^\dagger_{R,\sigma}\psi_{L,\sigma}\psi^\dagger_{L,-\sigma}\psi_{R,-\sigma}:, \tag{3.9}$$

$$H_2^c = v_F g_{2,c}\int dx\ (J_{R,\uparrow}+J_{R,\downarrow})(J_{L,\uparrow}+J_{L,\downarrow}), \tag{3.10}$$

$$H_2^s = v_F g_{2,s}\int dx\ (J_{R,\uparrow}-J_{R,\downarrow})(J_{L,\uparrow}-J_{L,\downarrow}), \tag{3.11}$$

$$H_3 = \frac{1}{2}v_F g_3 \int dx\ (:\psi^\dagger_{R,\sigma}\psi^\dagger_{R,-\sigma}\psi_{L,\sigma}\psi_{L,-\sigma}: + H.c.), \tag{3.12}$$

$$H_4^c = \frac{1}{2} v_F g_{4,c} \int dx \; [(J_{R,\uparrow} + J_{R,\downarrow})^2 + (J_{L,\uparrow} + J_{L,\downarrow})^2], \tag{3.13}$$

$$H_4^s = \frac{1}{2} v_F g_{4,s} \int dx \; [(J_{R,\uparrow} - J_{R,\downarrow})^2 + (J_{L,\uparrow} - J_{L,\downarrow})^2], \tag{3.14}$$

with currents $J_{R/L,\sigma}$ defined as $J_{R/L,\sigma} =: \psi^\dagger_{R/L,\sigma} \psi_{R/L,\sigma} :$. The coupling constants are indexed as in ref. [44]. In this expression H_1 describes *backward* scattering, H_2 and H_4 describe *dispersive* and *forward* scattering, respectively, and H_3 describes *umklapp* scattering (Fig. 3.4).

If the couplings g_1 and g_3 are zero, i.e. only forward and dispersive scatterings are present, then the model can be solved exactly and is called the spin-full *Tomonaga-Luttinger model* [48, 49]. This model can be exactly solved by *bosonization* [50, 51], the idea of which is to represent fermionic operators in terms of bosonic ones.

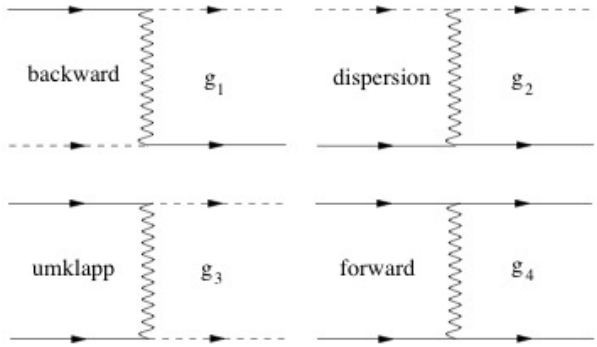

Figure 3.4: Diagrams for the interaction presented in Eqs. (3.9)-(3.14). Solid (dashed) arrows represent the right (left) moving electrons. The spin is suppressed in the diagrams but incoming electrons must have opposite spins for backward and umklapp scattering processes.

The fermionic currents form a $U(1)$ Kac-Moody algebra [52] and obey the following commutation relation:

$$[J_{r,\sigma}(x), J_{r',\sigma'}(x')] = -\frac{i}{2\pi} r \delta_{rr'} \delta_{\sigma\sigma'} \partial_x \delta(x - x'). \tag{3.15}$$

As before, r, r' take values R, L if they appear as subindices, otherwise $r = +, -$ respectively.

We define new *spin* and *charge* currents by

$$J_{r,c/s} = \frac{1}{\sqrt{2}} (J_{r,\uparrow} \pm J_{r,\downarrow}), \tag{3.16}$$

which obey the same commutation relation as in Eq. (3.15).

The Kac-Moody algebra can be satisfied by introducing bosons $\varphi_{c/s}$, with conjugate momenta $\Pi_{c/s}$, obeying

$$[\varphi_\alpha(x), \Pi_{\alpha'}(x')] = i \delta_{\alpha\alpha'} \delta(x - x'), \tag{3.17}$$

with α an index taking values c, s. A straightforward calculation shows that

$$J_{r,c/s} = \frac{1}{\sqrt{4\pi}}(\partial_x \varphi_{c/s} - r\Pi_{c/s}) \tag{3.18}$$

also satisfy a $U(1)$ Kac-Moody algebra.

We are now in a position to write the free Hamiltonian in bosonized form. Using normal ordering one can show that

$$:\psi^\dagger_{R,\sigma}\partial_x\psi_{R,\sigma}: - :\psi^\dagger_{L,\sigma}\partial_x\psi_{L,\sigma}: \;= -\pi(J^2_{R,\sigma} + J^2_{L,\sigma}). \tag{3.19}$$

Using Eqs. (3.18) and (3.19) the free Hamiltonian can be expressed in terms of free spin and charge bose fields:

$$H_0 = \sum_{\alpha=c,s} \frac{v_F}{2} \int dx \left[\Pi^2_\alpha + (\partial_x \varphi_\alpha)^2\right]. \tag{3.20}$$

The corresponding Lagrangian can be written as

$$L_0 = \sum_{\alpha=c,s} \frac{1}{2} \int dx \left[\frac{1}{v_F}(\partial_t \varphi_\alpha)^2 - v_F(\partial_x \varphi_\alpha)^2\right], \tag{3.21}$$

with canonical momentum defined as

$$\Pi_\alpha = \frac{1}{v_F}\partial_t \varphi_\alpha. \tag{3.22}$$

From the equation of motion of bose fields, which is the *Klein-Gordon* equation

$$\left(\frac{1}{v_F^2}\partial_t^2 - \partial_x^2\right)\varphi_\alpha = 0, \tag{3.23}$$

it is evident that we can write the bose field as a sum of left- and right-moving fields:

$$\varphi_\alpha(x,t) = \phi_{L,\alpha}(x + v_F t) + \phi_{R,\alpha}(x - v_F t). \tag{3.24}$$

Defining the *dual field* ϑ_α as

$$\Pi_\alpha = \partial_x \vartheta_\alpha \tag{3.25}$$

we can show that it is also a solution to the equation of motion and can be written as

$$\vartheta_\alpha = \phi_{L,\alpha}(x + v_F t) - \phi_{R,\alpha}(x - v_F t). \tag{3.26}$$

To make the bosonization procedure complete, we should find the representation of fermionic operators in terms of bosonic ones. The following formula

$$\psi_{r,\sigma} = \frac{\eta_{r,\sigma}}{\sqrt{2\pi\alpha}} \exp\left(2\pi r i \int^x dx' J_{r,\sigma}(x')\right), \tag{3.27}$$

obeys the required fermion anticommutation relations and is the correct representation. Here the so called *Klein factors* $\eta_{r,\sigma}$ are Hermitian operators with anticommutation relations $\{\eta_{r,\sigma}, \eta_{r',\sigma'}\} = 2\delta_{rr'}\delta_{\sigma\sigma'}$ (forming a *Clifford algebra*), which ensure

the correct anticommutation relations between different fermion species. Eq. (3.27) can be rewritten as

$$\psi_{r,\sigma} = \frac{\eta_{r,\sigma}}{\sqrt{2\pi\alpha}} \exp\left(ir\sqrt{4\pi}\phi_{r,\sigma}\right). \tag{3.28}$$

Some care is needed to properly account for the extension of the Hilbert space due to the Klein factors. The Hamiltonian and all physical observables must be diagonal in Klein factor space and the choice of a particular eigenstate decouples the rest of the Klein Hilbert space. This can be achieved by adopting a suitable representation for the Klein factors and then diagonalizing products of the Klein factors.

In terms of the new bosonic fields the interaction terms (3.9)-(3.14) can be expressed as

$$H_1 = \frac{v_F g_1}{2\pi^2} \int dx \cos(\sqrt{8\pi\varphi_s}), \tag{3.29}$$

$$H_2^c = \frac{v_F g_{2,c}}{2\pi} \int dx \left[(\partial_x\varphi_c)^2 - \Pi_c^2\right], \tag{3.30}$$

$$H_2^s = \frac{v_F g_{2,s}}{2\pi} \int dx \left[(\partial_x\varphi_s)^2 - \Pi_s^2\right], \tag{3.31}$$

$$H_3 = \frac{v_F g_3}{2\pi^2} \int dx \cos(\sqrt{8\pi\varphi_c}), \tag{3.32}$$

$$H_4^c = \frac{v_F g_{4,c}}{2\pi} \int dx \left[\Pi_c^2 + (\partial_x\varphi_c)^2\right], \tag{3.33}$$

$$H_4^s = \frac{v_F g_{4,s}}{2\pi} \int dx \left[\Pi_s^2 + (\partial_x\varphi_s)^2\right]. \tag{3.34}$$

Specializing to the Tomonaga-Luttinger Hamiltonian, i.e. $H_0 + H_{int}$ with $g_1 = g_3 = 0$, we have

$$H_{TL} = \sum_{\alpha=c,s} \frac{v_\alpha}{2} \int dx \left[K_\alpha \Pi_\alpha^2 + \frac{1}{K_\alpha}(\partial_x\varphi_\alpha)^2\right], \tag{3.35}$$

with

$$K_\alpha = \sqrt{\frac{\pi - g_{2,\alpha} + g_{4,\alpha}}{\pi + g_{2,\alpha} + g_{4,\alpha}}}, \qquad v_\alpha = v_F\sqrt{\left(1 + \frac{g_{4,\alpha}}{\pi}\right)^2 - \left(\frac{g_{2,\alpha}}{\pi}\right)^2}. \tag{3.36}$$

By rescaling the fields, $\tilde{\varphi}_\alpha = \varphi_\alpha/\sqrt{K_\alpha}$ and $\tilde{\Pi}_\alpha = \sqrt{K_\alpha}\Pi_\alpha$, i.e. performing a *Bogoliubov rotation*, one finally obtains

$$H_{TL} = \sum_{\alpha=c,s} \frac{v_\alpha}{2} \int dx \left[\tilde{\Pi}_\alpha^2 + (\partial_x\tilde{\varphi}_\alpha)^2\right]. \tag{3.37}$$

We see that this is a Hamiltonian for free *spin* and *charge* bosons, which propagate with different velocities. In other words the theory can not be described by electron-type quasiparticles but rather in terms of collective waves which separately

carry spin and charge and are bosonic in nature (in distinction to the fermionic quasiparticles in the Fermi liquid). This fact is a manifestation of *spin-charge separation*.

Having obtained the Tomonaga-Luttinger Hamiltonian, which encodes the dispersive (Eqs. (3.10), (3.11)) and forward (Eqs. (3.13),(3.14)) scattering processes, we have to ask what is the effect from backward (Eq. (3.9)) and umklapp (Eq. (3.12)) scattering processes. If the system is away from half-filling (the case which will be discussed throughout the thesis) $g_3 = 0$, so there is no contribution from the umklapp process. This is due to the fast $4k_F$ oscillations which integrate to zero. As for backscattering, if $|g_1| < 2\pi(K_s - 1)$ this process is *marginally irrelevant* (in renormalization group sense) and the system flows to the $g_1 = 0$ case (Eq. (3.37)). If $|g_1| > 2\pi(K_s - 1)$, then the backscattering is *marginally relevant* and the system develops a spin gap. The corresponding RG flow is shown in Fig. 3.5.

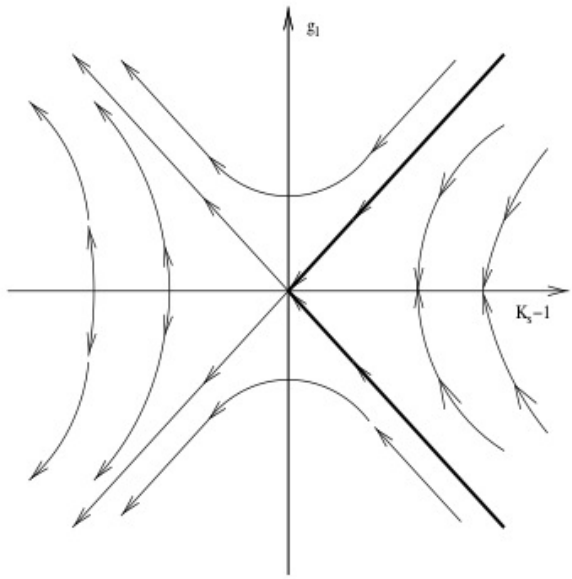

Figure 3.5: RG flow in the presence of the backward scattering. Thick arrows mark the SU(2) line.

This summarizes the so called *Abelian* bosonization of 1D interacting electrons. The name comes from the fact that the bose fields have $U(1)$ Abelian symmetry. Abelian bosonization may be used to describe the spin sector of one-dimensional electrons, but this description is not manifestly spin-rotation invariant. There exists another version of bosonization, the so called *non-Abelian* bosonization [53], where the description remains manifestly $SU(2)$ invariant. The corresponding boson theory is called the Wess-Zumino-Witten (WZW) model [52].

In this case charge and spin currents are expressed in the following way:

$$\begin{aligned} J_r(x) &= :\psi^\dagger_{r,\sigma}(x)\psi_{r,\sigma}(x):, \\ \boldsymbol{J}_r(x) &= \frac{1}{2}:\psi^\dagger_{r,\sigma}(x)\boldsymbol{\sigma}_{\sigma\sigma'}\psi_{r,\sigma'}(x):, \end{aligned} \tag{3.38}$$

with $\boldsymbol{\sigma}$ being a vector of Pauli matrices and σ, σ' summed over. The currents obey the following commutation relations:

$$\begin{aligned} \left[J_r(x), J_r(x')\right] &= -\frac{i}{\pi}\delta_{rr'}\partial_x\delta(x-x'), \\ [J^a_r(x), J^b_{r'}(x')] &= -\frac{ik}{2\pi}\delta_{rr'}\delta_{ab}\partial_x\delta(x-x') + i\epsilon_{abc}\delta_{rr'}J^c_r(x)\delta(x-x'), \end{aligned} \tag{3.39}$$

where k is called the *level* of the WZW model (being equal to the number of "channels" of the original electron system). Here for simplicity we discuss only the $k = 1$ case.

Using the definitions in Eq. (3.38) the free Hamiltonian can be written as

$$H_0 = \int dx \left[\frac{\pi v_F}{2}(J^2_R + J^2_L) + \frac{2\pi v_F}{3}(\boldsymbol{J}^2_R + \boldsymbol{J}^2_L)\right], \tag{3.40}$$

and the interaction terms (3.9)-(3.14) as

$$H_1 = -2v_F g_1 \int dx\ (J^x_R J^x_L + J^y_R J^y_L), \tag{3.41}$$

$$H^c_2 = v_F g_{2,c} \int dx\ J_R J_L, \tag{3.42}$$

$$H^s_2 = 4v_F g_{2,s} \int dx\ J^z_R J^z_L, \tag{3.43}$$

$$H_3 = \frac{v_F g_3}{2\pi^2} \int dx\ \cos(\sqrt{8\pi}\varphi_c), \tag{3.44}$$

$$H^c_4 = \frac{1}{2} v_F g_{4,c} \int dx\ (J^2_R + J^2_L), \tag{3.45}$$

$$H^s_4 = \frac{2}{3} v_F g_{4,s} \int dx\ (\boldsymbol{J}^2_R + \boldsymbol{J}^2_L). \tag{3.46}$$

If $g_1 = -2g_{2,s}$, H_1 and H^s_2 combine into a single rotation-invariant interaction:

$$H_1 + H^s_2 = -2v_F g_1 \boldsymbol{J}_R \cdot \boldsymbol{J}_L. \tag{3.47}$$

In the $SU(2)$ invariant case H reads (non half-filled case):

$$\begin{aligned} H &= \int dx \left[\left(\frac{\pi v_F}{2} + \frac{v_F g_{4,c}}{2}\right)(J^2_R + J^2_L) + v_F g_{2,c} J_R J_L\right] + \\ &+ \int dx \left[\left(\frac{2\pi v_F}{3} + \frac{2 v_F g_{4,s}}{3}\right)(\boldsymbol{J}^2_R + \boldsymbol{J}^2_L) - 2v_F g_1 \boldsymbol{J}_R \cdot \boldsymbol{J}_L\right]. \end{aligned} \tag{3.48}$$

The charge sector can be brought to the canonical form (3.40) by the *Bogoliubov rotation*

$$J_{L/R} = \cosh\theta\ \mathcal{J}_{L/R} + \sinh\theta\ \mathcal{J}_{R/L}, \tag{3.49}$$

with $e^{2\theta} = K_c$.

In the spin sector the last term is marginally irrelevant and the system flows to the canonical form (3.40), with $K_s = 1$. It can be shown that the separatrix $|g_1| = 2\pi(K_s - 1)$ is determined by the condition of rotational invariance, $g_1 = -2g_{2,s}$, and is hence called the $SU(2)$ invariant line (see Fig. 3.5).

Summarizing the above:

$$H = \int dx \left[\frac{\pi v_c}{2}(\mathcal{J}_R^2 + \mathcal{J}_L^2) + \frac{2\pi v_s}{3}(\boldsymbol{J}_R^2 + \boldsymbol{J}_L^2) \right], \tag{3.50}$$

where $v_c = v_F\sqrt{(1 + g_{4,c}/\pi)^2 - (g_{2,c}/\pi)^2}$ and $v_s = v_F(1 + g_{s,4}/\pi)$.

This form of the Hamiltonian is known as the *Sugawara* form [52], which is expressed in currents. Eq. (3.50) can also be written in terms of two WZW models ($U(1)$ for charge and $SU(2)$ for spin). The non-Abelian symmetry of the bosonic spin fields gives the name to this version of the bosonization.

3.3 Bosonization for the Boundary Problem

In the previous section I presented the bosonization for an infinite system with translational invariance. In the present section I will discuss bosonization in the case of a boundary. An immediate observation is that the translational invariance is broken and left- and right-moving fields are not independent anymore. Thus there is a need to suitably modify the bosonization procedure.

We consider an interacting electron liquid on a semi-infinite line, $x \geq 0$, subject to an open boundary condition (OBC) at the end $x = 0$. Following standard Luttinger-liquid approach discussed in the previous section, we linearize the spectrum and decompose the electron field Ψ_σ into left- (L) and right- (R) moving chiral fermions at the two Fermi points $\pm k_F$,

$$\Psi_\sigma(x) = e^{-ik_F x}\psi_{L\sigma}(x) + e^{ik_F x}\psi_{R\sigma}(x). \tag{3.51}$$

Imposing an open *(Dirichlet)* boundary condition at a "ghost position" $x = -a$,

$$\Psi_\sigma(-a) = e^{ik_F a}\psi_{L\sigma}(-a) + e^{-ik_F a}\psi_{R\sigma}(-a) = 0, \tag{3.52}$$

and assuming that the chiral fermions are slowly varying on the scale of a, it follows that

$$\psi_{R\sigma}(0) = e^{i\gamma}\psi_{L\sigma}(0), \tag{3.53}$$

where $\gamma = \pi + 2k_F a = \pi(1 + n_e)$, with n_e the filling factor ($n_e = 1$ for a half-filled band). Although not essential here, the "softening" of the boundary – implied by imposing the Dirichlet condition at $x = -a$ – is sometimes useful for modeling the

dependence of the scattering phase shift γ on the shape of an edge- or impurity-potential. Using Eq. (3.53) to analytically continue to negative coordinates, the right-movers may be represented by left-movers as

$$\psi_{R\sigma}(x) = e^{i\gamma}\psi_{L\sigma}(-x), \quad x > 0. \tag{3.54}$$

We can then express the boundary problem in left-moving fermions only, now taking values on the full line $-\infty < x < \infty$. At this point we can use the standard bosonization presented in the Sec. 3.2 provided that the interactions can be absorbed in the free bosonic Hamiltonian.

To bosonize the interaction terms Eq. (3.9) - (3.14) I closely follow the route given in [54, 55]. Writing the interaction in left-moving fields only makes the interacting Hamiltonian nonlocal. Dispersive and forward scattering, although non-local now, are still quadratic in the currents and can be readily diagonalized. As for backscattering a renormalization group analysis can be applied as in the translationally invariant system. It can be shown that for $K_s > 1$ backscattering is irrelevant, and that for an SU(2) invariant system K_s reaches the fixed point value $K_s = 1$ as for the translationally invariant system. Thus the problem is reduced to simply unfolding the semi-infinite system to an infinite one to which I shall return in a moment.

Using the standard bosonization formulas given in Sec. 3.2 for the semi-infinite system we write the left- and right-moving fermion fields as coherent superpositions of free bosonic charge and spin fields, $\phi_{rc} = (\phi_{r\uparrow}+\phi_{r\downarrow})/\sqrt{2}$ and $\phi_{rs} = (\phi_{r\uparrow}-\phi_{r\downarrow})/\sqrt{2}$, with $r = L, R$:

$$\begin{aligned}
\psi_{L\sigma}(t,x) &= \frac{\eta_{L\sigma}}{\sqrt{2\pi\alpha}} \exp\left(-i\sqrt{2\pi}(\cosh\theta\ \phi_{Lc}(x,t) + \sinh\theta\ \phi_{Rc}(x,t) + \sigma\phi_{Ls}(x,t))\right) \\
\psi_{R\sigma}(t,x) &= \frac{\eta_{R\sigma}}{\sqrt{2\pi\alpha}} \exp\left(i\sqrt{2\pi}(\cosh\theta\ \phi_{Rc}(x,t) + \sinh\theta\ \phi_{Lc}(x,t) + \sigma\phi_{Rs}(x,t))\right)
\end{aligned} \tag{3.55}$$

The Hamiltonian density is then given by:

$$\mathcal{H} = \sum_{j=c,s} \frac{v_j}{2}\left((\partial_x\phi_{Lj})^2 + (\partial_x\phi_{Rj})^2\right). \tag{3.56}$$

To make progress we analytically continue the charge ϕ_{Lc} and spin ϕ_{Ls} boson fields in (3.55) to $x < 0$ such that the boundary condition in Eq. (3.53) is satisfied:

$$\begin{aligned}
\phi_{Lc}(t,-x) &= -\phi_{Rc}(t,x) + \frac{\gamma}{\sqrt{2\pi K_c}} \\
\phi_{Ls}(t,-x) &= -\phi_{Rs}(t,x), \quad x > 0.
\end{aligned} \tag{3.57}$$

Using (3.57) in the bosonization formulas (3.55) we can write

$$\begin{aligned}
\psi_{L\sigma}(t,x) = \frac{e^{i\gamma(1-K_c)/2K_c}\eta_{L\sigma}}{\sqrt{2\pi\alpha}} \exp(\ &- i\sqrt{2\pi}(\cosh\theta\phi_{Lc}(t,x) - \sinh\theta\phi_{Lc}(t,-x) \\
&+ \sigma\phi_{Ls}(t,x))).
\end{aligned} \tag{3.58}$$

The logic of the construction just sketched is strictly valid only for a translational invariant system where all interaction processes can be classified into dispersive,

forward, backward, or umklapp scattering (see Fig. 3.4). For a system with an open boundary, translational invariance is broken and a two-particle interaction leads to additional scattering processes. As shown by V. Meden and co-workers [56], however, the theory in Eq. (3.56) still captures the universal low-energy physics. Perturbative arguments suggest that the energy range where it applies increases with the range of the interaction of the original microscopic theory. Whether in a particular application the energy range will be sufficiently large so as to observe Luttinger liquid behavior can probably only be answered by experiments.

3.4 Bosonization for SWCNTs

We shall see in this section that the formalism described in Sec. 3.2 can be adapted so as to apply to an armchair SWCNT in the *Luttinger liquid regime* [57]. This is the regime where the temperature is above 0.1 - 1 K (depending on the range of the effective Coulomb interaction in the tube), and at which backscattering becomes irrelevant. In this case the low-energy electronic properties of a metallic SWCNT are expected to be well described as a Luttinger liquid with an additional channel index [58, 59].

Let us first briefly review how the notion of a Luttinger liquid arises in the description of the metallic SWCNTs. As was realized early on, their unusual electronic properties originate in the special band structure of π electrons in graphite [60]. For the case that we choose to study here, an (n, n) "armchair" tube[1], the dispersion relation is gapless precisely at the corners of the hexagonal first Brillouin zone, implying that there are only two independent Fermi points $\pm\mathbf{K} = (\pm k_F, 0)$ (see Fig. 3.6). Moreover, at low energies electron modes encircling the waist of the tube can be neglected as they are energetically costly ($\sim \mathcal{O}(1\text{ eV})$), and one is left with a one-dimensional situation where electrons move only along the direction x of the tube (with y the transverse direction), and with a dispersion that is approximately linear (all the way up to 1 eV). A low-energy expression for the electron field can thus be written as

$$\Psi_\sigma(x, y) = \sum_{p,\alpha} \chi_{p\alpha}(x, y)\psi_{p\alpha\sigma}(x), \tag{3.59}$$

where $\chi_{p\alpha}(x, y) \sim f(y)\mathrm{e}^{-i\alpha k_F x}$ are Bloch functions defined separately on each sublattice $p = \pm$ of the 2D graphite honeycomb lattice (such that they vanish on the other), with $\psi_{p\alpha\sigma}(x)$ the corresponding 1D fermion operators. The index $\alpha = \pm$ labels the two Fermi points, and $\sigma = \uparrow, \downarrow$ is the usual spin index. To make contact with standard LL theory one passes to a chiral fermion basis, trading the sublattice fields $\psi_{p\alpha\sigma}(x)$ for left (L) and right (R) movers $\tilde{\psi}_{r\alpha\sigma}(x), r = L, R$:

$$\psi_{p\alpha\sigma}(x) = \tilde{u}_{Lp}\mathrm{e}^{-iq_F x}\tilde{\psi}_{L\alpha\sigma}(x) + \tilde{u}_{Rp}\mathrm{e}^{iq_F x}\tilde{\psi}_{R\alpha\sigma}(x). \tag{3.60}$$

Here $\tilde{u}_{L+} = \tilde{u}_{L-} = 1$ and $\tilde{u}_{R+} = -\tilde{u}_{R-} = i$, and q_F is an "effective" Fermi momentum measured with respect to the Fermi points $\pm k_F$ of the two channels.

[1] The index n measures the circumference of the tube in units of the graphene periodicity.

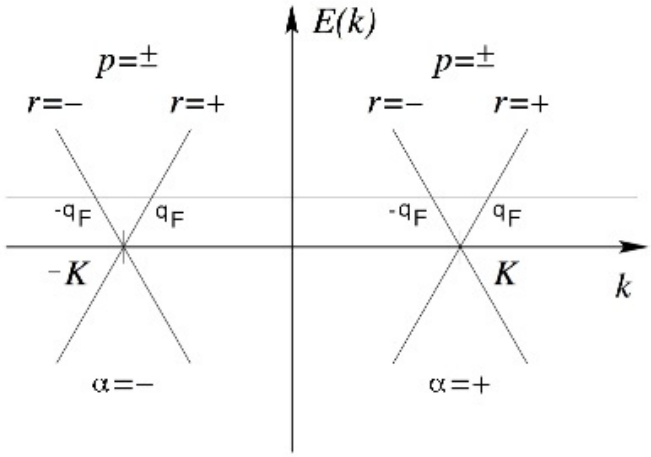

Figure 3.6: Low-energy band structure of the metallic armchair SWNT. Electron operators at different Fermi points labeled by $\alpha = \pm$, and sublattices $p = \pm$ combine to build right and left movers ($r = \pm$).

In analogy with standard LL theory, it is convenient to introduce a basis of total and relative ($\delta = \pm$) charge ($j = c$) and spin ($j = s$) chiral boson fields $\phi_{rj\delta}$ ($r = L, R$):

$$\begin{aligned}
\phi_{rc+} &= \frac{1}{4\pi}\sum_{\alpha,\sigma}\phi_{r\alpha\sigma} \\
\phi_{rc-} &= \frac{1}{4\pi}\sum_{\alpha\sigma}\alpha\phi_{r\alpha\sigma} \\
\phi_{rs+} &= \frac{1}{4\pi}\sum_{\alpha\sigma}\sigma\phi_{r\alpha\sigma} \\
\phi_{rs-} &= \frac{1}{4\pi}\sum_{\alpha,\sigma}\alpha\sigma\phi_{r\alpha\sigma}
\end{aligned} \tag{3.61}$$

and write the bosonization formula

$$\begin{aligned}
\tilde{\psi}_{L\alpha\sigma} = \frac{\eta_{L\alpha\sigma}}{\sqrt{2\pi\alpha}}\exp(-i\sqrt{\pi}[&\cosh\theta\phi_{Lc+}(x) + \sinh\theta\phi_{Rc+}(x) \\
&+ \alpha\phi_{Lc-}(x) + \sigma\phi_{Ls+}(x) + \alpha\sigma\phi_{Ls-}(x)]),
\end{aligned} \tag{3.62}$$

(with $\tilde{\psi}_{R\alpha\sigma}$ obtained by taking the complex conjugate of the right-hand-side of Eq. (3.62) and switching $L \leftrightarrow R$).

As shown via an RG analysis in Ref. [57], at finite temperatures and sufficiently large values of the index n, only forward scattering of electrons in the tube are

important. It follows that for this case the effective low-energy Hamiltonian density is given by

$$\mathcal{H} = \sum_{\substack{j=c,s \\ \delta=\pm}} \frac{v_{j\delta}}{2} \left((\partial_x \phi_{Lj\delta})^2 + (\partial_x \phi_{Rj\delta})^2 \right), \tag{3.63}$$

i.e. two copies of the standard LL Hamiltonian in (3.56). Since the Coulomb interaction couples only to the total charge density, only the interaction parameter K_{c+} takes a value different from unity:

$$K_{c+} = (1 + 4\tilde{V}_0(q \approx 0)/\pi v_F)^{-1/2} \leq 1 \tag{3.64}$$

with $\tilde{V}_0(q \approx 0)$ the strength of the Coulomb interaction at small momentum transfer. The velocities of the different modes in (3.63) are given by $v_{j\delta} \approx v_F/K_{j\delta}$.

We now consider a semi-infinite tube $x \geq 0$. Imposing an OBC for the electron fields Ψ_σ at $x = -a$, and assuming that the chiral fermions are slowly varying on the scale of a, it follows that

$$\tilde{\psi}_{R\alpha\sigma}(t, 0) = \mathrm{e}^{i\tilde{\gamma}} \tilde{\psi}_{L\alpha\sigma}(t, 0), \tag{3.65}$$

where $\tilde{\gamma} = \pi + 2q_F a$. Following the procedure from Sec. 3.3, we continue analytically to negative coordinates, and use (3.65) to represent the right-moving fermions by left-moving fermions at $x < 0$.

With the OBC in (3.65) and the bosonization formula (3.62) we can continue the bosonic fields to negative coordinates, and express the theory in left-moving fields only. The modified bosonization formula is then written as

$$\tilde{\psi}_{L\alpha\sigma} = \frac{\mathrm{e}^{i\tilde{\gamma}(1-K_{c+})/2K_{c+}} \eta_{L\alpha\sigma}}{\sqrt{2\pi\alpha}} \exp(-i\sqrt{\pi}[\cosh\theta\phi_{Lc+}(x) - \sinh\theta\phi_{Lc+}(-x) + \alpha\phi_{Lc-}(x) + \sigma\phi_{Ls+}(x) + \alpha\sigma\phi_{Ls-}(x)]). \tag{3.66}$$

3.5 Bosonization in the Strong-Coupling Regime

Here I will discuss the bosonization in the strong-coupling regime (where interactions are much stronger than the kinetic energy), for which the applicability of the above procedure is not immediately obvious. A strongly interacting scenario can be realized for a low-density system. For zero temperature the energy of an electron can be estimated by the Fermi energy $E_F = (\pi\hbar n)^2/8m$. For low densities $n \ll a_B^{-1}$ the kinetic energy is small compared to the Coulomb potential energy $e^2 n/\epsilon$. Here ϵ is the dielectric constant and $a_B = \epsilon\hbar^2/me^2$ is the effective Bohr radius of the material. In the limit of low densities the system is driven to the *Wigner crystal* [61, 62] regime, which can be viewed (in a classical picture) as a system of electrons placed equidistantly in order to minimize the potential energy. Quantum fluctuations induce an exponentially small antiferromagnetic spin exchange $J > 0$ between the electrons. In the extreme case where $J \ll E_F$ is the smallest energy scale in the system, the behavior becomes that of the so called *spin incoherent* [63, 64, 65] regime. Here we take $J \to 0$ limit before $T \to 0$ limit. Conventional order of

limits, i.e. taking the $T \to 0$ limit first, leads to very different physics. For nonzero temperatures spin incoherent regime can be realized in the following limit $J \ll T \ll E_F$.

For such strong interactions that favor a Wigner crystal structure it is not clear that a Luttinger liquid picture is applicable. Since the electrons are localized at the lattice sites of the Wigner crystal, the procedure of linearization of the spectrum around the Fermi momenta $\pm k_F$ and the expansion of the electron field in left- and right-movers (see Eq. (3.2)) is not justified. Despite this one can show that a bosonic Hamiltonian similar to that in Eq. (3.37) correctly describes the low-energy properties of a 1D Wigner crystal [66]. To see how, we again turn to the classical picture and describe a 1D Wigner crystal as a system of electrons vibrating around their equilibrium positions. This is very similar to the classical description of phonons as lattice vibrations. For low-energies (long-wavelength limit) the vibrations can be described by elasticity theory. The energy of the system can be written as

$$H = \int dx \left[\frac{p^2}{2mn} + \frac{1}{2} mns^2 (\partial_x u)^2 \right], \tag{3.67}$$

where $u(x)$ is the displacement of the medium and $p(x)$ is the momentum density. Density fluctuations are given by $\delta n = -n\partial_x u$, and s plays the role of the speed of density waves.

The classical Hamiltonian describing the 1D Wigner crystal (3.67) can be straightforwardly quantized by imposing canonical commutations relation between $u(x)$ and $p(x)$,

$$[u(x), p(x')] = i\delta(x - x'). \tag{3.68}$$

The resulting quantum Hamiltonian describes the propagation of density fluctuation in the Wigner crystal, which is similar to the bosonic Hamiltonian in Eq. (3.37). Comparing the commutation relations in Eqs. (3.68) and (3.17) we introduce a bosonic field φ_c and its conjugate momentum $\Pi_c(x)$ by the following identification

$$u(x) \equiv -\frac{\sqrt{2}}{\sqrt{\pi} n} \varphi_c(x), \qquad p(x) \equiv -\frac{\sqrt{\pi} n}{\sqrt{2}} \Pi_c(x), \tag{3.69}$$

by use of which the density fluctuation acquires the standard Luttinger liquid form $\delta n = (\sqrt{2/\pi})\partial_x \varphi_c$.

Using (3.69) the Hamiltonian can straightforwardly be written as

$$H = \frac{v_c}{2} \int dx \left[K_c \Pi_c^2 + \frac{1}{K_c} (\partial_x \varphi_c)^2 \right]. \tag{3.70}$$

Here

$$v_c = s \qquad K_c = \frac{v_F}{s}, \tag{3.71}$$

where $v_F = \pi n/2m$ is the Fermi velocity for non-interacting electrons with spin.

Thus, we have managed to write the Hamiltonian for a 1D Wigner crystal in the bosonized form even though we did not know the bosonization formula which connects electron and boson fields. Now I shall present how to derive the "effective"

bosonization formula which achieves this goal. The procedure, which is presented in **Paper IV**, is a kind of a "reverse engineering". First we observe that in the $J \to 0$ limit electrons behave like *spinless* fermionic particle, i.e. only charge degrees of freedom survive and spin degrees of freedom just define the huge degeneracy of the ground state. Then we can simply omit the spin index and write

$$\Psi(x) = \psi_L(x) + \psi_R(x), \tag{3.72}$$

where $\psi_L(x)$ ($\psi_R(x)$) is the part of the electron operator that contains negative (positive) momenta.

In analogy with bosonization in the case of spinless fermions, we can write an "effective" bosonization formula in the long wavelength regime:

$$\psi_r(x) \approx \frac{1}{\sqrt{2\pi\alpha}} e^{ir\tilde{k}_F x} e^{ri\sqrt{\lambda}\phi_{cr}(x)}, \tag{3.73}$$

where $\tilde{k}_F$ and λ can be determined by demanding that the density operator ρ takes the form

$$\rho = \Psi^\dagger(x)\Psi(x) = n + (\sqrt{2/\pi})\partial_x\varphi_c. \tag{3.74}$$

By calculating the density using Eq. (3.73) and comparing the obtained result to Eq. (3.74) we find that

$$\tilde{k}_F = \pi n, \qquad \lambda = 8\pi. \tag{3.75}$$

The doubling of the Fermi momentum is in agreement with our description of spinless fermions, since now only single fermion can occupy a given momentum state. We can see that in this formulation the "noninteracting" case corresponds to $K_c = 1/2$ and describes free spinless fermions. In this novel bosonization scheme interactions are absorbed in two stages: Local interactions are incorporated in the "effective" noninteracting Hamiltonian and long-range interactions define the value of K_c. To see this we note that for a delta function interaction the description as noninteracting spinless fermions is exact and $K_c = 1/2$.

To obtain a more conventional description (with the noninteracting case corresponding to $K = 1$) we define a bosonic field $\varphi = \sqrt{2}\varphi_c$. Then the bosonization formula and the Hamiltonian take the form

$$\psi_r(x) \approx \frac{1}{\sqrt{2\pi\alpha}} e^{ir\tilde{k}_F x} e^{ri\sqrt{4\pi}\phi_r(x)}, \tag{3.76}$$

and

$$H = \frac{v_c}{2} \int dx \left[K\Pi^2 + \frac{1}{K}(\partial_x\varphi)^2 \right], \tag{3.77}$$

where $K = 2Kc = 2v_F/s = \tilde{v}_F/s$, in agreement with the doubling of the Fermi momentum $\tilde{k}_F$.

Given the formalism developed above, we can easily adapt it to the case of an electron system with an open boundary condition, in exact analogy with the procedure outlined in the previous section. In particular, the bosonization formula now reads:

$$\psi_L(x) \approx \frac{1}{\sqrt{2\pi\alpha}} e^{-i\tilde{k}_F x} e^{-i\sqrt{4\pi}(\cosh(\vartheta)\tilde{\phi}_L(x) - \sinh(\vartheta)\tilde{\phi}_L(-x))}. \tag{3.78}$$

3.6 Important Properties of Luttinger Liquids

In this section I present some important properties of Luttinger liquids, exhibiting Fermi as well as non-Fermi liquid characteristics. Starting with the low-temperature *thermodynamics*, it is straightforward to derive the *specific heat*, *magnetic susceptibility* and *compressibility*, given the free bosonic Hamiltonian that describes the Luttinger liquid [61].

The specific heat C has the form

$$C = \frac{1}{2}\left(\frac{v_F}{v_c} + \frac{v_F}{v_s}\right)\gamma_0 T, \tag{3.79}$$

where γ_0 is the specific heat coefficient for a noninteracting system with Fermi velocity v_F. The susceptibility and compressibility are also easy to obtain and have the form

$$\chi = \frac{v_F}{v_s}\chi_0 \quad \text{and} \quad \kappa = \frac{v_F K_c}{v_c}\kappa_0, \tag{3.80}$$

respectively, where χ_0 and κ_0 are the noninteracting values.

From the above expressions, the Wilson ratio is

$$R_W = \frac{\chi/\chi_0}{\gamma/\gamma_0} = \frac{2v_c}{v_c + v_s} \tag{3.81}$$

and given by a non-universal interaction-dependent quantity.

As we see, the thermodynamic properties show Fermi liquid behavior (only the coefficients get modified by non-universal expressions). However the system is a non-Fermi liquid as becomes evident when going beyond thermodynamics.

With the use of the bosonization formula (3.28) it is possible to calculate any correlation function. Then within linear response theory it is possible to investigate essentially all properties of the model. Here I will try to discuss those which are particularly important.

The absence of quasiparticles manifests itself in the *spectral function* $\rho(k,\omega)$, which is proportional to the imaginary part of the retarded Green's function

$$G^R(x,t;0,0) = -i\Theta(t)\langle\{\psi_\sigma(x,t),\psi_\sigma^\dagger(0,0)\}\rangle. \tag{3.82}$$

In Fig. 3.7 we see the spin-charge separation manifested in the double-peak structure of the spectral function. The absence of quasiparticles is apparent from the gap between positive and negative energy structures.

From the spectral function $\rho(k,\omega)$ the *momentum distribution function* $n(k)$ can be derived and is given by

$$n(k) = \frac{1}{2} - \text{const.} \times \text{sign}(k-k_F)|k-k_F|^\alpha - \text{const.} \times (k-k_F), \tag{3.83}$$

where $\alpha = (K_c + 1/K_c - 2)/4$. For the Luttinger liquid $n(k)$ is a continuous function in contrast to the Fermi liquid case, where $n(k)$ has a discontinuity at the chemical potential at zero temperature. The absence of a jump is a manifestation of the nonexistence of fermionic quasiparticles.

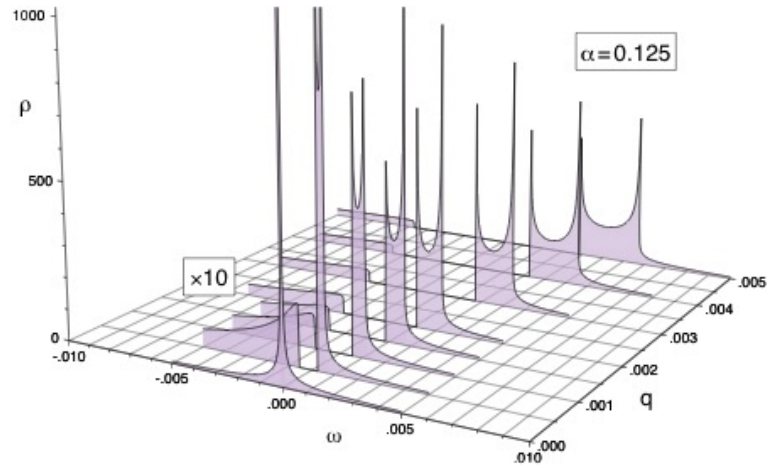

Figure 3.7: Spin-charge separation seen in the spectral function. The positions of the peaks and edges are determined by spin and charge velocities, $v_s < v_c$. Taken from the Ref. [67]

.

The *integrated spectral density* (density of states)

$$N(\omega) = \int_{-\infty}^{\infty} dk \rho(k, \omega) \tag{3.84}$$

shows scaling behavior $N(\omega) \propto |\omega|^{\alpha}$ at energies near the Fermi energy, while it would be constant ($\alpha = 0$) for a 1D Fermi liquid (if it existed!). This suppression of the integrated spectral density manifests itself in a suppressed rate of single-electron tunneling into a Luttinger liquid.

I should note that above properties are generic to *any marginal* theory, to which Luttinger liquids also belong. All the terms of the Luttinger liquid Hamiltonian are marginal, thus having scaling dimension $\Delta = 2$ (for (1+1)D case). The critical theory of such models is characterized by a line of fixed points, which gets parametrized by the parameters of the Hamiltonian. For the marginal theory coefficients and exponents of the observables continuously depend on non-universal quantity (K_c in the Luttinger liquid case).

3.7 Experimental Evidence for Luttinger Liquid Behavior

Here I will briefly discuss systems where experimentally observed non-Fermi liquid behavior has been argued to be a manifestation of Luttinger liquid behavior. These systems are *quasi one-dimensional conductors*, *fractional quantum Hall edge states*, *quantum wires* and *carbon nanotubes*, where in all cases the electron motion is effectively one-dimensional.

3.7.1 Quasi One-Dimensional Conductors

Good candidates for observing Luttinger liquid behavior are *quasi one-dimensional organic and inorganic conductors* [67]. In these systems the strong anisotropy makes the electron motion one-dimensional.

Well-studied representatives of organic quasi one-dimensional conductors are the *Bechgaard salts*. Their generic formula is $(TM)_2X$, where TM is a flat molecule that donates electrons and X is a negative ion that supplies a hole. TM is usually $TMTSF$ (*tetramethyl-tetraselenafulvalene*), or a similar molecule $TMTTF$ that contains sulphur instead of selenium. X is typically PF_6^- (*hexafluorophosphate*), ClO_4^- (*perchlorate*) or a similar anion. These molecules naturally stack in 1D structures with two TM molecules and one X ion per unit cell. The overlap between the electron clouds of neighboring molecules in the stacking direction is much larger than that between the stacks. At low temperatures ($\sim 20K$), true long-range order is able to develop because there is always some nonzero coupling between the stacks. Bechgaard salts exhibit a variety of orders and may show spin-Pierls, antiferromagnetic and even superconducting behaviors depending on the negative ion X [68]. However, at higher temperatures – where the coupling between the stacks is washed out by thermal fluctuations – the Bechgaard salts become truly 1D.

Photoemission (PES) [69] and nuclear magnetic resonance (NMR) [70] experiments on $(TMTSF)_2PF_6$ give circumstantial evidence for Luttinger liquid behavior. PES experiments show an anomalous low density of states near the Fermi level, scaling as $|\omega|^\alpha$ (with a nonzero α, in contrast to a 1D Fermi liquid which has a constant density of states). The NMR experiments have shown signals of spin-charge separation. The nuclear spin-lattice relaxation rate, $\mathcal{T}_1$ – which probes electron spin correlations at low temperature – varies as $\mathcal{T}_1 \sim T^{K_c}$. In the Fermi liquid limit $K_c = 1$, while for a Luttinger liquid $K_c < 1$ (repulsive interaction). From NMR experiments one deduces that $K_c \sim 0.15$, implying that $\alpha \sim 1.25$, in agreement with the PES experiments. One should note that the value of K_c is too small to be consistent with the standard theoretical predictions based on the Hubbard model, where the minimal value for K_c is $1/2$ and is achieved in the infinite interaction limit. However, in Ref. [71] it was shown that the presence of impurities or defects may substantially increase the effective values of K_c so as to get closer to the experimental data.

Several photoemission experiments have also been carried out on inorganic quasi one-dimensional metals such as $(TaSe_4)_2I$ and $BaVS_3$. Both angle-resolved photoemission (ARPES) experiments [72, 73] and angle-integrated photoemission (PES) experiments [74] support the conclusion that the very low density of states near the Fermi level is due to 1D electron correlations.

3.7.2 Fractional Quantum Hall Edge States

The prime candidates for observing Luttinger liquid behavior are the *edge states* of *fractional quantum Hall* liquid [75]. In the classical Hall effect, electrons moving in a magnetic field produce a transverse (to the current) potential difference V. In the quantum case the transverse resistance V/I exhibits plateaus as the magnetic field

is varied. These plateaus appear for particular filling factors ν, with the resistance having the values $h/\nu e^2$. The filling factor ν has integer values for the *integer effect* (IQHE) and fractional values for the *fractional effect* (FQHE).

IQHE edge states are described as one-dimensional *chiral* Fermi liquids [76], where the chirality is due to the skipping Landau orbits at the boundaries of a sample, with opposite directions for opposite edges. Due to the spatial separation between left and right moving excitations, *backscattering* from impurities or other electrons is suppressed. In contrast, FQHE edge states are described by *chiral* Luttinger liquids [77] due to the strong electron correlations, with Luttinger liquid interaction parameter $K = \nu$ (for filling fractions with only single edge mode).

Experiments on tunneling between edge states of the FQHE ($\nu = 1/3$) [78], and between 3D metal and edge states [79, 80] show a nontrivial power-law behavior of the tunneling conductance as a function of voltage and temperature. Even though the observed exponents are quite close to those predicted by Luttinger liquid theory [81, 82, 83], there are strong indications that the behavior is not universal (for a review see [84]). It was observed [85] that if one changes the magnetic field B slightly away from the center of the $\nu = 1/3$ plateau, but still staying on the plateau, the edge exponent varies linearly with B, rather than being locked to the bulk filling fraction (as one would expect from the theory). In addition, recent theoretical studies (see Ref. [86] and references therein) indicate that the behavior is not universal, thus it is not defined by the bulk only. It is shown that details of interactions and the edge potential, which can lead to edge reconstruction, are important for reconciling theory and experiment.

3.7.3 Quantum Wires

Natural candidates for one-dimensional electron systems are *quantum wires*. Quantum wires can be made either by gating a two dimensional electron gas formed at the *inversion layers of heterostructures* (e.g. at the interface of $GaAs$ and $AlGaAs$ [87]) or by *cleaved-edge overgrowth technique* [88]. In both cases electrons flow in a very narrow channel, leading to discrete transverse modes and effectively one dimensional electron transport (in a single-mode wire). One should note, however, that generally it is hard to fabricate wires sufficiently free from impurities that the backscattering does not destroy the collective modes.

Typical experiments on quantum wires measure a direct-current conductance. If the transport is ballistic with noninteracting electrons, the zero-temperature conductance is predicted to have a value in multiples of a universal quantity $G_Q = 2e^2/h$. In quantum wire experiments smaller values of G_Q are measured for low temperatures [89, 90]. At first glance the experiments appear to be in agreement with theory [83, 91, 92], but only if the wire is modeled to be infinitely long. Other groups theoretically showed [93, 94, 95] that transport is ballistic in *finite* (but clean) wires coupled to 3D leads. Unambiguous interpretations of experiments here face a great difficulty because it is hard to estimate how impurities and contacts with leads [96, 97] influence the results. In some cases it is even unclear whether properties of the 1D wire or the 3D leads are measured.

In experiments on $GaAs/AlGaAs$ [98] and $InSb$ [99] nanowires, power-law scaling of the conductance with temperature, and current with voltage is observed. These observations have been interpreted as Luttinger liquid behavior. In the experiment on momentum resolved tunneling between quantum wires [100] signatures of Luttinger liquid behavior are also observed. Very Recent experiments on polymer nanofibers [101], Niobium Selenide ($NbSe_3$) [102] and Molybdenum Selenide ($MoSe$) [103] nanowires also report Luttinger liquid like power law scaling of the conductance with temperature and voltage, but it is still under debate whether Luttinger liquid, Wigner Crystal or Environmental Coulomb Blockade Theory is the correct description.

3.7.4 Carbon Nanotubes

Carbon nanotubes are relatively newly discovered systems [104], where the low-temperature physics is predicted [105, 58, 57] to be governed by Luttinger liquid theory.

A single-walled carbon nanotube (SWCNT) is a rolled-up graphene sheet in a cylindrical structure, the diameter of which may be only a few nanometers, with a length up to several micrometers (for a review see Ref. [60, 106]). The properties of SWCNTs are fully described by two numbers (n, m), specifying the circumferential vector in an unrolled graphene sheet. The (n, m) numbers define whether a particular tube is a metal or a semiconductor. The remarkable electronic properties of carbon nanotubes are due to the special band structure of the π orbitals in graphite. The electron wavelength around the circumference of a nanotube is quantized due to the periodic boundary conditions, leading to discrete wavelengths. Because of the quantization of circumferential modes, the electronic states of the nanotube split into one-dimensional subbands. For SWCNTs, these subbands are separated on the scale of $1eV$. In metallic nanotubes only two subbands cross the Fermi energy. So even at room temperature metallic SWCNTs can be regarded as one-dimensional quantum wires.

Two independent transport experiments – one on individual SWCNTs [107], and the other on SWCNT bundles [108] – showed that SWCNTs behave like quantum wires, with effectively one-dimensional electron dynamics. Experiments on the electronic structure of nanotubes [109, 110] also showed the same behavior.

The low-temperature band structure of a metallic armchair SWCNT is shown in Fig. 3.6. The Fermi surface consists of two Fermi points $\pm\boldsymbol{K}$. Since the basis of the graphite consists of two atoms, there are two subbands in the system, with degenerate states at the Fermi points. Near the Fermi points the spectrum is linear.

The microscopic models of metallic armchair SWCNTs based on the Hubbard model [59] and the extended Hubbard model [111] predict that they become Mott insulators at half-filling. Away from half-filling (which can be realized e.g. by doping from gate electrodes or a substrate) R. Egger and A.O. Gogolin [58, 57] theoretically predicted that the low-temperature behavior of armchair nanotubes is described by Luttinger liquid theory.

Experimental work [112] of S.J. Tans and co-workers on transport properties of

individual SWCNTs showed the importance of electron correlations in this system. M. Bockrath and co-workers [113] showed that the conductance and the differential conductance scale as power laws with respect to temperature and bias voltage, respectively. By comparison to the theoretical prediction in Ref. [58, 57] they made the conclusion that it is a sign of Luttinger liquid behavior. Recent STM (scanning tunneling spectroscopy) experiment by J. Lee and co-workers [114] on SWCNT with a boundary provides a direct evidence for Luttinger liquid behavior. By measuring the standing waves due to the boundary, spin-charge separation as well as suppression of the density of states near the Fermi level was observed. However, as for the conjectures of Luttinger liquid behavior of the other systems discussed in this section, the above interpretations remain somewhat controversial.

4

Unified View for Critical Systems - Conformal Field Theory

One-dimensional quantum statistical physics models have a critical point at $T = 0$, which is called a *quantum critical point*. As the correlation length diverges at the critical point the system becomes scale invariant and *scaling operators* (e.g. the order parameter) show power-law behavior at low temperatures (near the critical point). It is known that 1D quantum statistics is equivalent to 2D classical statistics. So near the critical point we can define a corresponding (1+1)D Euclidean field theory model (giving a "coarse grained" description) which is invariant under *conformal transformations* and which is usually called a *conformal field theory* model (identifying one of the dimensions, usually an inverse temperature, as "time"). In this chapter we will briefly discuss the basic formalism of conformal invariance and its implications on correlation functions of the scaling fields. The interested reader can find a more detailed exposition of the subject in Ref. [52].

4.1 Conformal Invariance and Energy-Momentum Tensor

The *conformal group* is defined as the subgroup of coordinate transformations $\boldsymbol{x} \to \boldsymbol{x'}$ which keeps the metric tensor invariant up to a local scale factor,

$$g'_{\mu\nu}(\boldsymbol{x'}) = \Lambda(\boldsymbol{x}) g_{\mu\nu}(\boldsymbol{x}). \tag{4.1}$$

For an infinitesimal transformation $x^\mu \to x'^\mu = x^\mu + \epsilon^\mu(\boldsymbol{x})$, the metric changes (up to the first order) as follows:

$$g'_{\mu\nu} = \frac{\partial x_\alpha}{\partial x'_\mu} \frac{\partial x_\beta}{\partial x'_\nu} g_{\alpha\beta} = g_{\mu\nu} - (\partial_\mu \epsilon_\nu + \partial_\nu \epsilon_\mu). \tag{4.2}$$

The requirement that the transformation be conformal implies that

$$\partial_\mu \epsilon_\nu + \partial_\nu \epsilon_\mu = f(\boldsymbol{x}) g_{\mu\nu}, \tag{4.3}$$

where $f(\boldsymbol{x})$ is a local scaling factor, which is determined by taking a trace from both sides of Eq. (4.3). If we take $g_{\mu\nu}$ to be a flat Euclidean metric tensor $\eta_{\mu\nu} = diag(1, \ldots, 1)$, then

$$\partial_\mu \epsilon_\nu + \partial_\nu \epsilon_\mu = \frac{2}{D} \boldsymbol{\partial} \cdot \boldsymbol{\epsilon} \; \eta_{\mu\nu}. \tag{4.4}$$

This equation imposes certain constraints on the form of ϵ_μ. If $D \geq 3$, then ϵ_μ can be at most quadratic in coordinates

$$\epsilon_\mu = a_\mu + b_{\mu\nu} x^\nu + c_{\mu\nu\rho} x^\nu x^\rho. \tag{4.5}$$

This generates the following four independent transformations:

- *Translations*, with $\epsilon^\mu = a^\mu$,
- *Rigid rotations*, with $\epsilon^\mu = \omega^\mu_\nu x^\nu$ (ω is antisymmetric),
- *Dilatations*, with $\epsilon^\mu = \lambda x^\mu$,
- *Special conformal transformations*, with $\epsilon^\mu = 2(\boldsymbol{x} \cdot \boldsymbol{b}) x^\mu - b^\mu \boldsymbol{x}^2$.

The case of $D = 2$ deserves special attention. In this case Eq. (4.4) is equivalent to the *Cauchy-Riemann* equations,

$$\partial_1 \epsilon_1 = \partial_2 \epsilon_2 \qquad \partial_1 \epsilon_2 = -\partial_2 \epsilon_1. \tag{4.6}$$

This suggests the use of complex coordinates. It is natural to write $\epsilon \equiv \epsilon(z) = \epsilon^1 + i\epsilon^2$ and $\bar{\epsilon} \equiv \bar{\epsilon}(\bar{z}) = \epsilon^1 - i\epsilon^2$ in coordinates $z, \bar{z} = x^1 \pm i x^2$, with $\partial \equiv \partial_z = \frac{1}{2}(\partial_1 - i\partial_2)$ and $\bar{\partial} \equiv \partial_{\bar{z}} = \frac{1}{2}(\partial_1 + i\partial_2)$, and with the anti-diagonal metric $g_{z\bar{z}} = g_{\bar{z}z} = 1/2$, $g_{zz} = g_{\bar{z}\bar{z}} = 0$. It is useful to regard z and $\bar{z}$ as independent coordinates. In terms of the original coordinates $(x^1, x^2) \in \boldsymbol{\mathcal{R}}^2$, this amounts to taking instead $(x^1, x^2) \in \boldsymbol{\mathcal{C}}^2$, and then the transformation to z, $\bar{z}$ becomes a change of variables. When needed one can impose the condition $\bar{z} = z^*$, which defines the real plane.

We see that $\epsilon(z)$ can be any analytic function, which may not be well-defined everywhere on the complex plane. Thus, it generates only *local* conformal transformations. It is clear that in $D = 2$ we have *infinitely many* generators of conformal symmetry. This property is what enables exact solutions of *two-dimensional* conformal field theories.

A very important quantity is the *energy-momentum tensor* $T^{\mu\nu}$, which is defined through the variation of an action S, caused by a conformal transformation

$$\delta S = \int d^2x T^{\mu\nu} \partial_\mu \epsilon_\nu. \tag{4.7}$$

As the action is invariant under translations, rotations and dilatations this imposes constraints on the energy-momentum tensor. Translational invariance implies $\partial_\mu T^{\mu\nu} = 0$, which means that the energy-momentum tensor is conserved. Rotational invariance implies that the antisymmetric part of $T^{\mu\nu}$ should vanish, and

scale invariance implies that the trace of $T^{\mu\nu}$ should vanish. Summarizing, the energy-momentum tensor is conserved, symmetric and traceless.

In complex coordinates we can define two independent components of the energy momentum tensor

$$T(z) \equiv T_{zz} = T_{11} - T_{22} + 2iT_{12}, \tag{4.8}$$
$$\bar{T}(\bar{z}) \equiv T_{\bar{z}\bar{z}} = T_{11} - T_{22} - 2iT_{12}, \tag{4.9}$$

which satisfy $\partial_{\bar{z}} T(z) = \partial_z \bar{T}(\bar{z}) = 0$.

4.2 Correlation Functions and Operator Product Expansion

In this section we will find out what are the transformation properties of *correlation functions* of a conformal invariant theory. Here I will introduce the so called *primary* fields. Under a conformal transformation $z \to w(z)$, $\bar{z} \to \bar{w}(\bar{z})$ a primary field $\phi(z, \bar{z})$ transforms as

$$\phi'(w, \bar{w}) = \left(\frac{dw}{dz}\right)^{-h} \left(\frac{d\bar{w}}{d\bar{z}}\right)^{-\bar{h}} \phi(z, \bar{z}), \tag{4.10}$$

where $(h, \bar{h})$ are the *conformal dimensions* (or *conformal weights*). A field which satisfies the above property for global conformal transformations, but not for all local conformal transformation is called *quasi-primary*. Fields which are not primary are called *secondary* (a secondary field may or may not be quasi-primary). The energy-momentum tensor is an example of a secondary field, which is quasi-primary.

Let us consider a correlation function of n primary fields. For brevity we will write only the analytic (holomorphic) parts of the expression, since the anti-analytic (antiholomorphic) part has the same behavior. Using a path integral formulation:

$$\langle \phi_1(z_1) \dots \phi_n(z_n) \rangle = \frac{1}{Z} \int [\mathcal{D}\phi]\ \phi_1(z_1) \dots \phi_n(z_n) e^{-S[\phi]}. \tag{4.11}$$

Using the transformation properties (4.10) of primary fields, we find the following transformation rule for correlation functions:

$$\langle \phi_1'(w_1) \dots \phi_n'(w_n) \rangle_{\Gamma'} = \prod_{i=1}^{n} \left(\frac{dw}{dz}\right)_{w=w_i}^{-h_i} \langle \phi_1(z_1) \dots \phi_n(z_n) \rangle_{\Gamma}, \tag{4.12}$$

where Γ and Γ' indicate that the correlation functions are computed in different geometries. The correlation function on the RHS is evaluated in the old geometry, while on the LHS it is evaluated in the new geometry defined by the transformation $z \to w(z)$.

Symmetries of an action impose constraints on the correlation functions, which are known as *Ward identities*. Global conformal transformations impose the follow-

ing constraints on the correlation functions of n quasi-primary or primary fields:

$$\sum_i \partial_{z_i} \langle \phi_1(z_1) \dots \phi_n(z_n) \rangle = 0, \tag{4.13}$$

$$\sum_i (z_i \partial_{z_i} + h_i) \langle \phi_1(z_1) \dots \phi_n(z_n) \rangle = 0, \tag{4.14}$$

$$\sum_i (z_i^2 \partial_{z_i} + 2 z_i h_i) \langle \phi_1(z_1) \dots \phi_n(z_n) \rangle = 0. \tag{4.15}$$

For example, these equations fix the form of two-point functions (in the $\mathcal{C}^2$ geometry) to

$$\langle \phi_i(z_1) \phi_j(z_2) \rangle \sim \frac{\delta_{ij}}{(z_1 - z_2)^{2h_i}}, \tag{4.16}$$

which shows that the correlation function is nonzero only for fields with the same conformal dimensions.

Generally, a product of two fields can be expressed as

$$A(w)B(z) \sim \sum_{n=1}^{N} \frac{[AB]_n(z)}{(w-z)^n}, \tag{4.17}$$

where $N = \textit{integer part}\ (h_A + h_B)$ and $[AB]_n$ is a non-singular field of conformal dimension $h_n = h_A + h_B - n$. This expression is called *operator product expansion* (OPE) and "$\sim$" means "equal up to non-singular terms". It is important to remember that an OPE has meaning only within a correlation function.

We conclude this section by stating the transformation properties of the energy-momentum tensor $T(z)$. As it is a quasi-primary field it transforms as in Eq. (4.10) under global conformal transformations. For the local transformations

$$T'(w) = \left(\frac{dw}{dz}\right)^{-2} \left[T(z) - \frac{c}{12} \{w; z\} \right], \tag{4.18}$$

where c is the so called *central charge* and with $\{w; z\}$ the *Schwarzian derivative*:

$$\{w; z\} = \frac{d^3 w/dz^3}{dw/dz} - \frac{3}{2} \left(\frac{d^2 w/dz^2}{dw/dz} \right)^2. \tag{4.19}$$

4.3 Hilbert Space and Operator Formalism

In this section I will introduce the Hilbert space and operator formalism. The operator formalism in quantum mechanics relies on a choice of a reference frame, as it is not manifestly Lorentz invariant. This choice amounts to choosing the time direction. While the choice is natural in Minkowski space-time, it is somewhat arbitrary in Euclidean space. We are free to choose any direction for time. For a conformal field theory on the complex plane, it is useful to take concentric circles around the origin as the surfaces of constant time. The infinite past corresponds to

the origin and the infinite future to the point at infinity. This scheme is called *radial quantization*.

To define the Hilbert space we should first define a vacuum state $|0\rangle$, which is invariant under global conformal transformations. For an interacting field ϕ, we assume that the Hilbert space is the same as for a free field, except that the energy eigenstates are different (with the interaction switched on adiabatically). An "in" state is defined as an asymptotically free state in the infinite past

$$|\phi_{in}\rangle = \lim_{z,\bar{z}\to 0} \phi(z,\bar{z})|0\rangle. \tag{4.20}$$

The "out" state is defined as the Hermitian conjugate of the "in" state and is the asymptotically free state in the infinite future

$$\langle\phi_{out}| = |\phi_{in}\rangle^\dagger = \lim_{z,\bar{z}\to 0} \langle 0|\phi(z,\bar{z})^\dagger. \tag{4.21}$$

The Hermitian conjugate of a quasi-primary field is defined as

$$\phi(z,\bar{z})^\dagger = \bar{z}^{-2h} z^{-2\bar{h}} \phi(1/\bar{z}, 1/z), \tag{4.22}$$

which corresponds to the a time reversal from infinite past to infinite future.

Here I introduce the *conformal charge* Q_ϵ, connected to a conformal transformation $\epsilon(z)$ as

$$Q_\epsilon = \frac{1}{2\pi i} \oint dz \epsilon(z) T(z). \tag{4.23}$$

One can show that

$$\delta_\epsilon \phi(z) = -[Q_\epsilon, \phi(z)], \tag{4.24}$$

which means that the operator Q_ϵ is the generator of conformal transformations.

Performing the mode expansion of the energy-momentum tensor

$$T(z) = \sum_{n\in\mathbb{Z}} z^{-n-2} L_n, \qquad L_n = \frac{1}{2\pi i} \oint dz z^{n+1} T(z), \tag{4.25}$$

and taking into account the mode expansion of conformal transformations

$$\epsilon(z) = \sum_{n\in\mathbb{Z}} z^{n+1} \epsilon_n, \tag{4.26}$$

one can write

$$Q_\epsilon = \sum_{n\in\mathbb{Z}} \epsilon_n L_n, \tag{4.27}$$

where L_n (and $\bar{L}_n$) are the generators of conformal transformations. Since the infinitesimal form of global conformal transformations (Eq. (4.5)) is a second order polynomial, we can identify L_{-1}, L_0 and L_1 as the generators of such transformations. In particular, the operator $L_0 + \bar{L}_0$ generates the dilatations, which are time translations in radial quantization. Thus, $L_0 + \bar{L}_0$ is proportional to the Hamiltonian of the system.

The generators L_n and $\bar{L}_n$ obey the so called *Virasoro algebra*

$$\begin{aligned} [L_n, L_m] &= (n-m)L_{n+m} + \frac{c}{12}n(n^2-1)\delta_{n+m,0}, \\ [\bar{L}_n, \bar{L}_m] &= (n-m)\bar{L}_{n+m} + \frac{c}{12}n(n^2-1)\delta_{n+m,0}, \\ [L_n, \bar{L}_m] &= 0. \end{aligned} \tag{4.28}$$

To define the representations of the Virasoro algebra, we take L_0 ($\bar{L}_0$) to be diagonal in the representation space. If one requires that the vacuum is invariant under arbitrary conformal transformations, then

$$L_n|0\rangle = 0, \qquad n \geq -1. \tag{4.29}$$

We are interested in the properties of the so called *highest weight* state of the representation $|h, \bar{h}\rangle \equiv \phi(0,0)|0\rangle$. Since the Virasoro algebra decomposes into a direct sum of holomorphic and antiholomorphic parts, we can write $|h, \bar{h}\rangle = |h\rangle \otimes |\bar{h}\rangle$. One can show that

$$\begin{aligned} L_0|h\rangle &= h|h\rangle \\ L_n|h\rangle &= 0, \ n > 0 \\ L_{-n}|h\rangle &\sim |h+n\rangle, \ n > 0. \end{aligned} \tag{4.30}$$

We see that the operators L_{-n} ($n > 0$) act as *raising* operators. So we can write an arbitrary excited state connected to the particular highest weight state $|h\rangle$ as

$$L_{-n_1} L_{-n_2} \dots L_{-n_k}|h\rangle, \quad 1 \leq n_1 \leq n_2 \leq \dots \leq n_k, \tag{4.31}$$

with eigenvalue $h' = h + n_1 + n_2 + \dots + n_k \equiv h + N$. These states are also called *descendants* of $|h\rangle$ and N is called the *level* of the descendant. Conversely, operators L_n ($n > 0$) act as *lowering* operators on descendant states.

Summarizing all above we conclude that the Hilbert space of a conformal field theory is a sum of subsets (called *Verma modules* or *conformal towers*) generated by the highest weight states $|h\rangle$ and their descendants.

In addition to the conformal symmetry, which is connected to space-time properties, conformal field theories may have an additional internal *Lie group* symmetry G (e.g. spin rotational symmetry described in the previous chapter). Since the conformal invariance splits the theory into holomorphic and antiholomorphic sectors, a Lie group symmetry can be extended to a local holomorphic and antiholomorphic symmetry $G(z) \times G(\bar{z})$, a so called *affine symmetry*. There are two conserved currents $J(z) = \sum_{a=1}^{dim(G)} J^a(z)t^a$ and $\bar{J}(\bar{z}) = \sum_{a=1}^{dim(G)} \bar{J}^a(\bar{z})t^a$, which are generators of $G(z)$ and $G(\bar{z})$ respectively (with t^a being the elements of the Lie algebra g of G). The currents satisfy the Kac-Moody algebra, which in terms of mode expanded currents takes the form

$$[J^a_n, J^b_m] = i f_{abc} J^c_{n+m} + kn\delta_{ab}\delta_{n+m,0}, \tag{4.32}$$

where f_{abc} are the *structure constants* ($f_{abc} = \epsilon_{abc}$ in the $SU(2)$ case) of the Lie algebra and k is the *level* of the corresponding Kac-Moody algebra.

The generators of the Virasoro and Kac-Moody algebras satisfy the following commutator

$$[L_n, J^a_m] = -mJ^a_{n+m}. \tag{4.33}$$

Thus, generators of Virasoro and Kac-Moody algebras constitute an extended algebra with commutators given by Eqs. (4.28), (4.32), and (4.33). This algebra again is a *spectrum generating algebra* as in the case of the Virasoro algebra.

A primary field of the affine symmetry is defined as a field which transforms covariantly under $G(z) \times G(\bar{z})$ (in exact analogy with Virasoro primary fields). It can be shown that a Kac-Moody primary field is always a Virasoro primary, but the opposite is not true: A Virasoro primary can be a Kac-Moody descendant.

Also in exact analogy with the previous case, the Hilbert space of a conformal field theory with an affine symmetry is a sum of subsets generated by the highest weight states $|h\rangle$ and their Virasoro and Kac-Moody descendants.

4.4 Boundary Conformal Field Theory

So far we have been discussing conformal field theories on the infinite plane, i.e. infinite systems without boundaries. But many interesting physical problems (e.g. the Kondo model) are strongly influenced by the presence of boundaries. Here I discuss how conformal invariance can be applied to systems with boundaries.

The prototype for a system with a boundary is a system defined on the upper half-plane with some boundary condition on the real axis. Any other geometry can be considered trough a conformal transformation that maps the upper half-plane to the geometry of interest. For the model to be conformal invariant, conformal transformations must map the boundary into itself and preserve the boundary condition, i.e. the boundary must be conformally invariant. The conformal transformations $z \to z + \epsilon(z)$ map the real axis onto itself if and only if $\epsilon(\bar{z}) = \bar{\epsilon}(z)$ (implying that $\epsilon(z)$ must be real on the real axis). This strong constraint reduces the number of the conformal generators by half (but their number is still infinite): the holomorphic and antiholomorphic sectors of the theory are no longer independent. Based on this we can express a correlation function in terms of only holomorphic fields. This can be done by introducing a mirror image of the system, defined on the upper half-plane, to the lower half plane via a parity transformation. An antiholomorphic field $\bar{\phi}_{\bar{h}}(\bar{z})$ (with conformal dimension $\bar{h}$) on the upper half-plane is transformed to a holomorphic field $\phi_{\bar{h}}(z^*)$ (with conformal dimension $\bar{h}$) on the lower half-plane.

It follows that an n-point function in the upper half-plane (UHP)

$$\langle \phi_{h_1,\bar{h}_1}(z_1, \bar{z}_1) \dots \phi_{h_n,\bar{h}_n}(z_n, \bar{z}_n) \rangle_{UHP}, \tag{4.34}$$

can be rewritten as a purely holomorphic 2n-point function in the full plane

$$\langle \phi_{h_1}(z_1)\phi_{\bar{h}_1}(z_1^*) \dots \phi_{h_n}(z_n)\phi_{\bar{h}_n}(z_n^*) \rangle. \tag{4.35}$$

In the *boundary limit*, where the fields in the n-point function are close to the boundary compared to each other, a field $\phi_h(z)$ in the corresponding 2n-point function is close to its mirror image $\phi_{\bar{h}}(z^*)$. For this reason we can replace the product of a field and its mirror image by their OPE

$$\phi_h(z)\phi_{\bar{h}}(z^*) \sim \sum_i \frac{\phi_B^{(i)}(x)}{(z-z^*)^{(h+\bar{h}-h_i)}}, \tag{4.36}$$

where $\phi_B^{(i)}(x)$ is a *boundary operator* (with *boundary conformal dimension* h_i), which lives on the boundary $x \equiv (z+z^*)/2$. It is important to point out that these operators belong to the same operator algebra as the bulk fields. The boundary operator content is fully determined by the particular boundary condition imposed.

To identify boundary conformal dimensions one can exploit a well-known result [115], which relates them to the energy levels in a finite geometry. More explicitly, one considers a conformal field theory defined on the strip $\{w = w_1 + iw_2 \;\; | \;\; -\infty < w_1 < \infty, \;\; 0 \leq w_2 \leq L\}$, with w_1 Euclidean "time" and w_2 the "space" coordinate, and with a conformally invariant boundary condition, A, at the edges $w_2 = 0$ and $w_2 = L$ of the strip. By mapping this theory to the semi-infinite plane $\{z = \tau + ix \;\; | \;\; x \geq 0\}$ (using the conformal transformation $z = \exp(\pi w/L)$ and imposing the boundary condition A at $x = 0$), we can identify the boundary scaling dimension (in the semi-infinite plane) as

$$h_i = \frac{(E_i - E_0)L}{\pi}. \tag{4.37}$$

Here $\{E_i\}$ is the spectrum of energy levels in the strip geometry, which can be computed by a variety of methods, e.g. Bethe Ansatz or exact diagonalization.

To obtain the finite-temperature Green's function one can use a conformal map between zero- and finite-temperature geometries

$$w = \frac{\beta}{\pi} \arctan\left(\frac{\pi}{\beta} z\right), \tag{4.38}$$

which maps the complex plane $\{z = \tau + ix\}$ on which the zero-temperature theory is defined (with $\tau = it$ the Euclidean time) onto an infinite cylinder $\Gamma_j = \{w = \tau' + ix'\}$ of circumference $\beta = 1/T$.

Before concluding this section, let me mention that there exists another description of BCFT based on the notion of *boundary states* [116, 117]. This version of the theory, which in a sense is more fundamental, is particularly useful when studying quantum impurity problems at zero temperature. Since it will not be used here, I refer the interested reader to the literature [118].

5

Kondo and Luttinger Liquid Physics in Nanostructures

The main motivation behind Papers I and II is to understand the interplay between Kondo physics and effects from electron interactions. In particular, we are interested in interaction effects in 1D nanoscale structures, where Luttinger liquid correlations are important. We explore the possibility to observe single- and two-channel Kondo effects in these structures. By studying particular nanostructures one can address this issue and explore the "meeting point" of Kondo and Luttinger liquid physics. Since there are still issues to observe Luttinger Liquid and two-channel Kondo physics (see chapters 2 and 3), there is a need for more experimental and theoretical research. Our proposal in **Papers I** and **II** tries to overcome the limitations and unambiguously answer these questions.

5.1 Setup and a Model

We propose a 1D nanoscale structure which consists of a 1D quantum box side-coupled to a single-mode quantum wire via a point contact (Fig. 5.1). This kind of system could be built from a gated GaAs semiconductor [87] or cleaved edge overgrowth structure [88]. Here we are interested in how the charging of the box is affected by the electron correlations. We define a simple model where this setup can be analyzed in terms of Luttinger liquid and Kondo theories. By varying the external magnetic field one can explore both single- and two-channel Kondo physics. As the charging effects are encoded in the differential capacitance of the quantum box, we analyze its behavior at low temperatures and bias voltages. The fingerprint of Luttinger liquid and Kondo correlations should be possible to identify by charge measurements using the recently developed radio-frequency single electron transistor (RF-SET) electrometer technique [119, 120] (see Fig. 5.2). A SET consists of a small island connected to a source and a drain through small tunnel junctions. It is then

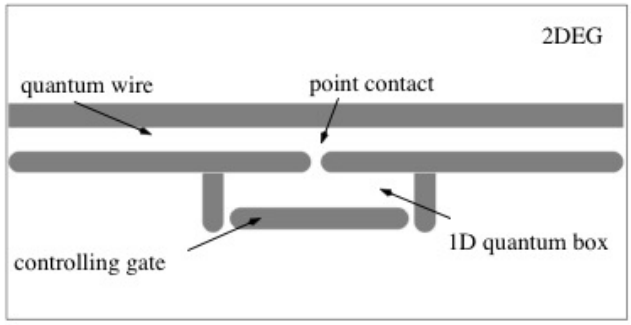

Figure 5.1: Schematic picture of the proposed setup. A 1D quantum box side-coupled to a quantum wire via a point contact. V is a gate voltage.

capacitively coupled to the quantum dot, charge of which is to be measured. This coupling induces a polarization charge on the SET that changes the differential resistance of the circuit. Usually the SET is biased by a dc current, and the drain-to-source voltage is monitored by a voltage amplifier. In the RF-SET realization which is faster and more sensitive, charge is detected by measuring the amplitude modulation of the reflected radio-frequency carrier wave from a resonant circuit containing the SET. There is a way to directly measure the capacitance of the box (which is the SET itself), by integrating it in a resonant circuit and measuring the gate-dependent phase shift of a reflected carrier wave [121].

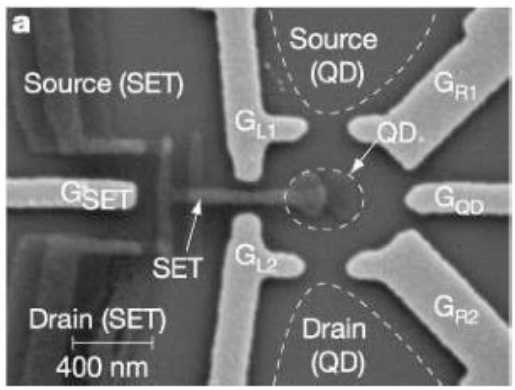

Figure 5.2: Electron micrograph of the RF-SET. Taken from the Ref. [120].

We take the quantum box to be sufficiently small to exhibit Coulomb blockade, but large enough for the electrons in the box to be modeled by a (confined) Luttinger liquid. More precisely, we study the limit $\delta E \ll k_B T_K \ll e^2/2C_\Sigma$, where δE is the average level spacing of the box close to the Fermi level, T_K is the temperature scale

at which the Kondo effect sets in, and $e^2/2C_\Sigma$ is the charging energy of the box (with C_Σ the full capacitance of the box). δE thus serves as a low-energy cutoff restricting the validity of our analysis.

Introducing second-quantized operators $a_{k\mu\alpha}$ for electrons in the wire ($\alpha = 0$) and the box ($\alpha = 1$) with momentum k and spin $\mu = \uparrow, \downarrow$, we model the set-up by the Hamiltonian

$$H = H_0 + H_I + H_C + H_T, \tag{5.1}$$

where

$$H_0 = \sum_{k,\mu,\alpha} \epsilon_k a^\dagger_{k\mu\alpha} a_{k\mu\alpha}, \tag{5.2}$$

$$H_I = \frac{1}{2} \sum_{\substack{\alpha,\alpha' \\ \mu,\mu'}} \sum_{k,k',q} V_{\alpha\alpha'}(q) a^\dagger_{k+q\,\mu\alpha} a^\dagger_{k'-q\,\mu'\alpha'} a_{k'\mu'\alpha'} a_{k\mu\alpha}, \tag{5.3}$$

$$H_C = \frac{Q^2}{2C_\Sigma} + VQ, \tag{5.4}$$

$$H_T = t \sum_{k,k',\mu} (a^\dagger_{k\mu 0} a_{k'\mu 1} + h.c.). \tag{5.5}$$

H_0 in Eq. (5.2) defines the non-interacting Hamiltonian, where we assume that the wire and the box are defined on the same substrate, so the spectrum ϵ_k and the Fermi energies are the same.

The interaction term H_I is written in the most general form, where $V_{\alpha\alpha'}(q)$ is the Fourier transform of the screened interaction potential (with the screening supplied by carriers in nearby gates). For simplicity we take this interaction to be the same *between* wire and box ($\sim V_{01}(q)$) as *in* the wire and the box ($\sim V_{00}(q) = V_{11}(q)$). Since we are interested in the long-wavelength limit $q \to 0$, we approximate the potential with its $q = 0$ value ($V_{01}(0) = V_{00}(0) \equiv g$). This is equivalent to considering the local interaction in coordinate space (cf. the discussion after Eq. (3.7)). In a real device one expects that $V_{01}(0) < V_{00}(0)$. However, as will be seen below, the value of the ratio $V_{01}(0)/V_{00}(0)$ at most influences subleading corrections to the charge fluctuations in the box, and for the purpose of extracting the leading behavior we may put it to unity, yielding a more transparent formalism.

H_C in Eq. (5.4) defines the charging energy. Here Q represents the charge in the box with respect to the (zero bias) Fermi level,

$$Q = e \sum_{k,\mu} [a^\dagger_{k\mu 1} a_{k\mu 1} - \theta(-\epsilon_k)], \tag{5.6}$$

and V is the gate voltage. While this interaction models only the *mean-field* Coulomb interaction among electrons in the box and does not influence the spectrum, the electron-electron interactions in H_I are dynamic and do alter the spectrum.

Finally, H_T in Eq. (5.5) governs the tunneling through the contact between the wire and the box, with t the tunneling rate. The momentum independence of t implies that the tunneling happens at a point. H_T thus models a *point contact*.

Here we also assume that *all* effects from the finite size of the box are taken into account by H_C. In particular, in H_0, H_I and H_T we take the length ℓ of the box to be the same as that of the extended wire.

5.2 Non-Abelian Bosonization

In this section we focus on $H_0 + H_I$, which represents the dynamic bulk piece of the Hamiltonian. We shall discuss two different scenarios depending on the strength of the magnetic field applied. For zero magnetic field we have a two-channel case, while for large magnetic fields the description becomes single-channel. This can be seen by observing that for zero magnetic field in addition to the spin quantum number we have a quantum number α which acts as a second channel. For strong magnetic fields the spin is suppressed and only one channel is present. H_I is most easily specified in the relevant low-energy limit where all scattering processes are confined to the neighborhood of the Fermi points $\pm k_F$. Assuming that the electron density is incommensurate with the lattice of the underlying substrate, the allowed low-energy processes can be classified into dispersive, forward and backward scattering (with the latter taking place only inside the wire or box since there is no exchange of wire and box electrons away from the point contact) (see Fig. 3.4). We then can use the Sugawara construction described in the section 3.2.

5.2.1 Single-Channel Case

Keeping only the local piece of the potential, and, for simplicity, setting $V_{01}(0) = V_{00}(0) \equiv g$ as discussed in the previous section, $H_0 + H_I$ can be expressed on diagonal Sugawara form (cf. to the Eq. (3.50)) as

$$H_0 + H_I \approx \sum_{\ell=\pm} \frac{1}{2\pi} \int dx \Big[\frac{v_c}{4} :J_\ell J_\ell: + \frac{v_F}{3} :\boldsymbol{J}_\ell^{[\alpha]} \cdot \boldsymbol{J}_\ell^{[\alpha]}: \Big], \tag{5.7}$$

where "$\approx$" is a reminder that (5.7) contains the local part of the interaction only. Here $v_c = v_F(1 + 4g/v_F)^{1/2}$, with v_F the Fermi velocity, and the normal ordering is taken with respect to the filled Dirac sea. The currents are defined by

$$\begin{aligned} J_\pm &= \mathrm{sh}\vartheta :\psi^\dagger_{\pm\alpha}\psi_{\pm\alpha}: + \mathrm{ch}\vartheta :\psi^\dagger_{\mp\alpha}\psi_{\mp\alpha}: \\ \boldsymbol{J}^{[\alpha]}_\pm &= \frac{1}{2} :\psi^\dagger_{\pm\alpha}\boldsymbol{\sigma}_{\alpha\alpha'}\psi_{\pm\alpha}: . \end{aligned} \tag{5.8}$$

with $2\vartheta = \mathrm{arctanh}(2g/(v_F + 2g))$, $\boldsymbol{\sigma}$ being the vector of Pauli matrices, and the indices $\alpha, \alpha' = 0, 1$ summed over. One immediately recognizes Eq. (5.7) as a Luttinger liquid Hamiltonian, with dynamically separated charge and *pseudospin* currents. Note that the spin current is absent in the description, in accordance with the above discussion. Here we have excluded the "backscattering" in the pseudospin sector, which represents an unphysical exchange of electrons between the wire and the box away from the point contact.

5.2.2 Two-Channel Case

In analogy with the single-channel case, $H_0 + H_I$ can be expressed on diagonal Sugawara form as

$$H_0 + H_I = \frac{1}{2\pi} \sum_{\substack{\ell=\pm \\ \eta=\alpha,\mu}} \int (\frac{v_c}{8} : J_\ell(x) J_\ell(x) : + \frac{v_{[\eta]}}{4} : \boldsymbol{J}_\ell^{[\eta]}(x) \cdot \boldsymbol{J}_\ell^{[\eta]}(x) :) dx, \quad (5.9)$$

with $v_c = v_F(1+6g/v_F)^{1/2}, v_{[\mu]} = v_{[\alpha]} = v_F - g$. The charge and *pseudospin* currents $J_\pm$ and $\boldsymbol{J}_\pm^{[\alpha]}$, respectively, are defined as in Eq. (5.8) but with $2\vartheta = \operatorname{arctanh}(3g/(v_F + 3g))$. Since the magnetic field is zero, the spin acquires dynamics, with the spin current given by

$$\boldsymbol{J}_\pm^{[\mu]} = \frac{1}{2} : \psi^\dagger_{\pm\mu\alpha} \boldsymbol{\sigma}_{\mu\mu'} \psi_{\pm\mu'\alpha} : . \quad (5.10)$$

We have removed two marginally irrelevant interactions in the spin and pseudospin sectors in Eq. (5.9), including an unphysical exchange process between wire and dot electrons away from the point contact.

5.3 Mapping onto a Kondo Problem

In this section we will show that $H_c + H_T$ can be mapped onto an anisotropic Kondo interaction near a degeneracy point (see section 2.2).

We probe the system with a gate voltage close to a degeneracy point, say $V = -e/2C_\Sigma$, by applying a small voltage bias u ($u \ll e/C_\Sigma$). Near the degeneracy point electrostatic energies of states with $Q = 0$ and $Q = e$ are close and equal to $E(0) = 0$ and $E(e) = eu$ respectively, while all other charge states have energies $E(Q) > e^2/2C_\Sigma \gg eu$. In the limit of a small tunneling rate t and temperature T (compared to the charging energy $e^2/2C_\Sigma$) we can then truncate the Hilbert space to the $Q = 0$ and $Q = e$ states since in this limit transitions to virtual states of higher energy are suppressed. Following an exact formulation of K.A. Matveev [26], we can project out all higher energy configurations by introducing the operators P_0 and P_1, which project to the states with 0 and 1 unit charges, respectively. Taking into account all of the above, $H_C + H_T$ can be written as

$$H_C + H_T = euP_1 + t \sum_{k,\mu,p} (a^\dagger_{k\mu 0} a_{p\mu 1} P_1 + a^\dagger_{p\mu 1} a_{k\mu 0} P_0). \quad (5.11)$$

To connect to the Kondo problem we adopt the following representation for charge states and projection operators:

$$|e> = \begin{pmatrix} 1 \\ 0 \end{pmatrix} \qquad |0> = \begin{pmatrix} 0 \\ 1 \end{pmatrix}, \quad (5.12)$$

$$P_0 = \begin{pmatrix} 0 & 0 \\ 0 & 1 \end{pmatrix} \qquad P_1 = \begin{pmatrix} 1 & 0 \\ 0 & 0 \end{pmatrix}. \quad (5.13)$$

By noticing that

$$a_{p\mu 1}P_1 = a_{p\mu 1}\begin{pmatrix} 0 & 0 \\ 1 & 0 \end{pmatrix} = a_{p\mu 1}S^- \tag{5.14}$$

$$a^\dagger_{p\mu 1}P_0 = a^\dagger_{p\mu 1}\begin{pmatrix} 0 & 1 \\ 0 & 0 \end{pmatrix} = a^\dagger_{p\mu 1}S^+ \tag{5.15}$$

$$P_1 = \frac{1}{2} - S^z, \tag{5.16}$$

which is valid in our two-level formulation, Eq. (5.11) can be expressed in the following way:

$$\begin{aligned} H_C + H_T &= \frac{1}{2}eu - euS^z + t\sum_{k,p,\mu}(a^\dagger_{k\mu 0}a_{p\mu 1}S^- + a^\dagger_{p\mu 1}a_{k\mu 0}S^+) \\ &= \frac{1}{2}eu - euS^z + \frac{t}{2}\sum_{\substack{k,p,\mu \\ \alpha,\alpha'}}(a^\dagger_{k\mu\alpha}\sigma^+_{\alpha\alpha'}a_{p\mu\alpha'}S^- + h.c.). \end{aligned} \tag{5.17}$$

After rewriting this equation in coordinate space, expanding in left- and right-moving fields, and omitting a constant we get

$$H_K = H_C + H_T = \frac{J_\perp}{2}\psi^\dagger_{\ell\mu\alpha}(0)\sigma^j_{\alpha\alpha'}\psi_{\ell'\mu'\alpha'}(0)S^j - hS^z\,, \tag{5.18}$$

where $J_\perp = 2t$ and $h = eu$, and where $\boldsymbol{S}$ is an additional *pseudospin* of magnitude $1/2$ that implements the constraint on the allowed states (with $\boldsymbol{S}$ localized at the position $x = 0$ of the point contact). Note that *all* indices in (5.18), $\ell, \ell' = L, R$; $\mu, \mu' = \uparrow, \downarrow$; $\alpha, \alpha' = 0, 1$; $j = x, y$, are summed over. We recognize H_K as an anisotropic two-channel Kondo interaction. To make the mapping complete we observe that

$$\langle Q(u)\rangle = e\left[\frac{1}{2} - \mu(h, J_\perp)\right], \tag{5.19}$$

where $\mu = \langle S^z\rangle$ is an average magnetization. Then the "impurity" susceptibility χ_{imp}, describing the response of the local pseudospin to a "magnetic field" $h \equiv eu$ at $x = 0$, can be mapped onto a differential capacitance c using the following equation:

$$\chi_{imp}(h, T) = \frac{1}{e^2}\frac{\partial\langle Q\rangle}{\partial u} \equiv c(u, T). \tag{5.20}$$

Equations (5.18)-(5.20) summarize the mapping onto a multichannel Kondo problem, where the spin plays the role of the channel index. The above description is valid for zero magnetic field. For strong magnetic fields the spin get polarized and the label μ in Eq. (5.18) takes only a single value (say $\uparrow$), which can be omitted. Thus for strong magnetic fields the $H_C + H_T$ is mapped onto the anisotropic single-channel Kondo model.

5.4 Kondo Effect in Luttinger Liquids

We see that the original problem has been replaced by that of a Kondo impurity in a Luttinger liquid. The task is now to calculate the susceptibility of a (pseudo)spin-1/2 impurity coupled to a Luttinger liquid (see Eq. (5.7) or Eq. (5.9)) by an anisotropic Kondo interaction H_K (Eq. (5.18)). As we see, the Kondo interaction can not be written in current form due to the *backscattering* from the impurity. This is different from the ordinary Kondo problem for electrons in a three-dimensional bulk material [2], which supports only *forward* scattering, making the present problem more difficult.

The problem of an $SU(2)$ Kondo impurity in a Luttinger liquid has been studied by various analytical and numerical methods. First this problem was addressed by D.-H. Lee and J. Toner [122], and A. Furusaki and N. Nagaosa [123]. The perturbative RG analysis of the latter authors – using a Coulomb gas representation – revealed that the backscattering terms become relevant for interacting electrons, taking the theory to a nontrivial fixed point. They conjectured that the ground state is governed by the strong-coupling fixed point where the impurity is completely screened and the fixed-point Hamiltonian consists of two semi-infinite Luttinger liquids and a spin singlet. P. Fröjdh and H. Johannesson [124, 125] approached the problem via a nonperturbative route, exploiting boundary conformal field theory (BCFT) [17]. They showed that there are only two types of scaling behaviors consistent with the symmetries of the problem: either a local Fermi liquid or the nontrivial fixed point proposed by the perturbative analysis. R. Egger and A. Komnik [126] subsequently studied this problem using a quantum Monte Carlo method. This numerically exact method, with no finite-size limitations, allowed them to simulate the whole temperature range. Their calculation of the magnetic susceptibility showed that the fixed point of the problem is indeed governed by the non-Fermi liquid fixed point.

The case of the multi-channel Kondo problem in a Luttinger liquid was first addressed by M. Granath and H. Johannesson [127, 128] using boundary conformal field theory (BCFT). Similar results as in the single-channel case are obtained: either a local Fermi liquid or a nontrivial fixed point is realized. Using renormalization group methods K. Le Hur showed that the amplitude for two-channel electron-impurity backscattering renormalizes to a strong coupling fixed point as the temperature is lowered [32], in exact analogy to the single-channel case.

An additional important effect from the electron interactions is the enhancement of the Kondo temperature [122, 123, 32]. For strong interactions the Kondo temperature is given by a power-law expression compared to exponential suppression for weak interactions.

To study our problem we will follow the nonperturbative route developed in Refs. [124, 125, 127, 128]. As discussed in the previous section, the effective Kondo formulation of our problem is based on the work of K.A. Matveev [26], where a similar lead-box system was discussed for *non-interacting* electrons in a 3D geometry. Other works based on the above formulation [33, 34, 129, 130, 131] discuss the case of a lead with an *end-coupled* box, which supports only forward scattering from the

impurity (in contrast to our case with a *side-coupled* box). As we shall see next, our proposal to side-couple the box to the quantum wire will lead to a very different low-temperature behavior.

5.5 Calculation of the Differential Capacitance

Near the boundary fixed point the Hamiltonian of the system can be written in the following way:

$$H = H^* + V = H^* + \sum_i \lambda_i \mathcal{O}^{(i)}, \tag{5.21}$$

where H^* is the critical Hamiltonian and $\mathcal{O}^{(i)}$ are boundary operators with conjugate scaling fields λ_i (to be defined below). Going to the imaginary time representation $t = -i\tau$ the partition function of the system, Z, can be written in the functional integral form

$$Z = Tre^{-\beta H} = \int [\mathcal{D}\phi] \exp\left(- \int_{-\beta/2}^{\beta/2} \mathcal{L}_E(\tau) d\tau \right), \tag{5.22}$$

where $\mathcal{L}_E$ is the Euclidean Lagrangian, i.e. the Hamiltonian (5.21) written in fields.

The partition function can be rewritten in the following form:

$$Z = Z_0 \left\langle \exp\left(- \int_{-\beta/2}^{\beta/2} V(\tau) d\tau \right) \right\rangle, \tag{5.23}$$

with the average defined as

$$\langle \dots \rangle = \frac{1}{Z_0} \int [\mathcal{D}\phi] \dots \exp\left(- \int_{-\beta/2}^{\beta/2} \mathcal{L}_{0E}(\tau) d\tau \right) \tag{5.24}$$

and Z_0 being the partition function of the theory at the fixed point

$$Z_0 = \int [\mathcal{D}\phi] \exp\left(- \int_{-\beta/2}^{\beta/2} \mathcal{L}_{0E}(\tau) d\tau \right). \tag{5.25}$$

We define the free energy F in standard way and write Eq. (5.23) as

$$e^{-\beta F(\beta, \{\lambda_i\})} = e^{-\beta F(\beta, 0)} \left\langle \exp\left(- \int_{-\beta/2}^{\beta/2} V(\tau) d\tau \right) \right\rangle, \tag{5.26}$$

with $V(\tau) = \sum_i \lambda_i \mathcal{O}^{(i)}(\tau)$. Then the impurity free energy F_{imp} is defined as

$$e^{-\beta F_{imp}(\beta, \{\lambda_i\})} = \left\langle \exp\left(- \int_{-\beta/2}^{\beta/2} V(\tau) d\tau \right) \right\rangle. \tag{5.27}$$

Using the *cumulant* (or *linked cluster*) expansion [132] F_{imp} can be written as

$$F_{imp}(\beta, \{\lambda_i\}) = \sum_{n=1}^{\infty} \frac{(-1)^{n+1}}{\beta n!} \int_{-\beta/2}^{\beta/2} d\tau_1 \cdots \int_{-\beta/2}^{\beta/2} d\tau_n \langle V(\tau_1) \cdots V(\tau_n) \rangle_c, \tag{5.28}$$

where $\langle \cdots \rangle_c$ denotes the *connected* n-point function. Given the expression (5.28) we can calculate the magnetic susceptibility (differential capacitance) perturbatively, using the definition

$$\chi_{imp} = -\frac{\partial^2 F_{imp}}{\partial h^2}. \tag{5.29}$$

So far we have presented the formalism. Next we shall identify the leading boundary operators that appear in (5.21) and that govern the physics near the fixed point ($T = 0$, $h = 0$).

5.5.1 Results for the Single-Channel Case

It has been shown in Ref. [125] that for the *isotropic* case the fixed point corresponds to a particular selection rule for quantum numbers of the BCFT embedding $U(1) \otimes U(1) \otimes SU(2)_2 \otimes Ising$. Here the two U(1) factors represent the spectra of left- and right-moving charge excitations, while the $SU(2)_2 \otimes Ising$ block derives from a coset construction of the $SU(2)_1 \otimes SU(2)_1$ left- and right-moving pseudospin excitation spectra (with the indices labeling the *levels* of the corresponding Kac-Moody algebras (see Sec. 4.3)).

We have two main criteria for accepting or rejecting a possible boundary operator. The first is a *symmetry argument* which says that we should include only operators which are compliant with the symmetry of the model. The second is the *non-interacting constraint* which says that in the non-interacting limit the low-temperature behavior is that of the one-channel Kondo model. In the *spin* sector we have the following conformal towers: $j = 0, 1/2, 1$ in the $SU(2)_2$ sector, and $\phi = 1$ (identity), σ (order parameter), and ϵ (energy density) in the Ising sector. Using the symmetry argument applied to the parity[1] and U(1) symmetries we can exclude the $j = 1/2, 1$ towers. Thus we are left with the following combinations of conformal towers (*gluing conditions*) in the spin sector [125]:

$$\begin{aligned} &(0)_2 \times (1), \\ &(0)_2 \times (\epsilon). \end{aligned} \tag{5.30}$$

Combining the spin sector with the charge sector we get the following possible

[1] Operators should have definite parity under channel exchange, with the two channels represented by left- and right-movers (for more details see Ref. [125]).

leading correction-to-scaling boundary operators (LCBOs):

$$J^z \otimes \epsilon \otimes 1_c \qquad \Delta = \frac{3}{2}, \tag{5.31}$$

$$J^z \otimes 1_I \otimes \mathcal{O}_c \qquad \Delta = 1 + \frac{1}{2K_c}, \tag{5.32}$$

$$T^s \otimes 1_I \otimes 1_c \qquad \Delta = 2, \tag{5.33}$$

$$J^z \otimes \epsilon \otimes \mathcal{O}_c \qquad \Delta = \frac{3}{2} + \frac{1}{2K_c}, \tag{5.34}$$

where we have included only operators with nontrivial contributions in the $SU(2)_2$ sector, since only they may contribute to the susceptibility. In the spin sector only the z component is chosen because of the $U(1)$ symmetry of the model. Using the second criterion we shall argue that only the operators in (5.33) and (5.34) can be present and contribute to the susceptibility. Moreover we shall see that the existence of the anisotropy does not generate additional relevant operators, implying that the system flows to the isotropic fixed point.

Starting with the operator in (5.31) we can eliminate it by two independent arguments: First, if it were present it would imply a two-channel behavior in the non-interacting limit, in violation of the known one-channel behavior. Secondly, if we were to include this operator we should also include the relevant operator $1_s \otimes \epsilon \otimes 1_c$, since (5.31) is its descendant. But a relevant operator can not appear since we know that the fixed point is stable when there is no magnetic field added. Adding a finite local magnetic field may invalidate this argument and for this case the operator may appear. As for the operator in (5.32), we can exclude it by exactly the same line of arguments: First, in the noninteracting limit it gives a two-channel behavior, which is not there. Secondly if we were to include this operator we should also include the relevant operator $1_s \otimes 1_I \otimes \mathcal{O}_c$ of which (5.32) is a descendant. But this operator cannot be present since we know that the fixed point is stable when no magnetic field is added. In fact, adding a magnetic field does not change the argument, since $1_s \otimes 1_I \otimes \mathcal{O}_c$ does not couple to the field. We are thus left with the operators in Eqs. (5.33) and (5.34), respectively.

Given these operators, $\mathcal{O}^{(1)} = T^s \otimes 1_I \otimes 1_c$ and $\mathcal{O}^{(2)} = J^z \otimes \epsilon \otimes \mathcal{O}_c$, the scaling behavior of $\chi_{imp}(T, h = 0)$ can be calculated via an expansion in their conjugate scaling fields λ_1 and λ_2. To simplify the calculation we replace the local field h in the definition of χ_{imp} by a uniform field coupling to the pseudospins of all electrons. This will change the amplitude of the impurity susceptibility [133], but since we shall be interested in the scaling exponents only, this change is immaterial. Using Eq. (5.29) with Eq. (5.28) we can then write

$$\chi_{imp}(T, 0) = \lambda_1 I[\mathcal{O}_3^{(1)}] + \frac{1}{2} \sum_{i=1,2} \lambda_i^2 I[\mathcal{O}_3^{(i)}, \mathcal{O}_4^{(i)}] + \cdots, \tag{5.35}$$

where

$$I[\mathcal{O}_3, ..., \mathcal{O}_j] \equiv \int_{-\infty}^{\infty} \frac{dx_1 dx_2}{4\pi^2 \beta} \int_{-\beta/2}^{\beta/2} d\tau_1 \ldots d\tau_j \langle J_1^z J_2^z \mathcal{O}_3 ... \mathcal{O}_j \rangle_c,$$

with $J^z_k \equiv J^z(\tau_k, x_k), k = 1, 2$ and $\mathcal{O}^{(1,2)}_j \equiv \mathcal{O}^{(1,2)}(\tau_j), j = 3, 4$.

To collapse the integrands to products of two-point functions we use the following operator product expansions [52]:

$$J^a(z)J^b(w) \sim \frac{2\delta_{ab}}{(z-w)^2} + \sum_c i f_{abc} \frac{J^c(w)}{z-w} + \cdots , \tag{5.36}$$

$$T^s(z)J^a(w) \sim \frac{J^a(w)}{(z-w)^2} + \frac{\partial J^a(w)}{z-w} + \cdots , \tag{5.37}$$

$$T^s(z)T^s(w) \sim \frac{3/4}{(z-w)^4} + \frac{2T^s(w)}{(z-w)^2} + \frac{\partial T^s(w)}{z-w} + \cdots . \tag{5.38}$$

This allows us to easily calculate the integrals and we obtain (using that $c(T, u{=}0) = \chi_{imp}(T, h{=}0)$):

$$c(T, u{=}0) = A + B(1/K_c - 1)T^{1/K_c} + CT^2 + \cdots , \tag{5.39}$$

with A, B and C constants, and where "$\cdots$" indicate subleading corrections. The short-range electron-electron interaction, encoded by the parameter K_c, is thus seen to induce a *nonanalytic term in the differential capacitance*, scaling as T^{1/K_c}, while vanishing in the noninteracting limit ($K_c = 1$).

Our result in (5.39) predicts a distinct signal of Luttinger liquid correlations in the proposed setup. For what temperatures should one expect to see it? Taking the 1D quantum box to have a length $\ell' \sim 1\mu m$ and choosing parameters assuming an experiment using a GaAs heterostructure [134], the energy spacing δE close to the Fermi level corresponds to roughly 0.5K. The temperature that sets the upper limit for the validity of our theory is the effective Kondo temperature T_K, with expression $T_K = E^*_C \exp(-1/2t\nu)$ in the limit $g\ell < 2t$ [123]. Here $E^*_C = E_C(1 - 4(t\nu)^2 + \cdots)$ is the renormalized charging energy [135], and ν is the density of states at the Fermi level. With $t \sim 0.2/\nu$ and $E_C \sim e^2/2C_\Sigma$, where $C_\Sigma \sim 30$aF in a typical device, we obtain $T_K \sim 2$K. With these estimates our prediction in (5.39) applies for temperatures in the interval $0.5\text{K} < T < 2\text{K}$.

Considering the narrowness of the estimated temperature interval, it may experimentally be easier to study the scaling of the capacitance with gate voltage at a fixed temperature (in the window $0.5\text{K} < T < 2\text{K}$). Approximating it by taking $T \to 0$, the scaling can be obtained by performing a *Wegner expansion* [136] of the effective ("Kondo language") impurity free energy. The Wegner expansion allows us to find the corrections to scaling coming from the nonlinearities of the scaling fields as well as the effects from the irrelevant fields. Here we are interested in the correction to the scaling as a result of the irrelevant fields. In the neighborhood of the critical point $T = 0, h = 0$ we thus write

$$F_{imp} = \text{const.} + Tf(\frac{h}{T^\Delta}) + g'T^{1-\Delta'} f'(\frac{h}{T^\Delta}) + \cdots . \tag{5.40}$$

Here f is a scaling function, $\Delta = 1/2$ is the boundary dimension acquired by the *local* magnetic field h, and f' is the gradient of f with respect to the leading irrelevant

scaling field g'. The corresponding operator $\epsilon \otimes \mathcal{O}_c$ is generated from the OPE of J^z with $J^z \otimes \epsilon \otimes \mathcal{O}_c$ and g' is thus proportional to h and carries RG eigenvalue $\Delta' = -(1/K_c - 1)/2 < 0$. In the limit $s \to \infty$, $f(s) \sim s^{1/\Delta}$. Thus, when $T \to 0$ the second term in Eq. (5.40) gives an analytic contribution $\sim h^2$. Inspection of the third term in (10) reveals that it can contribute a *finite* correction δF_{imp} only via a term $\sim s^{(1-\Delta')/\Delta}$ in the expansion of f', implying that $\delta F_{imp} \sim h^{1+(1-\Delta')/\Delta} = h^{2+1/K_c}$. Contributions from higher order terms in Eq. (5.40) are of O$[h^4]$. Summarizing, we obtain:

$$c(T=0,u) = D + E[K_c]u^{1/K_c} + Fu^2 + \cdots . \tag{5.41}$$

Here $D, E[K_c]$ and F are constants, with $E[K_c] \to 0$ as $K_c \to 1$. The window of applicability of the Eq. (5.41) is given by $\delta E \ll eu \ll T_H$, where T_H is an energy scale of the order of T_K [137].

5.5.2 Results for the Two-Channel Case

Let us first recall that the fixed point of the *isotropic* two-channel Kondo effect in a Luttinger liquid corresponds to a particular selection rule for quantum numbers of the BCFT embedding $\otimes_{i=1,2}$[U(1)$\otimes$SU(2)$_2\otimes$SU(2)$_2$]^i implied by the Hamiltonian in (5.9) [127, 128]. Here the U(1) factor represents charge, while the SU(2)$_2$ factors represent spin and pseudospin, with i labeling left and right moving fields. The Kondo interaction couples left and right movers, and therefore the symmetries above are broken down to their diagonal subgroups. For the charge sector this implies that any U(1) operator with dimension

$$\Delta_c = \frac{1}{4}n^2 e^{\pm 2\theta} + N; \qquad n, N \in \mathbb{N} \tag{5.42}$$

is allowed [127, 128]. Factorizing the diagonal subgroups in the spin and pseudospin sectors amounts to a coset construction at the level of conformal towers: The two SU(2)$_2$ towers in the spin and pseudospin sectors are decomposed into SU(2)$_4$ and a coset which is generated by the N=1 superconformal algebra (SCA) of central charge c=1. Primary states of the spin (pseudospin) SU(2)$_4$ sectors have conformal dimensions $j(j+1)/6$ with $j \in \{0, 1/2, 1, 3/2, 2\}$. The SCA in turn is divided into two sectors: the Ramond (R) and Neveu-Schwartz (NS) algebras with primary dimensions $\{1/24, 1/16, 3/8, 9/16\}$ and $\{0, 1/16, 1/6, 1\}$ respectively. In addition, the grade of a generic state is integer in the R sector, whereas it is half-integer in the NS sector. The scaling dimensions of LCBOs, which are the combinations of operators from charge, spin, pseudospin, and SCA sectors, are then given by

$$\Delta = \Delta_c + \sum_{j=s,p} (\Delta^j_{SU(2)_4} + \Delta^j_{SCA}), \tag{5.43}$$

where

$$\Delta^{s/p}_{SU(2)_4} = \frac{j(j+1)}{6} + N, \qquad j = 0, \frac{1}{2}, 1, \frac{3}{2}, 2; \quad N \in \mathbb{N} \tag{5.44}$$

$$\Delta^{s/p}_{SCA} = \{0, \frac{1}{16}, \frac{1}{6}, 1\} + \frac{N}{2}, \ \{\frac{1}{24}, \frac{1}{16}, \frac{3}{8}, \frac{9}{16}\} + N, \quad N \in \mathbb{N} \tag{5.45}$$

Valid LCBOs (i) must respect all remaining symmetries of the theory and (ii) must not violate the known critical scaling of observables in the non-interacting limit $g \to 0$. The criterion (i) restricts the choice of operators in each conformal sector, while the criterion (ii) defines the rules for combination of operators in different sectors to obtain the LCBOs.

Given the above construction and criteria, it is in principle straightforward to pinpoint the effect from the exchange anisotropy (broken pseudospin rotational symmetry) and the magnetic field (broken time reversal symmetry) in (5.18). In contrast to the $SU(2)_4$ invariant case above where only operators that transform as singlets are allowed, more operators now appear in the pseudospin sector. By inspection we find that the only relevant operator produced is the $j = 1$ primary field ϕ^z, with conformal dimension $\Delta_{\phi^z} = 1/3$. This operator is present only if pseudospin rotational *and* time reversal symmetries are simultaneously broken. In the limit of vanishing magnetic field the anisotropy is irrelevant, implying that the magnetic field is a relevant perturbation, as for the two-channel Kondo model for non-interacting electrons [31]. There are two more operators appearing because of the broken pseudospin symmetry: The first descendant J^z of the $j = 0$ identity operator, and the $j = 2$ primary field ϕ^{zz}, both being exactly marginal of dimension $\Delta = 1$.

For the *isotropic* problem the leading behavior of the impurity susceptibility $\chi(T, h)$ is driven by the same operator (of dimension $\Delta = 3/2$) as for noninteracting electrons, giving rise to a logarithmic divergence as $T \to 0$ or $h \to 0$ [127, 128]. In our construction the LCBO driving the behavior is a combination of the first descendant of the pseudospin j=1 $SU(2)_4$ conformal tower with $\Delta = 1/6$ NS field. To explore whether a faster divergence may result from any of the new composite operators generated from the broken pseudospin symmetry, we have to identify those of scaling dimension $\Delta < 3/2$ (since they may produce more leading contributions) and then test them against criteria (i) and (ii) above.

We can identify two distinct classes of possible LCBOs. The first class contains operators with dimensions $\Delta < 3/2$, which do not depend on the Luttinger liquid interaction parameter K_c (thus containing the identity operator from the charge sector) and hence they should be present in the non-interacting limit as well. Since these contributions do not vanish in non-interacting limit, taking into account constraint (ii) we conclude that the operators from this class should not be included in the calculation. The second class contains operators with dimensions $\Delta(K_c) < 3/2$, which depend on the Luttinger liquid interaction parameter K_c (thus containing non-trivial operators from the charge sector). Our calculations using the expansion described in the previous section show that the contributions to the observables from these operators do not vanish in the non-interacting limit. Thus again using constraint (ii) we conclude that these operators should neither be included in the calculation.

It follows that the leading behavior of the differential capacitance $c(T, u)$ of our proposed set-up exhibits the same logarithmic scaling as in the two-channel Kondo effect for noninteracting electrons:

$$c(T, u{=}0) = A \ln\left(\frac{T_K}{T}\right) + \cdots, \quad T \ll T_K \tag{5.46}$$

and

$$c(T=0,u) = B \ln\left(\frac{T_H}{eu}\right) + \cdots, \quad eu \ll T_H \tag{5.47}$$

where $T_H \approx T_K$ [137]. Here A and B are constants, and "$\cdots$" indicate subleading terms.

As we already noted above our analysis is valid in the regime $\delta E \ll T \ll T_K$, which in general is expected to be rather narrow. As shown by K. Le Hur, the amplitude for two-channel electron-impurity backscattering renormalizes to a strong coupling fixed point as the temperature is lowered [32]. This is in exact analogy with the single-channel Kondo problem in a Luttinger liquid, where this effect was first noted [122, 123]. The flow to strong coupling produces a crossover from an exponentially suppressed Kondo temperature $T_K \sim E_c e^{-1/2t\nu}$ for $g \ll J_\perp$ to a power law $T_K \sim E_C(2t\nu)^{2/(1-K_c)}$ for $g \gg J_\perp$. Using the crossover formula from Ref. [122, 123] with input parameters chosen for a GaAs based device [134] and with $t\nu \lesssim 0.2$, one finds that while T_K in the noninteracting limit ($K_c = 1$) is comparable to or below the level spacing in the box, T_K becomes almost an order of magnitude larger as K_c approaches 0.6 (which is easily reached in a low-density quantum wire [138]). Although the temperature window that opens is probably too narrow for a full-fledged two-channel Kondo scaling to develop, it should at least allow for a controlled experimental study of its transient behavior. Using a *metallic* quantum wire/box with its much larger effective electron mass would stretch the window by another order of magnitude (provided that the electron density can be suppressed by proper gating of the device). We here point to the recent observation that electron-shell effects can stabilize arbitrarily long metallic quantum wires, making the fabrication of a metallic device a viable and realistic prospect [139].

5.6 Summary and Discussion

In this section we address the question how the boundaries of the box, as well as the finite range and the anisotropy of the screened Coulomb interaction, influence the physics. Although these features must be accounted for in a faithful modeling of an experimental sample, they will not *qualitatively* change the charge fluctuation effects derived in Eqs. (5.39), (5.41), (5.46), and (5.47). As to the boundary effects from the quantum box, these will suppress the spectral weight at the Fermi level, at low energies reducing the effective value of K_c [140]. The finite range R of the screened Coulomb interaction further depresses K_c [138]. Both effects are moderate, though, and as long as the renormalized K_c is larger than $1/2$ above analysis remains valid. Turning to the expected anisotropy $V_{01}(0) \equiv g' < V_{00}(0) = g$, this will generate an exactly marginal term proportional to $(g-g')J_L^z J_R^z$ in the pseudospin sector, to be added to H_{el}, in addition to shift the velocities in Eqs.(5.7) and (5.9). It is evident that the breaking of isotropy in the pseudospin sector of the bulk Hamiltonian does not generate new LCBOs, since it is already broken locally (by the Kondo Hamiltonian in Eq. (5.18)). As far as we are interested in boundary properties, and since there is no difference between the symmetric and anisotropic bulk cases locally

at the boundary, the results obtained in Secs. 5.5.1 and 5.5.2 remain unchanged.

We predict that for the single-channel scenario the differential capacitance of a quantum box side-coupled to a quantum wire exhibits a nonanalytic scaling in temperature and gate voltage, with *the same scaling exponent in both cases*. For the two-channel scenario the differential capacitance of the system exhibits logarithmic two-channel Kondo divergences with temperature T (voltage u) for $T \ll T_K$ ($eu \ll T_H$). This leading behavior is *not* modified by the strong 1D electron correlations in the wire and the box. The Kondo temperature T_K (or T_H in the case of voltage scaling) can be significantly larger compared to a device with non-interacting electrons. While design constraints for a semiconductor implementation probably only allows for crossover effects to be observed, the fabrication of a device with metallic nanowires should yield access to the proposed behavior. We expect that high-precision charge [119, 120] or capacitance [121] measurements should be able to detect the effects above. An experimental verification may shed new light on the elusive Luttinger liquid and two-channel Kondo behaviors of electrons in one dimension.

6

STM Response of a Luttinger Liquid with Edges and Impurities

6.1 Overview of the STM Probe

Scanning tunneling microscopy (STM) provides a unique tool for spatially resolving the electronic structure of a sample. Being a local probe it is particularly useful for studying effects from interactions and edges and/or impurities. STM was invented by G. Binnig and H. Rohrer in 1982 [141, 142] and was recognized by the Nobel Prize in 1986 [143]. The probe consists of an atomically sharp tip placed near a surface of a sample so that electrons may tunnel between the tip and the sample (see Fig. 6.1). The resulting tunneling current encodes the local electronic structure of the sample. After properly analyzing the STM data it is also possible to identify the atomic structure of the sample. Theoretical works on STM stem from J. Bardeen's [144] transfer Hamiltonian formalism of tunneling. His ideas were applied to STM by J. Tersoff and D.R. Hamman [145, 146], and by A. Baratoff [147]. An equivalent STM theory based on a scattering approach was also developed at the same time [148, 149, 150].

In the following I will present the basics of STM, following Refs. [145, 146]. In the simplest approach, when the presence of the STM tip does not affect the sample, the tunneling current at zero temperature is given by

$$I(V,x) \propto \frac{2e}{\pi} \int_0^{eV} N(\omega,x) N_{STM}(\omega - eV) d\omega, \tag{6.1}$$

where $N(\omega, x)$ is the local single-electron density of states for a conduction electron at a position x with energy ω, and $N_{STM}(\omega)$ is the density of states of the STM tip. An individual tip is difficult to characterize in detail, and for metallic tips one simply takes $N_{STM}(\omega)$ to be a constant, call it ρ_0, at low voltage bias and temperature. With this approximation the local differential tunneling conductance can be directly related to the local density of states by differentiating $I(V, x)$ in Eq. (6.1):

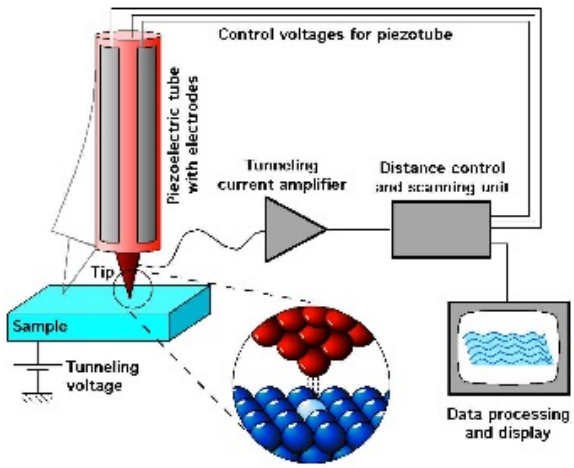

Figure 6.1: Schematic view of the STM setup [by Michael Schmid, TU Wien].

$$\frac{dI(V,x)}{dV} \propto \frac{2e^2}{\pi}\rho_0 N(V,x). \tag{6.2}$$

For non-zero temperatures the expression for $I(V,x)$ is modified to

$$I(V,x;\beta) \propto \frac{2e}{\pi}\rho_0 \int_{-\infty}^{\infty} [f(\omega - eV,\beta) - f(\omega,\beta)]A(\omega,x;\beta)d\omega. \tag{6.3}$$

Here $f(\omega,\beta)$ is the Fermi-Dirac distribution, and $A(\omega,x;\beta)$ is the finite-temperature local spectral weight (LSW) of the conduction electrons at $T = 1/\beta$. Writing

$$f(\omega - eV,\beta) - f(\omega,\beta) = (1 - f(\omega,\beta))f(\omega - eV,\beta) - (1 - f(\omega - eV,\beta))f(\omega,\beta) \tag{6.4}$$

one can see that the first [second] term represents tunneling from [to] the STM tip to [from] the sample. At zero temperature this factor simply changes the integration limits to those in Eq. (6.1), with $A(\omega,x;\beta)$ reducing to $N(\omega,x)$. Given Eq. (6.3), the local differential conductance at finite temperature can be written as

$$\frac{dI(V,x;\beta)}{dV} \propto \frac{2e}{\pi}\rho_0 \int_{-\infty}^{\infty} \frac{d}{dV} f(\omega - eV,\beta)A(\omega,x;\beta)d\omega. \tag{6.5}$$

It follows that the line shape properties of the local tunneling conductance are directly determined by the LSW.

The LSW gives the probability distribution for the energy ω of an electron added to the system at a position x, i.e. the probability that the N-particle states $|m\rangle$ of energy ϵ_m are connected to the $(N+1)$-particle states $|n\rangle$ of energy $\epsilon_n = \epsilon_m + \omega$ by the addition of an extra electron of energy ω and coordinate x:

$$A(\omega,x;\beta) = \frac{1 + \exp(-\beta\omega)}{Z} \sum_{m,n} \exp(-\beta E_m)\, |\langle n|\Psi_\sigma^\dagger(x)|m\rangle|^2\, \delta(\omega - E_n + E_m). \tag{6.6}$$

Here Z is the partition function of the N-particle system, and $\Psi_\sigma^\dagger(x)$ creates an electron with spin σ at x. At zero temperature $A(\omega, x; \beta = \infty)$ simply enumerates the states that can be obtained from the ground state by adding an extra electron of energy ω at a position x. By definition, this is precisely the single-electron local density of states $N(\omega, x)$ that appears in Eqs. (6.1) and (6.2).

It is possible to extract the LSW in the standard way by first calculating the single-electron retarded Green's function

$$G^R(t, x; \beta) = -i\Theta(t)\langle\{\Psi_\sigma(t, x), \Psi_\sigma^\dagger(0, x)\}\rangle_\beta, \tag{6.7}$$

and then use that [132]

$$A(\omega, x; \beta) = -\frac{1}{\pi}\mathrm{Im}\int_0^\infty G^R(t, x; \beta)\mathrm{e}^{i\omega t}dt. \tag{6.8}$$

In the next section I will present the results derived in **Paper III** using bosonization, which give the first complete and accurate analytical expression for the finite-temperature LSW for a semi-infinite Luttinger liquid with an open boundary condition.

6.2 STM Response of the Standard Luttinger Liquid

Since the calculations and results are presented in great detail in **Paper III**, I will here only provide a short summary. As was shown in the previous section, to derive the LSW and therefore the STM response one should first calculate the retarded Green's function. This is done using the bosonization scheme described in the Sec. 3.3 from which the zero-temperature expression is obtained. Then using the BCFT formalism (described in Sec. 4.4) we can easily derive the finite temperature form of the retarded Green's function using Eq. (4.38). It is then straightforward, in principle, to perform the Fourier transform with respect to time and thus obtain the LSW. It is worth emphasizing that careful attention must be given to the branch cuts of the integrand so as to obtain a well-defined expression. Taking into account all of the above, one obtains for the LSW in Eq. (6.8)

$$\begin{aligned} A(\omega, x, \beta) &= \frac{4}{\pi}\int_0^\infty dt \cos\omega t Re G_{LL}(t, x, x; \beta) \\ &+ \frac{2}{\pi}\int_{-\infty}^\infty dt \cos(2k_F x + \gamma - \omega t) Re\, G_{LL}(t, x, -x; \beta), \end{aligned} \tag{6.9}$$

where $G_{LL}(t, x, x'; \beta) = \langle\psi_{L\sigma}(t, x)\psi_{L\sigma}^\dagger(0, x')\rangle_\beta$ is the chiral Green's function.

In the next subsection I will highlight the most important results and ask the reader to consult **Paper III** for further details.

6.2.1 Properties of the LSW

Here we focus on three aspects of the LSW of particular interest for STM experiments: Its *asymmetric line shape* as a function of energy, oscillation patterns revealing *spin-charge separation*, and *thermal effects*.

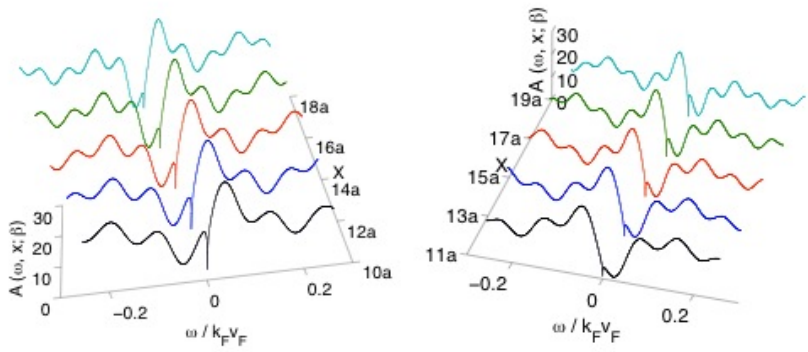

Figure 6.2: $A(\omega, x; \beta)$ for $K = 0.7$, $v_c/v_F \approx 1.43$, $v_c/v_s \approx 3$, $T/k_F v_F = 2.6 \times 10^{-6}$, $n_e = 0.97$, shown for even and odd sublattices.

Asymmetric line-shape

One of the most striking features of the LSW is the *asymmetry* of its line shape at small energies (see Fig. 6.2). This property is due to the phase $2k_F x + \gamma$ appearing in the second term of $A(\omega, x; \beta)$ (see Eq. (6.9)). The phase causes a shift of the periodic structure of $A(\omega, x; \beta)$ with respect to the Fermi level, and accordingly determines how the spectral weight suppression close to the Fermi level affects the line shape. The shift depends upon the filling factor n_e since, for fixed x, n_e determines the values of k_F and γ. The LSW is asymmetric in general, but for particular fillings for which $2k_F na + \gamma = \pi m \, (m \in \mathbb{Z})$ it becomes a symmetric function of ω. By inspection of Eq. (6.9) one finds that for a given interaction strength the asymmetry tends to zero very close to the boundary ($2\omega x/v_s \ll 1$) and very far from the boundary ($2\omega x/v_c \gg 1$, "bulk" regime) and reaches a maximum in the intermediate region. It is important to realize that the shift of the periodic structure with respect to the Fermi level is present also for the non-interacting case when the LSW takes the simple form $A(\omega, x; \beta) \sim \cos(2k_F x + \gamma - 2\omega x/v_F)$. We conclude that the shift is a pure boundary effect, and is due to the interference of the incoming and reflected electrons at the boundary. In contrast, the dip of the spectral weight at the Fermi level is an interaction effect. The asymmetric line shape comes from a combination of boundary and interaction effects.

In Fig. 6.2 we show the energy and coordinate dependence of the LSW for even and odd sublattices. The Friedel oscillations on the scale of the lattice spacing a are easily visible as a flip of the asymmetry when going from one graph to the other. Note that the asymmetry with energy varies with the distance to the boundary since the phase $2k_F x + \gamma$ also varies with distance.

It is interesting to note the similarity of the typical asymmetric line shapes in Fig. 6.2 with that of a Fano resonance [151, 152] when ω is close to the Fermi level. A Fano resonance is known to develop in the LSW for non-interacting electrons when

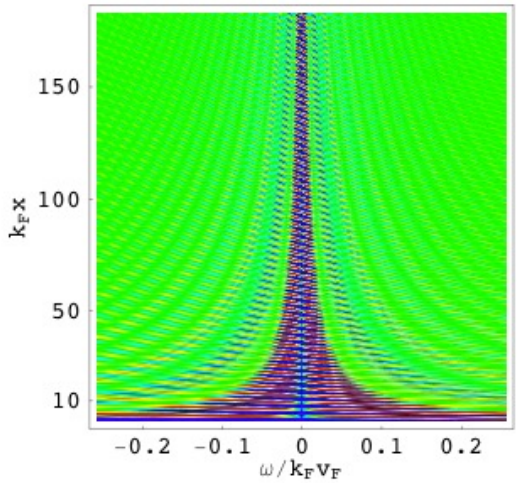

Figure 6.3: $A(\omega, x; \beta)$ for $K = 0.7$, $v_c/v_F \approx 1.43$, $v_c/v_s \approx 3$, $T/k_F v_F = 2.6 \times 10^{-4}$, $n_e = 0.97$.

coupled e.g. to a magnetic impurity, the effect being produced by the interference between resonating and nonresonating electron paths through the impurity [153]. As we have seen, the asymmetry in the present case instead comes from the combined effect of electron interactions (causing a dip in the LSW at the Fermi level) and the reflection of electrons off the boundary (causing a phase shifted oscillation in the LSW). As one expects the Fano line shape to survive for *interacting* electrons coupled to a magnetic impurity it is indeed satisfying to see this feature reproduced by the open boundary for which the impurity gets traded at low temperatures.

Spin-charge separation

The proximity to an open edge (or impurity) reveals a key property of interacting electrons in one dimension – *spin-charge separation*. The effect shows up in the LSW as characteristic oscillations at intermediate distances from the boundary. Very far from the boundary ($2\omega x/v_s \gg 1$) $A(r, \omega; \beta)$ is a monotone function scaling as ω^α near the Fermi level, with bulk exponent $\alpha = (K_c + K_c^{-1})/4 - 1/2$ at low temperatures [67]. Extremely close to the boundary ($2\omega x/v_s \ll 1$) $A(r, \omega; \beta)$ has a similar structure, but with an enhanced suppression near the Fermi level, $A(r, \omega; \beta) \sim \omega^{\alpha_B}$, with boundary exponent $\alpha_B = (K_c^{-1} - 1)/2$ at low temperatures [154, 54, 71] (see Fig. 6.3, with color coding in arbitrary units). As one moves away from the immediate vicinity of the boundary an oscillation pattern emerges, which becomes most pronounced when $2\omega x/v_s \sim \mathcal{O}(1)$. This oscillatory feature (see Fig. 6.4) is due to a superposition of propagating collective spin and charge waves. The two panels correspond to two different choices of K_c, with two different values of the ratio v_c/v_s, leading to the

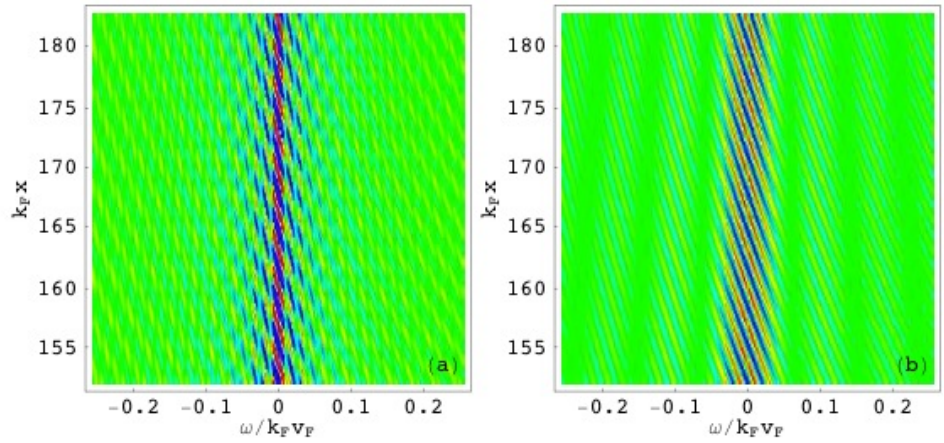

Figure 6.4: $A(\omega, x; \beta)$ for $T/k_F v_F = 2.6 \times 10^{-6}$, $n_e = 0.97$, with $K = 0.7$, $v_c/v_F \approx 1.43$, $v_c/v_s \approx 3$ (a) and $K = 0.9$, $v_c/v_F \approx 1.11$, $v_c/v_s \approx 1.26$ (b). The color coding is the same as in Fig. 6.3.

two different peak structures. By close inspection of the graphs one can easily read off the corresponding velocity ratios. To see how, let us make a "cut" of the two panels in Fig. 6.4 at a distance $x = 100a$ from the boundary, yielding the panels in Fig. 6.5.

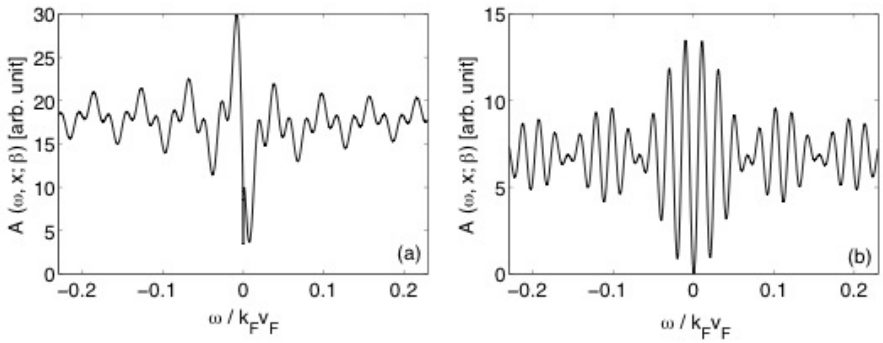

Figure 6.5: $A(\omega, x; \beta)$ for $T/k_F v_F = 2.6 \times 10^{-6}$, $n_e = 0.97$, with $x = 50a$, $K = 0.7$, $v_c/v_F \approx 1.43$, $v_c/v_s = \lambda_c/\lambda_s \approx 3$ (a) and $x = 100a$, $K = 0.9$, $v_c/v_F \approx 1.11$, $v_c/v_s = \lambda_c/\lambda_s \approx 1.26$ (b).

When $K_c = 0.7$ (see Fig. 6.5(a)) the spin and charge velocities differ significantly. For this case the short wavelength ($\lambda_s = \pi v_s/x$) spin oscillations are modulated by long wavelength charge oscillations ($\lambda_c = \pi v_c/x$). We note that there

are three spin oscillations per one charge oscillation which is in agreement with the fact that in this case $\lambda_c/\lambda_s = v_c/v_s \approx 3$ (see Fig. 6.5 (a). When K_c gets closer to unity (non-interacting limit) the spin and charge velocities approach each other and the spin-charge separation manifests itself as a beating pattern, provided that K_c is not identical to unity (see Fig. 6.5(b) where $K_c = 0.9$). The short wavelength ($\lambda = 2\pi v_s v_c/x(v_s + v_c)$) oscillations are now amplitude-modulated by long wavelength oscillations ($\lambda' = 2\pi v_s v_c/x(v_c - v_s)$). We see that there are about six short wavelength oscillations per "bubble" of the long wavelength amplitude modulations, which is in agreement with the fact $\lambda'/\lambda \approx 12$ in this case, corresponding to $\lambda_c/\lambda_s = v_c/v_s \approx 1.26$.

The spin-charge oscillations in the LSW are also present in real space as has been discussed before [155]. The oscillations as a function of energy might be easier to observe, however, since here there are no superimposed Friedel oscillations. We also remark that the existence of the beating pattern for values of K_c close to unity was proposed in Ref. [156] as a diagnostic tool for spin-charge separation in possible tunneling experiments of an LL where an STM tip is used as an impurity.

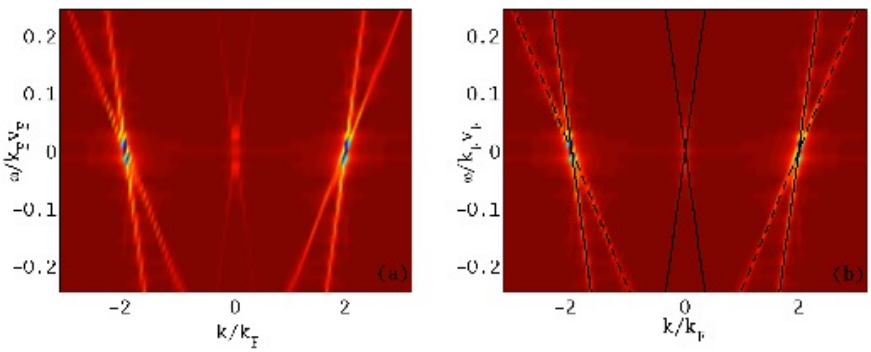

Figure 6.6: Fourier transform of the LSW for $K = 0.7$, $v_c/v_F \approx 1.43$, $v_c/v_s \approx 3$, $T/k_F v_F = 2.6 \times 10^{-4}$, $n_e = 0.97$ (a) and the same graph with charge (solid lines) and spin (dashed lines) wave dispersions superimposed (b).

One can map the dispersion of the spin and charge waves by taking a Fourier transform of the LSW (see Fig. 6.6(a)). This Fourier transform should not be mixed up with the momentum or angle resolved spectral weight, which is measured in photoemission experiments, although it shows similar features of spin-charge separation. The dominant weights in the transform correspond to the $\omega(k)$ dependence of the excitations. The dispersion lines at $k = 0$ come from the non-oscillatory part of the LSW and represent the charge excitations, since the non-oscillatory part contains only charge oscillations. This feature at $k = 0$ is also a clear indication of interaction effects and disappears as $K_c \to 1$. The dispersion lines at $k \neq 0$ come from the Friedel terms, and contain spin and charge branches shifted from $k = 0$ by $\pm 2k_F$. The mirror symmetry about $k = 0$ reflects the standing wave nature of

the oscillations. In Fig. 6.6(b) the dispersion relations $\omega(k) = \pm k v_c/2$ at $k \approx 0$ and $\omega(k) = (\pm k - 2k_F)v_{c/s}/2$ at $k \approx \pm 2k_F$ are plotted on top of the Fourier transform and agree excellently with the location of the maxima. This provides an important test of our numerical integration for obtaining the LSW in Eq. (6.9).

Thermal effects

On general grounds one expects that thermal effects become visible only for energies $\omega \lesssim T$ and distances $x \gtrsim \lambda_T = v_s/T$. Choosing e.g. $T \lesssim 10\text{K}$ and $v_F \approx 10^5\text{m/s}$ (a typical value for a quasi-1D organic metal for which Luttinger liquid theory should be applicable [51]) this implies that the spin-charge peak structure as seen in Fig. 6.4 will remain intact for distances not too far from the edge ($2x/\beta v_s \ll 1$). For $2x/\beta v_c \gtrsim 1$ the spin and charge waves loose their coherence before reaching the edge and therefore spin-charge separation is destroyed.

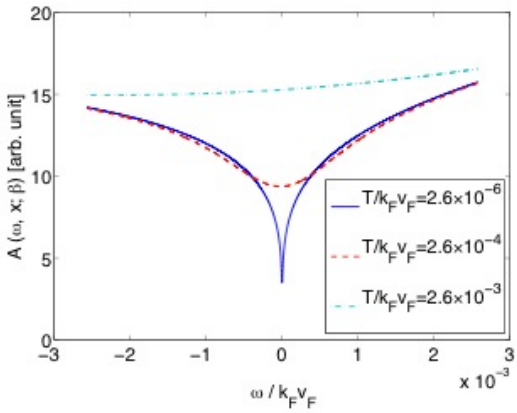

Figure 6.7: $A(\omega, x; \beta)$ for $K = 0.7$, $v_c/v_F \approx 1.43$, $v_c/v_s \approx 3$, $x = 10a$, $n_e = 0.97$ at different temperatures.

A more interesting issue is the fate of the asymptotic scaling behavior of the LSW near the Fermi level as the temperature increases. In earlier work it was found that the "uniform part" of the LSW (corresponding to the first term in (6.9) crosses over to ω^2 scaling in both boundary ($2\omega x/v_s \ll 1$) and bulk regimes ($2\omega x/v_c \gg 1$) when $\omega\beta < 1$ [140]. The effect was found to originate in the exponential damping of the density correlations for unequal times due to thermal fluctuations. By performing an expansion of the *full* LSW in Eq. (6.9) with the small parameter $\omega\beta$ we find that the power law is now modified to

$$A(\omega, x; \beta) \sim A + B\omega + C\omega^2, \quad \omega\beta \ll 1 \tag{6.10}$$

where A, B and C depend on the temperature and the distance from the boundary. We depict the crossover from boundary scaling $\sim \omega^{(K_c^{-1}-1)/2}$ for $\omega\beta \gg 1$ to thermal scaling $\sim A + B\omega + C\omega^2$ for $\omega\beta \ll 1$ in Fig. 6.7. Note that one is able to observe this

crossover for $2x/\beta v_s \ll 1$. For $2x/\beta v_c \gtrsim 1$ the boundary scaling is completely washed out. Since in this regime $G_{LL}(t, x, -x; \beta)$ is exponentially suppressed compared to $G_{LL}(t, x, x; \beta)$, it follows that $A(\omega, x; \beta) \sim A + C\omega^2$, and the line shape becomes symmetric.

6.2.2 Properties of the Local Tunneling Conductance

The *local differential tunneling conductance*, defined in Eq. (6.5), exhibits the very same features as the LSW. The only difference is that the fine structure of the differential conductance is thermally smeared via the temperature dependence of the Fermi-Dirac distribution. This can clearly be seen by examining the energy dependence at some fixed distance from the boundary, as done in Fig. 6.8, and then comparing to the corresponding graphs for the LSW in Fig. 6.5. As the smearing occurs on the scale of T, spin-charge separation is wiped out for temperatures $T \gtrsim \lambda_s$. The distance x from the boundary determines the wavelength of the oscillations in energy space, so in most cases it should be possible to find a range for x which shows many waves in the energy interval where LL theory applies that are not washed out by temperature, i.e. $1/\Delta \ll x/v_c \ll 1/T$, where Δ is the bandwidth. Note that the inequality above coincides with the criterion for observing spin-charge separation in the LSW, discussed in the previous subsection.

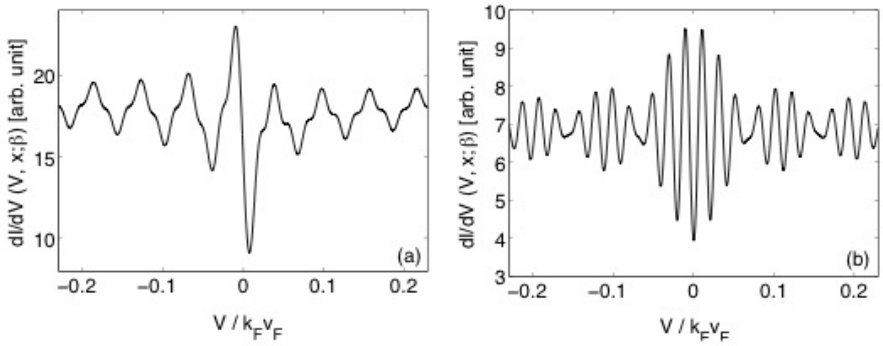

Figure 6.8: $dI/dV(V, x; \beta)$ for $T/k_F v_F = 2.6 \times 10^{-3}$, $n_e = 0.97$, with $x = 50a$, $K = 0.7$, $v_c/v_F \approx 1.43$, $v_c/v_s = \lambda_c/\lambda_s \approx 3$ (a) and $x = 100a$, $K = 0.9$, $v_c/v_F \approx 1.11$, $v_c/v_s = \lambda_c/\lambda_s \approx 1.26$ (b).

6.3 STM Response of the Armchair SWCNTs

Here we present results for the two-channel Luttinger liquid, with parameters suitable for modeling the armchair SWCNTs. To calculate the STM response we follow the same procedure as in the previous section, but now we use the bosonization scheme described in Sec. 3.4. We see that in the simplest case when the end of the

tube is modeled by an open boundary condition, we get the same qualitative behavior as for the single-channel Luttinger liquid case. The LSW is given by Eq. (6.9) also in this case, only the second term has opposite signs for different sublattices of the SWCNT. As a consequence all features of the LSW described in the previous section - *asymmetry, spin-charge peak structure, and thermal effects* - are present also in this case, and we therefore focus only on issues which are important for experimentally observing the distinctive features in the local tunneling conductance dI/dV.

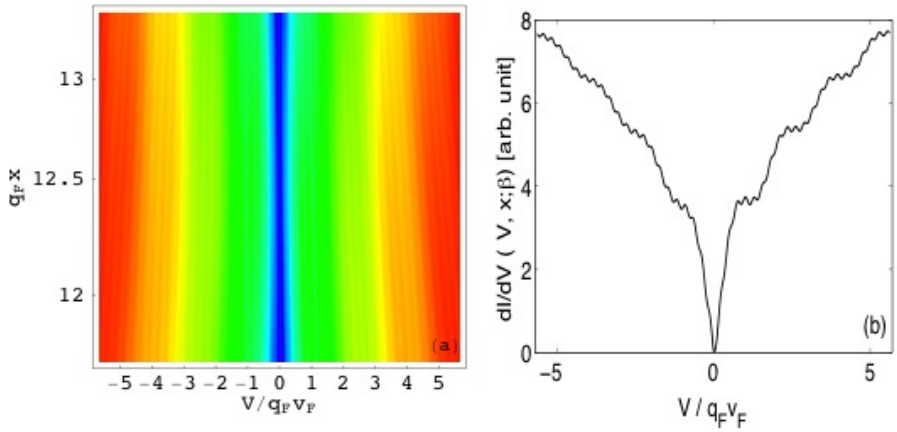

Figure 6.9: $dI/dV(V, x; \beta)$ for $T/q_F v_F \approx 5 \times 10^{-3}$, $K = 0.18$, $v_{c+}/v_F \approx 5$, $n_e = 0.1$, $\tilde{\gamma} = 0$ (a) and cut at $x = 150a$ (b).

The most conspicuous feature of the LSW in this case is the very large wavelength of the real space Friedel oscillations. Recall that these oscillations are caused by the spatial dependence of the phase factor in the second term of $A(\omega, x, ; \beta)$ (see Eq. (6.9)). Since the "effective" Fermi momentum q_F is much smaller than k_F [57], the resulting Friedel oscillations will have a wave length much larger than the lattice spacing. Thus, if one measures dI/dV from STM on an armchair tube over some finite range it is quite possible that the Friedel oscillations will not be visible at all. This property is well illustrated by the plot in the first panel of Fig. (6.9). We have here chosen a value of K_{c+} according to Eq. (3.64), with $\tilde{V}_0(q \approx 0)$ estimated from experimental data given in Ref. [107] (see also [57]). The second panel shows a "cut" at a fixed distance ($x = 150a$) from the boundary. By close inspection one can pinpoint five short wave length oscillations with energy (coming from the three slowly propagating modes $\phi_{s\pm}, \phi_{c-}$) per one long-wavelength oscillation (from the charge mode ϕ_{c+}), which is in agreement with the fact that $v_{c+}/v_F \approx 5$. It is clear from panel (b) that in order to experimentally resolve the peak structure one needs a voltage significantly larger than the width of the central dip. Alternatively, one can take the measurement further away from the boundary. However, since v_{c+}/v_F is large, there is only a small range of distances from the edge for which it is possible

to see the long- and short-wavelength oscillations at the same time.

When applying the results to SWCNTs several important issues should be taken into account. The dominant effect is the complicated interference pattern of the Bloch waves, which strongly depends on the geometry of the boundary condition and the chirality of the tubes [157]. Nonetheless, an enhanced velocity, a suppressed spectral weight and a characteristic power law of decaying oscillations are clear signatures of interaction effects which all have been seen in experiments [114]. A more complete theoretical analysis would also have to include the effects of backscattering, band structure, longer-range interactions and the mixing of the channels near the boundary. These problems are deferred to a future project.

6.4 Summary and Discussion

We have derived the full finite-temperature LSW for a Luttinger liquid with an edge or impurity (modeled as an open boundary condition), relevant to high-precision STM measurements. We have also generalized our approach to the "two-channel" case that describes SWCNTs in the Luttinger liquid regime, which is qualitatively similar to the single-channel case.

The LSW (determining the local differential tunneling conductance in STM measurements) exhibits a very rich structure as a function of temperature, distance from the impurity, and the strength of the electron interaction. Depending on the choice of parameters one is able to see *asymmetric Fano-like line shapes* and *spin and charge oscillations*. The Fano-like asymmetries are caused by an interplay of boundary and interaction effects, and, as shown in **Paper III**, are closely linked to the Friedel oscillations in real space. Spin and charge oscillations appear due to the interference of propagating spin and charge waves reflected from the boundary.

We have discussed how to consistently determine the key parameters of a Luttinger liquid (the interaction parameter K_c, and the spin and charge velocities) from experimental measurements of the tunneling conductance. We have also extensively discussed various thermal effects with focus on their influence on the Fano-like asymmetries and spin-charge oscillations in the LSW as a function of energy. The thermal suppression of the coherence of spin and charge waves makes it hard to detect interaction effects in the LSW and even more so in the local differential tunneling conductance (where the finite-temperature LSW gets weighted by the Fermi-Dirac distribution): For temperatures $T \gtrsim v_s/x$ (where v_s is the speed of the spin excitations, and x is the distance to the edge or the impurity) the characteristic power law behavior near the Fermi level is completely washed out and replaced by an interaction-independent analytic scaling. For these temperatures spin-charge separation also becomes virtually impossible to detect.

In conclusion, the results obtained in **Paper III** provide guidelines for identifying and interpreting signals of electron correlations in STM data on SWCNTs and other one-dimensional systems, and as such should be useful in the search for realizations of Luttinger liquid physics.

7

Boundary Behavior of Spin-Incoherent Interacting Electrons in 1D

7.1 Review of the Spin-Incoherent Regime

Recently the spin-incoherent regime of one-dimensional strongly interacting, very low density electrons has attracted a lot of interest [63, 64, 65]. For zero temperature the kinetic energy of an electron can be estimated by the Fermi energy $E_F = (\pi\hbar n)^2/8m$. For low densities, $n \ll a_B^{-1}$, the kinetic energy is small compared to the Coulomb potential energy $e^2 n/\epsilon$. Here ϵ is the dielectric constant and $a_B = \epsilon\hbar^2/me^2$ is the effective Bohr radius of the material. In the limit of low densities the system is driven to the *Wigner crystal* [62] regime, which can be viewed as a classical system of electrons placed equidistantly to minimize the potential energy. Quantum fluctuations induce an exponentially small antiferromagnetic spin exchange $J > 0$ between the electrons. In the extreme case, where $J \ll E_F$ is the smallest energy scale, the behavior of the system is that of *spin incoherent* [63, 64, 65] electrons. For nonzero temperatures the spin-incoherent regime is realize in the limit $J \ll T \ll E_F$. The physics of the spin-incoherent regime has been addressed using Bethe's Ansatz [63, 64] and a bosonized path integral approach [65]. Surprisingly, it was found that the spin incoherence dramatically influences the correlations of charge excitations, leading to a power-law decay in the charge sector with an interaction-dependent non-unitary exponent.

Here I will discuss the bosonization scheme introduced in Ref. [65] in more detail, since the calculations that follow are based on it. We have already seen in Sec. 3.5, that in the regime of $J \ll T \ll E_F$ the behavior of the system can be described as a system with decoupled spin and charge degrees of freedom. The charge sector can be described as spinless fermions and can be readily bosonized (see Sec. 3.5).

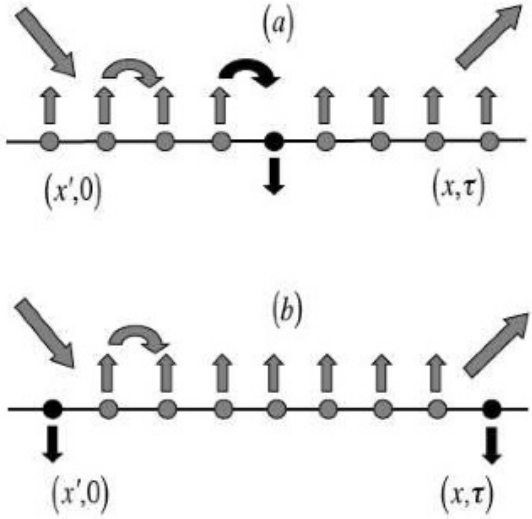

Figure 7.1: Two possible world line configurations: (a) excluded, since spin flip is not allowed and (b) allowed, since all intermediate electrons have the same spin.

The spin sector is described by a lattice of localized spins coupled via a Heisenberg Hamiltonian, which in the limit $J \ll T \ll E_F$ represents the massively degenerate spin incoherent system.

Since we are calculating the Green's function for spinful electrons

$$G(x,\tau) = \langle \Psi_\sigma(x,\tau)\Psi^\dagger_\sigma(0,0)\rangle \tag{7.1}$$

we will first do a nontrivial averaging in the spin sector and then in the charge sector using the bosonization scheme presented in Sec. 3.5. The spin averaging can be done using a *first quantized path integral* representation for $G(x,\tau)$, with spin-up electron world lines inserted at $(0,0)$ and removed at (x,τ). Large Coulomb repulsion restricts the topology of the electron world lines to *noncrossing* paths, which is identical to those of spinless fermions. This restriction demands that in order for an electron created at coordinate $(0,0)$ to be annihilated at a large distance (x,τ), all intermediate world lines should have the same spin (see Fig. 7.1). For N intermediate world lines, the probability that $N+1$ spins are the same is 2^{-N}. Since in the limit $J \ll T$ all spin configurations have the same weight after spin averaging the Green's function has the form

$$G(x,\tau) \;=\; \langle 2^{-N(x,\tau)}\Psi(x,\tau)\Psi^\dagger(0,0)\rangle, \tag{7.2}$$

where the average is taken in the charge sector and where $N(x,\tau)$ is given by

$$N(x,\tau) = n|x| + \frac{1}{\sqrt{\pi}}(\varphi(x,\tau) - \varphi(0,0)), \tag{7.3}$$

as can be easily seen from Eq. (3.74).

One should note that the Green's function in Eq. (7.2) is written in a different but equivalent form compared to the one given in Ref. [65]. Our formulation is more general and can be readily generalized for the case of spin-incoherent electrons in the presence of boundaries and impurities.

7.2 Boundary Green's Function

We shall here focus on the case of a 1D semi-infinite electron system with an open boundary condition (OBC) at one end. To calculate the Green's function we follow the procedure described in the previous section. The calculation of the Green's function then translates into the calculation of the following correlator for spinless fermions:

$$\begin{aligned} G(x,x',\tau) &= \langle 2^{-N(x,x',\tau)}\Psi(x,\tau)\Psi^\dagger(x',0)\rangle \\ &= G_{LL}(x,x',\tau) + G_{RR}(x,x',\tau) + G_{LR}(x,x',\tau) + G_{RL}(x,x',\tau), \end{aligned} \tag{7.4}$$

where

$$G_{\ell\ell'}(x,x',\tau) = \langle 2^{-N(x,x',\tau)}\psi_\ell(x,\tau)\psi^\dagger_{\ell'}(x',0)\rangle \quad \ell,\ell' = L,R. \tag{7.5}$$

We see that LR and RL terms appear in addition to the LL and RR contributions, which is a generic feature when an impurity or a boundary is present in a 1D system system (cf. the similar calculation in **Paper III**). Since the translational symmetry is broken, the Green's function does not depend only on relative coordinate as in Eq. (7.1).

Eq. (7.4) is straightforwardly calculated using the bosonic Hamiltonian in Eq. (3.77). It is convenient to introduce relative (r) and center-of-mass (R) coordinates

$$\begin{aligned} r &= x - x' \\ R &= \frac{x+x'}{2}, \end{aligned} \tag{7.6}$$

which makes it easier to separate boundary and bulk contributions.

The four correlators in Eq. (7.5) are calculated using the bosonization formula (3.78) given in the Sec. 3.5 (cf. the analogous calculations in **Paper III**). The Green's function gets modified due to the boundary, which can be seen in the LL piece

$$\begin{aligned} G_{LL}(x,x',\tau) &= \langle 2^{-N(x,x',\tau)}\psi_L(x,\tau)\psi^\dagger_L(x',0)\rangle \\ &= \frac{1}{2\pi\alpha} e^{-\frac{\ln 2}{\pi}\tilde{k}_F|r|} e^{-i\tilde{k}_F r} e^{i\zeta_{LL}} \\ &\times \frac{1}{(\alpha\ \mathrm{sign}\tau + v_c\tau + ir)} \frac{1}{((\alpha\ \mathrm{sign}\tau + v_c\tau)^2 + r^2)^{-2\Delta_1+2\Delta_2}} \\ &\times \left(\frac{\sqrt{(\alpha^2+(2R+r)^2)(\alpha^2+(2R-r)^2)}}{(\alpha\ \mathrm{sign}\tau + v_c\tau)^2 + 4R^2} \right)^{2\Delta_1+2\Delta_3}, \end{aligned} \tag{7.7}$$

where the phase factor ζ_{LL} has the form

$$\begin{aligned}\zeta_{LL} &= \frac{\ln 2}{4\pi}K\left(\ln\frac{(\alpha^2+(2R+r)^2)(\alpha^2+(2R-r)^2)}{((\alpha\ \mathrm{sign}\tau+v_c\tau)^2+4R^2)^2}+2\ln\frac{(\alpha\ \mathrm{sign}\tau+v_c\tau)^2+r^2}{\alpha^2}\right)\\ &+ \frac{\ln 2}{4\pi}\left(\ln\frac{(\alpha-i(r+2R))(\alpha-i(r-2R))}{(\alpha+i(r+2R))(\alpha+i(r-2R))}+2\ln\frac{\alpha\ \mathrm{sign}\tau+v_c\tau+ir}{\alpha\ \mathrm{sign}\tau+v_c\tau-ir}\right). \quad (7.8)\end{aligned}$$

We see the exponential decay in the spin sector with power law decaying part in charge sector, which we anticipated. In addition we see that the charge part gets modified by the presence of the boundary: the factor in the brackets in Eq. (7.7) is the boundary effect.

The LR part of the Green's function, which is a pure boundary effect, can also be readily obtained and has the following form

$$\begin{aligned}G_{LR}(x,x',\tau) &= \langle 2^{-N(x,x',\tau)}\psi_L(x,\tau)\psi_R^\dagger(x',0)\rangle\\ &= e^{-\frac{\ln 2}{\pi}\tilde{k}_F|r|}e^{-i2\tilde{k}_FR}e^{i\zeta_{LR}}\\ &\times \frac{1}{(\alpha\ \mathrm{sign}\tau+v_c\tau+i2R)}\frac{1}{((\alpha\ \mathrm{sign}\tau+v_c\tau)^2+4R^2)^{2\Delta_1+2\Delta_2}}\\ &\times \left(\sqrt{(\alpha^2+(2R+r)^2)(\alpha^2+(2R-r)^2)}((\alpha\ \mathrm{sign}\tau+v_c\tau)^2+r^2)\right)^{2\Delta_1}\\ &\times \left(\frac{\sqrt{(\alpha^2+(2R+r)^2)(\alpha^2+(2R-r)^2)}}{(\alpha\ \mathrm{sign}\tau+v_c\tau)^2+r^2}\right)^{2\Delta_3}, \quad (7.9)\end{aligned}$$

where the phase factor ζ_{LR} reads

$$\begin{aligned}\zeta_{LR} &= \frac{\ln 2}{4\pi}K\ln\frac{\alpha^2+(2R+r)^2}{\alpha^2+(2R-r)^2}\\ &+ \frac{\ln 2}{4\pi}\left(\ln\frac{(\alpha-i(r+2R))(\alpha-i(r-2R))}{(\alpha+i(r+2R))(\alpha+i(r-2R))}+2\ln\frac{\alpha\ \mathrm{sign}\tau+v_c\tau+ir}{\alpha\ \mathrm{sign}\tau+v_c\tau-ir}\right) \quad (7.10)\end{aligned}$$

The exponents in Eqs. (7.7) and (7.9) are given by the following expressions:

$$\begin{aligned}\Delta_1 &= \frac{K}{8}\left(\frac{\ln 2}{\pi}\right)^2,\\ \Delta_2 &= \frac{1}{8}\left(\frac{1}{K}+K-2\right), \quad (7.11)\\ \Delta_3 &= \frac{1}{8}\left(\frac{1}{K}-K\right),\end{aligned}$$

where the exponent Δ_1 is modified due to the spin averaging performed in Eq. (7.4) (cf. to Eq. (26) in **Paper III**).

Using the expressions for G_{LL} and G_{LR} in Eqs. (7.7) and (7.9), respectively, we can immediately write the corresponding expressions for the RR and the RL pieces of the Green's function:

$$\begin{aligned}G_{RR}(x,x',\tau) &= G^*_{RR}(x,x',\tau),\\ G_{RL}(x,x',\tau) &= G^*_{LR}(x,x',\tau). \quad (7.12)\end{aligned}$$

Having obtained the full expression for the boundary Green's function we can now study the boundary and bulk regimes by taking the proper limits. The bulk Green's function is obtained from Eq. (7.4) by taking the $R \to \infty$ limit. For the G_{LL} piece we then recover the same expression as in Refs. [63, 65]:

$$\begin{aligned} G_{LL}(x,x',\tau) &= \frac{1}{2\pi\alpha} e^{-\frac{\ln 2}{\pi}\tilde{k}_F|r|} e^{-i\tilde{k}_F r} e^{i\zeta_{LL}} \\ &\times \frac{1}{(\alpha\ \mathrm{sign}\tau + v_c\tau + ir)} \frac{1}{((\alpha\ \mathrm{sign}\tau + v_c\tau)^2 + r^2)^{-2\Delta_1+2\Delta_2}}. \end{aligned} \tag{7.13}$$

On the other hand G_{LR} decays as a power-law and disappears in the bulk limit:

$$G_{LR}(x,x',\tau) \sim \frac{1}{R^K} \tag{7.14}$$

For the boundary case, when $v_c\tau >> r, R$:

$$\begin{aligned} G_{LL}(x,x',\tau) &\sim \frac{1}{\tau^{1/K}} \\ G_{LR}(x,x',\tau) &\sim \frac{1}{\tau^{1/K}}. \end{aligned} \tag{7.15}$$

The boundary exponent $\Delta_{boundary} = 1/K$ obtained by us is the same as that found in Refs. [158, 159, 160], where the Green's function was directly calculated in the above extreme boundary case.

7.3 Summary and Discussion

We have studied the boundary behavior of spin-incoherent interacting electrons in one dimension. Our effective low-energy bosonization approach for strongly interacting systems (see Sec. 3.5) allowed us to generalize the approach to boundary systems. We have derived the *full* boundary Green's function, and shown that it has the correct limiting behavior in boundary as well as bulk regimes. Our result, obtained in **Paper IV**, not only reproduces known result in boundary and bulk regimes, respectively, it also allows the study of the crossover regimes not addressed before. Having access to the full Green's function will be very important for the study of phenomena appearing at intermediate times, as measured on the scale defined by the distance to the boundary.

Bibliography

[1] P.W. Anderson, "More is Different," *Science* **177** (1972) 393–396.

[2] A.C. Hewson, *The Kondo Problem to Heavy Fermions.* Cambridge University Press (Cambridge), 1993.

[3] W.J. de Haas and J. de Boer, "The Electrical Resistance of Platinum at Low Temperatures," *Physica* **1** (1934) 609.

[4] W.J. de Haas, J. de Boer, and G.J. van den Berg, "The Electrical Resistance of Gold, Copper and Lead at Low Temperatures," *Physica* **1** (1934) 1115.

[5] J. Kondo, "Resistance Minimum in Dilute Magnetic Alloys," *Prog. Theor. Phys.* **32** (1964) 37.

[6] P.W. Anderson and G. Yuval, "Exact Results in the Kondo Problem: Equivalence to a Classical One-Dimensional Coulomb Gas," *Phys. Rev. Lett.* **23** (1969) 89–92.

[7] G. Yuval and P.W. Anderson, "Exact Results for the Kondo Problem: One-Body Theory and Extension to Finite Temperature," *Phys. Rev. B* **1** (1970) 1522–1528.

[8] P.W. Anderson, G. Yuval, and D.R. Hamann, "Exact Results in the Kondo Problem. II. Scaling Theory, Qualitatively Correct Solution, and Some New Results on One-Dimensional Classical Statistical Models," *Phys. Rev. B* **1** (1970) 4464–4473.

[9] P.W. Anderson, "A Poor Man's Derivation of Scaling Laws for the Kondo Problem," *J. Phys. C: Solid State Phys.* **3** (1970) 2436–2441.

[10] K.G. Wilson, "Renormalization Group-Critical Phenomena and Kondo Problem," *Rev. Mod. Phys.* **47** (1975) 773–840.

[11] P. Noziéres, "A "Fermi-Liquid" Description of the Kondo Problem at Low Temperatures," *J. Low Temp.* **17** (1974) 31–42.

[12] N. Andrei, "Diagonalization of the Kondo Hamiltonian," *Phys. Rev. Lett.* **45** (1980) 379–382.

[13] P. Wiegmann, "Exact Solution of the $s-d$ Exchange Model at $T=0$," *Pisma Eksp. Teor. Fiz* **31** (1980) 392–398.

[14] P. Noziéres and A. Blandin, "Kondo Effect in Real Metals," *J. de Phys.* **41** (1980) 193–211.

[15] N. Andrei and C. Destri, "Solution of the Multichannel Kondo Problem," *Phys. Rev. Lett.* **52** (1984) 364–367.

[16] A.M. Tsvelik and P.B. Wiegmann, "Solution of the N-Channel Kondo Problem (Scaling and Integrability)," *Z. Phys. B* **54** (1984) 201–206.

[17] I. Affleck and A.W.W. Ludwig, "Critical Theory of Overscreened Kondo Fixed Point," *Nucl. Phys.* **360** (1991) 641–696.

[18] L. Kouwenhoven and L. Glazman, "Revival of the Kondo Effect," *Physics World* (Jan, 2001) 33–38.

[19] G.M. Whitesides and J.C. Love, "The Art of Building Small," *Scientific American* (Sep, 2001) 39–47.

[20] M.A. Kastner, "Artificial Atoms," *Physics Today* (Jan, 1993) 24–31.

[21] L. Kouwenhoven and C. Marcus, "Quantum Dots," *Physics World* (Jun, 1998) 35–39.

[22] L.I. Glazman and M.E. Raikh, "Resonant Kondo Transparency of a Barrier with Quasilocal Impurity States," *JETP Letters* **47** (1988) 452–455.

[23] T.K. Ng and P.A. Lee, "On-Site Coulomb Repulsion and Resonant Tunneling," *Phys. Rev. Lett.* **61** (1988) 1768–1771.

[24] I.O. Kulik and R.I. Shekhter, "Kinetic Phenomena and Charge Discreteness Effects in Granulated Media," *Sov. Phys. JETP* **41** (1975) 308–316.

[25] M. Pustilnik, L.I. Glazman, D.H. Cobden, and L.P. Kouwenhoven, "Magnetic-Field-Induced Kondo Effects in Coulomb Blockade Systems," *Lecture Notes in Physics* **579** (2001) 3–24.

[26] K.A. Matveev, "Quantum Fluctuations of the Charge of a Metal Particle Under the Coulomb Blockade," *Sov. Phys. JETP* **72** (1991) 892–899.

[27] D. Goldhaber-Gordon, H. Shtrikman, D. Mahalu, D. Abusch-Magder, U. Meirav, and M.A. Kastner, "Kondo Effect in a Single-electron Transistor," *Nature* **391** (1998) 156–159.

[28] S.M. Cronenwett, T.H. Oosterkamp and L.P. Kouwenhoven, "A Tunable Kondo Effect in Quantum Dots," *Science* **281** (1998) 540–544.

[29] W.G. van der Wiel, S. De Franceschi, T. Fujisawa, J.M. Elzerman, S. Tarucha, and L.P. Kouwenhoven, "The Kondo Effect in the Unitary Limit," *Science* **289** (2000) 2105–2108.

[30] J. Nygård, D.H. Cobden, and P.E. Lindelof, "Kondo Physics in Carbon Nanotubes," *Nature* **408** (2000) 342–346.

[31] I. Affleck, A.W.W. Ludwig, H.-B. Pang, and D.L. Cox, "Relevance of Anisotropy in the Multichannel Kondo Effect: Comparison of Conformal Field Theory and Numerical Renormalization-Group Results," *Phys. Rev. B* **45** (1992) 7918–7935.

[32] K. Le Hur, "Kondo Effect in Crossed Luttinger Liquids," *Phys. Rev. B* **61** (2000) 1853–1858.

[33] E. Lebanon, A. Schiller, and V. Zevin, "Noncrossing Approximation for the Anisotropic Kondo Model: Charge Fluctuations in a Quantum Box," *Phys. Rev. B* **64** (2001) 245338.

[34] K. Le Hur and G. Seelig, "Capacitance of a Quantum Dot from the Channel-Anisotropic Two-Channel Kondo Model," *Phys. Rev. B* **65** (2002) 165338.

[35] Y. Oreg and D. Goldhaber-Gordon, "Two-Channel Kondo Effect in a Modified Single Electron Transistor," *Phys. Rev. Lett* **90** (2003) 136602.

[36] E. Lebanon, A. Schiller, and F.B. Anders, "Enhancement of the Two-Channel Kondo Effect in Single-Electron Boxes," *Phys. Rev. B* **68** (2003) 155301.

[37] F.B. Anders, E. Lebanon, and A. Schiller, "Coulomb Blockade and Non-Fermi-Liquid Behavior in Quantum Dots," *Phys. Rev. B* **70** (2004) 201306(R).

[38] C.J. Bolech and N. Shah, "Prediction of the Capacitance Line Shape in Two-Channel Quantum Dots," *Phys. Rev. Lett* **95** (2005) 036801.

[39] P. Simon, J. Salomez, and D. Feinberg, "Transport Spectroscopy of a Kondo quantum dot coupled to a finite size grain," *ArXiv, cond-mat/0602172* (2006).

[40] I. Rau, R. Potok, and D. Goldhaber-Gordon, "The Two-Channel Kondo Effect in a Semiconductor Nanostructure," *unpublished* (2006). Talk at the APS March Meeting in Baltimore.

[41] D. Pines and P. Noziéres, *The Theory of Quantum Liquids*, vol. I. Addison-Wesley Publishing (New York), 1966.

[42] R. Shankar, "Renormalization-Group Approach to Interacting Fermions," *Rev. Mod. Phys.* **66** (1994) 129–192.

[43] C.M. Varma, Z. Nussinov, and W. van Saarloos, "Singular or Non-Fermi Liquids," *Phys. Rep.* **361** (2002) 267–417.

[44] D. Sénéchal, "An Introduction to Bosonization," *Cond-Mat/9908262* (1999).

[45] F.D.M. Haldane, ""Luttinger Liquid Theory" of One-Dimensional Quantum Fluids: I. Properties of the Luttinger Model and their Extension to the general 1D Interacting Spinless Fermi Gas," *J. Phys. C: Solid State Phys.* **14** (1981) 2585–2609.

[46] P. Jordan and E. Wigner, "Über das Paulische Äquivalenzverbot," *Z. Phys.* **47** (1928) 631–651.

[47] E. Lieb, T. Schultz, and D. Mattis, "Two Soluble Models of an Antiferromagnetic Chain," *Ann. Phys.* **16** (1961) 407–466.

[48] S. Tomonaga, "Remarks on Bloch's Method of Sound Waves Applied to Many-Fermion Problems," *Prog. Theor. Phys.* **5** (1950) 544.

[49] J.M. Luttinger, "An Exactly Soluble Model of a Many-Fermion System," *J. Math. Phys.* **4** (1963) 1154.

[50] A.O. Gogolin, A.A. Nersesyan, and A.M. Tsvelik, *Bosonization and Strongly Correlated Systems.* Cambridge University Press (Cambridge), 1998.

[51] T. Giamarchi, *Quantum Physics in One Dimension.* Oxford University Press (Oxford), 2004.

[52] P. Di Francesco, P. Mathieu, and D. Sénéchal, *Conformal Field Theory.* Graduate Texts in Contemporary Physics. Springer-Verlag (New York), 1997.

[53] E. Witten, "Non-Abelian Bosonization in 2 Dimensions," *Commun. in Math. Phys.* **92** (1984) 455–472.

[54] M. Fabrizio and A.O. Gogolin, "Interacting One-Dimensional Electron Gas with Open Boundaries," *Phys. Rev. B* **51** (1995) 17827–17841.

[55] S. Eggert and I. Affleck, "Magnetic Impurities in Half-Integer-Spin Heisenberg Antiferromagnetic Chains," *Phys. Rev. B* **46** (1992) 10866–10883.

[56] V. Meden , W. Metzner, U. Schollwöck, O. Schneider, T. Stauber, K. Schönhammer, "Luttinger Liquids with Boundaries: Power-Laws and Energy Scales," *Eur. Phys. J. B* **16** (2000) 631–646.

[57] R. Egger and A.O. Gogolin, "Correlated Transport and Non-Fermi-Liquid Behavior in Single-Wall Carbon Nanotubes," *Eur. Phys. J. B* **3** (1998) 281–300.

[58] R. Egger and A.O. Gogolin, "Effective Low-Energy Theory for Correlated Carbon Nanotubes," *Phys. Rev. Lett.* **79** (1997) 5082–5085.

[59] L. Balents and M.P.A. Fisher, "Correlation Effects in Carbon Nanotubes," *Phys. Rev. B* **55** (1997) R11973–R11976.

[60] R. Saito, G. Dresselhaus, and M.S. Dresselhaus, *Physical Properties of Carbon Nanotubes*. Imperial College Press, London, 1998.

[61] H.J. Schulz, G. Cuniberti, and P. Pieri, *Fermi Liquids and Luttinger Liquids*. In *Field Theories for Low-Dimensional Condensed Matter Systems - Spin Systems and Strongly Correlated Electrons*. Springer, 2000.

[62] H. J. Schulz, "Wigner Crystal in One Dimension," *Phys. Rev. Lett.* **71** (1993) 1864–1867.

[63] V.V. Cheianov and M.B. Zvonarev, "Nonunitary Spin-Charge Separation in a One-Dimensional Fermion Gas," *Phys. Rev. Lett.* **92** (2004) 176401.

[64] V.V. Cheianov and M.B. Zvonarev, "Zero Temperature Correlation Functions for the Impenetrable Fermion Gas," *J. Phys. A: Math. Gen.* **37** (2004) 2261–2297.

[65] G.A. Fiete and L. Balents, "Green's Function for Magnetically Incoherent Interacting Electrons in One Dimension," *Phys. Rev. Lett.* **93** (2004) 226401.

[66] K.A. Matveev, "Conductance of a Quantum Wire at Low Electron Density," *Phys. Rev. B* **70** (2004) 245319.

[67] J. Voit, "One-Dimensional Fermi Liquids," *Rep. Prog. Phys.* **58** (1995) 977–1116.

[68] C. Bourbonnais and D. Jérome, "One-Dimensional Conductors," *Physics World* (September, 1998) 41–45.

[69] B. Dardel, D. Malterre, M. Grioni, P. Weibel, Y. Baer, J. Voit, and D. Jérome, "Possible Observation of a Luttinger-Liquid Behavior from Photoemission Spectroscopy of One-Dimensional Organic Conductors," *Europhys. Lett.* **24** (1993) 687–692.

[70] P. Wzietek, F. Creuzet, C. Bourbonnais, D. Jérome, K. Bechgaard, and P. Batail, "Nuclear Relaxation and Electronic Correlations in Quasi-One-Dimensional Organic Conductors. II. Experiments," *J. Phys. I France* **3** (1993) 171–201.

[71] S. Eggert, H. Johannesson, and A. Mattsson, "Boundary Effects on Spectral Properties of Interacting Electrons in One Dimension," *Phys. Rev. Lett.* **76** (1996) 1505–1508.

[72] Y. Hwu, P. Alméras, M. Marsi, H. Berger, F. Lévy, M. Grioni, D. Malterre, and G. Margaritondo, "Photoemission Near the Fermi Energy in One Dimension," *Phys. Rev. B* **46** (1992) 13624–13626.

[73] M. Nakamura, A. Sekiyama, H. Namatame, A. Fujimori, H. Yoshihara, T. Ohtani, A. Misu, and M. Takano, "Metal-Semiconductor Transition and Luttinger-Liquid Behavior in Quasi-One-Dimensional $BaVS_3$ Studied by Photoemission Spectroscopy," *Phys. Rev. B* **49** (1994) 16191–16201.

[74] B. Dardel, D. Malterre, M. Grioni, P. Weibel, Y. Baer, and F. Lévy, "Unusual Photoemission Spectral Function of Quasi-One-Dimensional Metals," *Phys. Rev. Lett.* **67** (1991) 3144–3147.

[75] R.B. Laughlin, "Anomalous Quantum Hall Effect: An Incompressible Quantum Fluid with Fractionally Charged Excitations," *Phys. Rev. Lett.* **50** (1983) 1395–1398.

[76] B. I. Halperin, "Quantized Hall Conductance, Current-Carrying Edge States, and the Existence of Extended States in a Two-Dimensional Disordered Potential," *Phys. Rev. B* **25** (1982) 2185–2190.

[77] X.-G. Wen, "Topological Orders and Edge Excitations in Fractional Quantum Hall States," *Adv. Phys.* **44** (1995) 405–473.

[78] F.P. Milliken, C.P. Umbach, and R.A. Webb, "Indications of a Luttinger Liquid in the Fractional Quantum Hall Regime," *Solid State Commun.* **97** (1996) 309–313.

[79] A.M. Chang, L.N. Pfeiffer, and K.W. West, "Observation of Chiral Luttinger Behavior in Electron Tunneling into Fractional Quantum Hall Edges," *Phys. Rev. Lett.* **77** (1996) 2538–2541.

[80] A. M. Chang, M. K. Wu, C. C. Chi, L. N. Pfeiffer, and K. W. West, "Plateau Behavior in the Chiral Luttinger Liquid Exponent," *Phys. Rev. Lett.* **86** (2001) 143–146.

[81] X.-G. Wen, "Chiral Luttinger Liquid and the Edge Excitations in the Fractional Quantum Hall States," *Phys. Rev. B* **41** (1990) 12838–12844.

[82] X.-G. Wen, "Theory of the Edge States in Fractional Quantum Hall-Effects," *Int. J. Mod. Phys. B* **6** (1992) 1711–1762.

[83] C.L. Kane, "Transmission Through Barriers and Resonant Tunneling in an Interacting One-Dimensional Electron Gas," *Phys. Rev. B* **46** (1992) 15233–15262.

[84] A. M. Chang, "Chiral Luttinger Liquids at the Fractional Quantum Hall Edge," *Rev. Mod. Phys.* **75** (2003) 1449–1505.

[85] M. Grayson, D. C. Tsui, L. N. Pfeiffer, K. W. West, and A. M. Chang, "Continuum of Chiral Luttinger Liquids at the Fractional Quantum Hall Edge," *Phys. Rev. Lett.* **80** (1998) 1062–1065.

[86] Xin Wan, F. Evers, and E. H. Rezayi, "Universality of the Edge-Tunneling Exponent of Fractional Quantum Hall Liquids," *Phys. Rev. Lett.* **94** (2005) 166804.

[87] C.W.J. Beenakker and H. van Houten, *Quantum Transport in Semiconductor Nanostructures*, vol. 44 of *Solid State Physics Advances in Research and Applications*. Academic Press (New York), 1991.

[88] L. Pfeiffer, K.W. West, H.L. Stormer, J.P. Eisenstein, K.W. Baldwin, D. Gershoni, and J. Spector , "Formation of a High Quality Two-Dimensional Electron Gas on Cleaved GaAs," *Appl. Phys. Lett* **56** (1990) 1697–1699.

[89] S. Tarucha, T. Honda, and T. Saku, "Reduction of Quantized Conductance at Low Temperatures Observed in 2 to 10μ m-long Quantum Wires," *Solid State Commun.* **94** (1995) 413–418.

[90] A. Yacoby, H.L. Stormer, N.S. Wingreen, L.N. Pfeiffer, K.W. Baldwin, and K.W. West, "Nonuniversal Conductance Quantization in Quantum Wires," *Phys. Rev. Lett.* **77** (1996) 4612–4615.

[91] C. L. Kane and M.P.A. Fisher, "Transport in a One-Channel Luttinger Liquid," *Phys. Rev. Lett.* **68** (1992) 1220–1223.

[92] M. Ogata and H. Fukuyama, "Collapse of Quantized Conductance in a Dirty Tomonaga-Luttinger Liquid," *Phys. Rev. Lett.* **73** (1994) 468–471.

[93] D.L. Maslov and M. Stone, "Landauer Conductance of Luttinger Liquids with Leads," *Phys. Rev. B* **52** (1995) R5539–R5542.

[94] V. Ponomarenko, "Renormalization of the One-Dimensional Conductance in the Luttinger-Liquid Model," *Phys. Rev. B* **52** (1995) R8666–R8667.

[95] I. Safi and H.J. Schulz, "Transport in an Inhomogeneous Interacting One-Dimensional System," *Phys. Rev. B* **52** (1995) R17040–R17043.

[96] A.M. Chang, "Resistance of a Perfect Wire," *Nature* **411** (2001) 39 – 40.

[97] R. de Picciotto, H.L. Stormer, L.N. Pfeiffer, K.W. Baldwin, and K.W. West, "Four-Terminal Resistance of a Ballistic Quantum Wire," *Nature* **411** (2001).

[98] M. Rother, W. Wegscheider, R. A. Deutschmann, M. Bichler, and G. Abstreiter, "Evidence of Luttinger Liquid Behavior in GaAs/AlGaAs Quantum Wires," *Physica E* **6** (2000) 551–554.

[99] S.V. Zaitsev-Zotov, Yu. A. Kumzerov, Yu. A. Firsov, and P. Monceau, "Luttinger-Liquid-Like Transport in Long InSb Nanowires," *J. Phys.: Condens. Matter* **12** (2000) L303–L309.

[100] O.M. Auslaender, A. Yacoby, R. de Picciotto, K.W. Baldwin, L.N. Pfeiffer, and K. W. West, "Tunneling Spectroscopy of the Elementary Excitations in a One-Dimensional Wire," *Science* **295** (2002) 825–828.

[101] A.N. Aleshin, H.J. Lee, Y.W. Park, and K. Akagi, "One-Dimensional Transport in Polymer Nanofibers," *Phys. Rev. Lett.* **93** (2004) 196601.

[102] E. Slot, M.A. Holst, H.S.J. van der Zant, and S.V. Zaitsev-Zotov, "One-Dimensional Conduction in Charge-Density-Wave Nanowires," *Phys. Rev. Lett.* **93** (2004) 176602.

[103] L. Venkataraman, Y.S. Hong, and P. Kim, "Electron Transport in a Multichannel One-Dimensional Conductor: Molybdenum Selenide Nanowires," *Phys. Rev. Lett.* **96** (2006) 076601.

[104] S. Iijima, "Helical Microtubules of Graphitic Carbon," *Nature* **354** (1991) 56.

[105] C.L. Kane, L. Balents, and M.P.A. Fisher, "Coulomb Interactions and Mesoscopic Effects in Carbon Nanotubes," *Phys. Rev. Lett.* **79** (1997) 5086–5089.

[106] C. Dekker, "Carbon Nanotubes as Molecular Quantum Wires," *Physics Today* **52** (1999), no. 5, 22–28.

[107] S.J. Tans, M.H. Devoret, H. Dai, A. Thess, R.E. Smalley, L.J. Geerligs, and C. Dekker, "Individual Single-Wall Carbon Nanotubes as Quantum Wires," *Nature* **386** (1997) 474–477.

[108] M. Bockrath, D.H. Cobden, P.L. McEuen, N.G. Chopra, A. Zettl, A. Thess, and R.E. Smalley , "Single-Electron Transport in Ropes of Carbon Nanotubes," *Science* **175** (1997) 1922–1925.

[109] J.W.G. Wildöer, L.C. Venema, A.G. Rinzler, R.E. Smalley, and C. Dekker, "Electronic Structure of Atomically Resolved Carbon Nanotubes," *Nature* **391** (1998) 59–62.

[110] T.W. Odom, J.-L. Huang, P. Kim, and C.M. Lieber, "Atomic Structure and Electronic Properties of Single-Walled Carbon Nanotubes," *Nature* **391** (1998) 62–64.

[111] Yu.A. Krotov, D.-H. Lee, and S.G. Louie, "Low Energy Properties of (n,n) Carbon Nanotubes," *Phys. Rev. Lett.* **78** (1997) 4245–4248.

[112] S.J. Tans, M.H. Devoret, R.J.A. Groeneveld, and C. Dekker, "Electron-Electron Correlations in Carbon Nanotubes," *Nature* **395** (1998) 761–764.

[113] M. Bockrath, D.H. Cobden, J. Lu, A.G. Rinzler, R.E. Smalley, L. Balents, and P.L. MacEuen, "Luttinger-Liquid Behaviour in Carbon Nanotubes," *Nature* **397** (1999) 598–601.

[114] J. Lee, S. Eggert, H. Kim, S.-J. Kahng, H. Shinohara, and Y. Kuk, "Real Space Imaging of One-Dimensional Standing Waves: Direct Evidence for a Luttinger Liquid," *Phys. Rev. Lett.* **93** (2004) 166403.

[115] J.L. Cardy, "Conformal Invariance and Universality in Finite-Size Scaling," *J. Phys. A: Math. Gen.* **17** (1984) L385–L387.

[116] J.L. Cardy, "Conformal Invariance and Surface Critical Behavior," *Nucl. Phys. B* **240** (1984) 514–532.

[117] J.L. Cardy, "Boundary Conditions, Fusion Rules and the Verlinde Formula," *Nucl. Phys. B* **324** (1989) 581–596.

[118] I. Affleck, "Conformal Field Theory Approach to the Kondo Effect," *Acta Phys. Polon. B* **26** (1995) 1869–1932.

[119] R.J. Schoelkopf, P. Wahlgren, A.A. Kozhevnikov, P. Delsing, and D.E. Prober, "The Radio-Frequency Single-Electron Transistor (RF-SET): A Fast and Ultrasensitive Electrometer," *Science* **280** (1998) 1238–1242.

[120] W. Lu, Z. Ji, L. Pfeiffer, K.W. West, and A.J. Rimberg, "Real-Time Detection of Electron Tunnelling in a Quantum Dot," *Nature* **423** (2003) 422–425.

[121] T. Duty, G. Johansson, K. Bladh, D. Gunnarsson, C. Wilson, and P. Delsing, "Observation of Quantum Capacitance in the Cooper-Pair Transistor," *Phys. Rev. Lett.* **95** (2005) 206807.

[122] D.-H. Lee and J. Toner, "Kondo Effect in a Luttinger Liquid," *Phys. Rev. Lett.* **69** (1992) 3378–3381.

[123] A. Furusaki and N. Nagaosa, "Kondo Effect in a Tomonaga-Luttinger Liquid," *Phys. Rev. Lett.* **72** (1994) 892–895.

[124] P. Fröjdh and H. Johannesson, "Kondo Effect in a Luttinger Liquid: Exact Results from Conformal Field Theory," *Phys. Rev. Lett.* **75** (1995) 300–303.

[125] P. Fröjdh and H. Johannesson, "Magnetic Impurity in a Luttinger Liquid: A Conformal Field Theory Approach," *Phys. Rev. B* **53** (1996) 3211–3236.

[126] R. Egger and A. Komnik, "Scaling and Criticality of the Kondo Effect in a Luttinger Liquid," *Phys. Rev. B* **57** (1998) 10620–10629.

[127] M. Granath and H. Johannesson, "Two-Channel Kondo Effect in a Luttinger Liquid," *Z. Phys. B* **103** (1997) 225–229.

[128] M. Granath and H. Johannesson, "Multichannel Kondo Effect in an Interacting Electron System: Exact Results for the Low-Temperature Thermodynamics," *Phys. Rev. B* **57** (1998) 987–992.

[129] A. Furusaki and K.A. Matveev, "Occupation of a Resonant Level Coupled to a Chiral Luttinger Liquid," *Phys. Rev. Lett.* **88** (2002) 226404.

[130] E.B. Kolomeisky, R.M. Konik, and X. Qi, "Quantum Fluctuations of Charge and Phase Transitions of a Large Coulomb-Blockaded Quantum Dot," *Phys. Rev. B* **66** (2002) 075318.

[131] E.H. Kim, Y.B. Kim, C. Kallin, "From Quantum Critical to Two-Channel Kondo Physics via Charge Fluctuations in a Quantum Dot," *J. Phys.: Condens. Matter* **15** (2003) 7047–7053.

[132] G.D. Mahan, *Many-Particle Physics*. Kluwer Academic/Plenum Publishers (New York), 3rd ed., 2000.

[133] G. Zaránd, T. Costi, A. Jeres, and N. Andrei, "Thermodynamics of the Anisotropic Two-channel Kondo Problem," *Phys. Rev. B* **65** (2002) 134416.

[134] A.R. Goñi, A. Pinczuk, J.S. Weiner, B.S. Dennis, L.N. Pfeiffer, and K.W. West, "Observation of Magnetoplasmons, Rotons, and Spin-Flip Excitations in GaAs Quantum Wires," *Phys. Rev. Lett.* **70** (1993) 1151–1154.

[135] X. Wang, R. Egger, and H. Grabert, "Coulomb Charging Energy for Arbitrary Tunneling Strength," *Europhys. Lett.* **38** (1997) 545–550.

[136] F.J. Wegner, "Corrections to Scaling Laws," *Phys. Rev. B* **5** (1972) 4529–4536.

[137] N. Andrei, K. Furuya, and J. H. Lowenstein, "Solution of the Kondo Problem," *Rev. Mod. Phys.* **55** (1983) 331–402.

[138] W. Häusler, L. Kecke, and A.H. MacDonald, "Tomonaga-Luttinger Parameters for Quantum Wires," *Phys. Rev. B* **65** (2002) 085104.

[139] J. Bürki and C.A. Stafford, "On the Stability and Structural Dynamics of Metal Nanowires," *Applied Physics A* **81** (2005) 1519–1525.

[140] A.E. Mattsson, S. Eggert, and H. Johannesson, "Properties of a Luttinger Liquid with Boundaries at Finite Temperature and Size," *Phys. Rev. B* **56** (1997) 15615–15628.

[141] G. Binning, H. Rohrer, Ch. Gerber, and E. Weibel, "Surface Studies by Scanning Tunneling Microscopy," *Phys. Rev. Lett.* **49** (1982) 57–61.

[142] G. Binning, H. Rohrer, Ch. Gerber, and E. Weibel, "(111) Facets as the Origin of Reconstructed Au(110) Surfaces," *Surface Sci.* **131** (1983) L379–L384.

[143] G. Binning and H. Rohrer, "Nobel Lecture: Scanning Tunneling Microscopy - From Birth to Adolescence," *http://nobelprize.org/physics/laureates/1986/binnig-lecture.pdf* (1986).

[144] J. Bardeen, "Tunnelling from a Many-Particle Point of View," *Phys. Rev. Lett.* **6** (1961) 57–59.

[145] J. Tersoff and D. R. Hamann, "Theory and Application for the Scanning Tunneling Microscope," *Phys. Rev. Lett.* **50** (1983) 1998–2001.

[146] J. Tersoff and D. R. Hamann, "Theory of the Scanning Tunneling Microscope," *Phys. Rev. B* **31** (1985) 805–813.

[147] A. Baratoff, "Theory of Scanning Tunneling Microscopy - Methods and Approximations," *Physica B* **127** (1984) 143.

[148] N. Garcia, C. Ocal, and F. Flores, "Model Theory for Scanning Tunneling Microscopy: Application to Au(110) (12)," *Phys. Rev. Lett.* **50** (1983) 2002–2005.

[149] N. Garcia and F. Flores, "Theoretical Studies for Scanning Tunneling Microscopy," *Physica B* **127** (1984) 137.

[150] E. Stoll, A. Baratoff, A. Selloni, and P. Carnevali, "Current Distribution in the Scanning Vacuum Tunnel Microscope: a Free-Electron Model," *J. Phys. C: Solid State Phys.* **17** (1984) 3073–3086.

[151] U. Fano, "Sullo spettro di assorbimento dei gas nobili presso il limite dello spettro d'arco," *Nuovo Cimento* **12** (1935) 154–161. English translation can be found at ArXiv, Cond-Mat/0502210.

[152] U. Fano, "Effects of Configuration Interaction on Intensities and Phase Shifts," *Phys. Rev.* **124** (1961) 1866–1878.

[153] O. Újsághy, J. Kroha, L. Szunyogh, and A. Zawadowski, "Theory of the Fano Resonance in the STM Tunneling Density of States due to a Single Kondo Impurity," *Phys. Rev. Lett.* **85** (2000) 2557–2560.

[154] C.L. Kane and M.P.A. Fisher, "Transmission Through Barriers and Resonant Tunneling in an Interacting One-Dimensional Electron Gas," *Phys. Rev. B* **46** (1992) 15233–15262.

[155] S. Eggert, "Scanning Tunneling Microscopy of a Luttinger Liquid," *Phys. Rev. Lett.* **84** (2000) 4413–4416.

[156] I. Ussishkin and L.I. Glazman, "Signatures of Spin-Charge Separation in Scanning Probe Microscopy," *Phys. Rev. Lett.* **93** (2004) 196403.

[157] C.L. Kane and E.J. Mele, "Broken Symmetries in Scanning Tunneling Images of Carbon Nanotubes," *Phys. Rev. B* **59** (1999) R12759–R12762.

[158] G.A. Fiete, K. Le Hur and L. Balents, "Transport in a Spin-Incoherent Luttinger Liquid," *Phys. Rev. B* **72** (2005) 125416.

[159] G.A. Fiete, J. Qian, Y. Tserkovnyak and B.I. Halperin, "Theory of Momentum Resolved Tunneling into a Short Quantum Wire," *Phys. Rev. B* **72** (2005) 045315.

[160] M. Kindermann, P. W. Brouwer, and A. J. Millis, "Interference as a Probe of Spin Incoherence in Strongly Interacting Quantum Wires," *ArXiv, cond-mat/0603604* (2006).

Papers I-IV

Paper I

P. Kakashvili and H. Johannesson,
"Measuring Luttinger Liquid Correlations from Charge Fluctuations in a Nanoscale Structure",
Phys. Rev. Lett. **91**, 186403 (2003).

Measuring Luttinger Liquid Correlations from Charge Fluctuations in a Nanoscale Structure

Paata Kakashvili and Henrik Johannesson

Institute of Theoretical Physics, Chalmers University of Technology and Göteborg University, SE-412 96 Göteborg, Sweden

(Received 24 June 2003; published 28 October 2003)

We suggest an experiment to study Luttinger liquid behavior in a one-dimensional nanostructure, avoiding the usual complications associated with transport measurements. The proposed setup consists of a quantum box, biased by a gate voltage, and side coupled to a quantum wire by a point contact. Close to the degeneracy points of the Coulomb blockaded box, and in the presence of a magnetic field sufficiently strong to spin polarize the electrons, the setup can be described as a Luttinger liquid interacting with an effective Kondo impurity. Using exact nonperturbative techniques, we predict that the differential capacitance of the box will exhibit distinctive Luttinger liquid scaling with temperature and gate voltage.

DOI: 10.1103/PhysRevLett.91.186403 PACS numbers: 71.10.Pm, 73.21.–b, 73.23.Hk

It is theoretically well established that interacting electrons in one dimension (1D) do not form a Fermi liquid, but rather a composite—a *Luttinger liquid* [1]—where *all* low-lying excitations are collective, and separately carry charge and spin. Despite intense efforts, however, there are very few experiments that unambiguously point to Luttinger liquid behavior in a real 1D electron system. Quantum wires [2] and single-walled carbon nanotubes [3] are prime examples of systems where the electron dynamics is effectively one dimensional. Still, interpretations of relevant experimental data based on Luttinger liquid theory remain controversial. In most experiments until now, one has measured *transport* properties, and it has been notoriously difficult to assess the extent to which external sources, contacts, impurities, etc., influence the results.

In this Letter, we propose a *nontransport* experiment on a 1D nanoscale structure which avoids the problems mentioned above. The system is composed by a 1D quantum box side coupled to a single-mode quantum wire via a point contact (Fig. 1), and could be built from a gated GaAs semiconductor or cleaved edge overgrowth structure [2]. A magnetic field is applied such that the electrons become spin polarized. The charging of the box is then monitored as a function of an applied gate voltage or, alternatively, as a function of temperature at a fixed voltage bias. Using a simple model, we show that this setup can be analyzed in terms of Luttinger liquid theory. We find that the differential capacitance of the quantum box has a nonanalytic dependence on temperature and gate voltage, with a scaling exponent that encodes the electron correlations of the system. This fingerprint of Luttinger liquid behavior should be possible to identify by charge measurements using the recently developed single-electron transistor electrometer technique [4], given proper choice of parameters and design of the setup.

We take the quantum box to be sufficiently small to exhibit Coulomb blockade [5], but large enough for the electrons in the box to be modeled by a (confined) Luttinger liquid. More precisely, we study the limit $\delta E \ll k_B T_K \ll e^2/2C_\Sigma$, where δE is the average level spacing of the box close to the Fermi level, T_K is the temperature scale at which correlation effects set in (to be defined below), and $e^2/2C_\Sigma$ is the charging energy of the box (with C_Σ the full capacitance of the box). δE thus serves as a low-energy cutoff restricting the validity of our analysis [6].

The system can be modeled by a Hamiltonian

$$H = H_{el} + H_c + H_{\rm tun}, \tag{1}$$

where

$$H_{el} = \sum_{k,\alpha} \epsilon_k a^\dagger_{k,\alpha} a_{k,\alpha} + \sum_{q,\alpha,\beta} \hat{U}_{\alpha\beta}(q) \rho_{q,\alpha} \rho_{-q,\beta}, \tag{2}$$

$$H_c = \frac{Q_1^2}{2C_\Sigma} + \zeta V Q_1, \tag{3}$$

$$H_{\rm tun} = \frac{t}{\ell} \sum_{k,p} (a^\dagger_{k,0} a_{p,1} + \text{H.c.}). \tag{4}$$

Here $a_{k,\alpha}$ are the electron destruction operators in the wire ($\alpha = 0$) and the box ($\alpha = 1$), with the energy ϵ_k measured from the Fermi level ϵ_F. In the interaction term $\rho_{q,\alpha}$ are the Fourier components of the corresponding density operators in the wire and the box, and

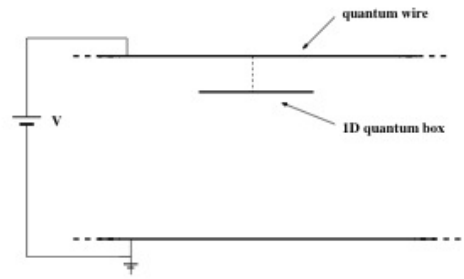

FIG. 1. Schematic picture of the proposed setup. A 1D quantum box side coupled to a quantum wire via a point contact. V is a gate voltage.

$\hat{U}_{\alpha\alpha}(q)\,[\hat{U}_{01}(q)]$ is the Fourier transform of the screened interaction potential *in* the wire and the box [*between* the wire and the box] (with the screening supplied by carriers in nearby gates). Since the wire and the box are defined on the same substrate, we shall take $\hat{U}_{00}(q) = \hat{U}_{11}(q)$, assuming that their transverse widths are the same. The charging energy of the box is described by H_c, with Q_1 measuring the surplus charge in the box with respect to the (zero bias) Fermi level, ζ being a dimensionless parameter which depends on the layout of the sample, and V the gate voltage. The last term, $H_{\rm tun}$, governs the tunneling between the wire and the box, with t the tunneling rate through the point contact. Note that all effects from the finite size of the 1D box (including Coulomb blockade) are carried by H_c, and that in H_{el} and $H_{\rm tun}$ the length ℓ of the box for simplicity is taken to be the same as that of the extended wire (here assumed to be sufficiently large for additional charging effects to be ignored). Also note that, while H_c encapsulates only the *mean-field* Coulomb interaction among electrons in the box, the electron-electron interaction in H_{el} is dynamic and influences the spectrum already for a fixed number of electrons in the wire and the box.

To make progress, we decompose the electron fields $\psi_\alpha(x) \sim \int dk\, e^{ikx} a_{k,\alpha}$ in left $[\psi_{L,\alpha}(x)]$ and right $[\psi_{R,\alpha}(x)]$ components (with x the coordinate along the wire), expanded about the two Fermi points $\pm k_F$ of the linearized spectrum. Keeping only the "local" piece $U_{\alpha\beta}(x) = \hat{U}_{\alpha\beta}(0)\delta(x)$ of the potential, and setting $\hat{U}_{01}(0) = \hat{U}_{00}(0) \equiv g$, H_{el} can be expressed on diagonal Sugawara form [7] as

$$H_{el} \approx \frac{1}{2\pi}\int dx\Big[\frac{v_c}{4}(:J_R J_R: + :J_L J_L:) + \frac{v_F}{3}(:\boldsymbol{J}_R\cdot\boldsymbol{J}_R: + :\boldsymbol{J}_L\cdot\boldsymbol{J}_L:)\Big], \quad (5)$$

where "$\approx$" is a reminder that (5) contains the local part of the interaction only. Here $v_c = v_F(1 + 4g/v_F)^{1/2}$, with v_F the Fermi velocity, and the normal ordering is taken with respect to the filled Dirac sea. The currents are defined by

$$J_{R/L} = \sinh\vartheta :\psi^\dagger_{R/L,\alpha}\psi_{R/L,\alpha}: + \cosh\vartheta :\psi^\dagger_{L/R,\alpha}\psi_{L/R,\alpha}:,$$

$$\boldsymbol{J}_{R/L} = \tfrac{1}{2}:\psi^\dagger_{R/L,\alpha}(x)\boldsymbol{\sigma}_{\alpha\alpha'}\psi_{R/L,\alpha'}(x):,$$

with $2\vartheta = \operatorname{arctanh}[2g/(v_F + 2g)]$, $\boldsymbol{\sigma}$ being the vector of Pauli matrices, and the indices $\alpha, \alpha' = 0, 1$ summed over.

One immediately recognizes H_{el} in (5) as a Luttinger liquid Hamiltonian, with dynamically separated charge and "pseudospin" currents $J_{L/R}$ and $\boldsymbol{J}_{L/R}$, respectively [8]. Taking into account the boundaries of the box [9], as well as the finite range of the screened Coulomb interaction [10], will add more structure to Eq. (5). Also, in a more realistic theory one expects that $\hat{U}_{01} < \hat{U}_{00}$, implying that the manifest SU(2) pseudospin symmetry of H_{el} in (5) gets broken. However, for transparency and ease of notation, we here choose to work with the simple theory where H_{el} is represented by (5), and return below to discuss the more general case.

Having built in the Luttinger liquid correlations into the model via (5), we now explore how these influence the charging of the box. Let us first recall that in a "classical" picture the charge in a quantum box biased by a gate voltage V can change only when V is tuned to the discrete values $-ne/2\zeta C_\Sigma$ (with n an odd integer) for which the Coulomb blockade is lifted [5]. This leads to the celebrated "Coulomb staircase" with steps at the *degeneracy points* at which the charging energy for $(n/2) \pm 1/2$ electrons is the same. This simple picture is modified by quantum charge fluctuations, enhanced by the coupling of the box to the quantum wire.

To study the fluctuation effects, we probe the system with a gate voltage close to a degeneracy point, for example $\zeta V = -e/2C_\Sigma + u$, with $u \ll e/C_\Sigma$ (i.e., u is a small voltage bias away from the chosen degeneracy point). In the limit of small t, we can then truncate the Hilbert space to the $Q_1 = 0$ and $Q_1 = e$ states (since in this limit transitions to virtual states of higher energy are suppressed). Following an exact formulation of Matveev [11], the resulting two-level system $H_c + H_{\rm tun}$ in (1) can be mapped onto an anisotropic Kondo interaction

$$H_K = \frac{J_\perp}{2}\psi^\dagger_{\mu,\alpha}(0)\sigma^j_{\alpha\alpha'}\psi_{\mu',\alpha'}(0)S^j - hS^z, \quad (6)$$

where $J_\perp = 2t$ and $h = eu$, and where $\boldsymbol{S}$ is an additional "pseudospin" of magnitude $1/2$ that implements the constraint on the allowed states (with $\boldsymbol{S}$ localized at the position $x = 0$ of the point contact). Note that *all* indices in (6) ($\mu, \mu' = L, R$; $\alpha, \alpha' = 0, 1$; $j = x, y$) are summed over. It is here important to realize that the presence of backscattering terms in H_K is due to the fact that the quantum box is *side coupled* to the wire via the point contact. This is different from the case of an *end-coupled* box, which supports only forward Kondo scattering [11–13]. As it turns out, it is precisely the backscattering in (6) that imprints Luttinger liquid characteristics on the charging of the box, measured by the average $\langle Q_1\rangle$. Its dependence on the gate voltage is given by the *differential capacitance* $c(u, T) = -[1/(\zeta e^2)][\partial\langle Q_1\rangle/\partial V]$, which, via the Matveev mapping [11], gets modeled by an impurity susceptibility $\chi_{\rm imp}(h, T) = \partial\langle S^z\rangle/\partial h \equiv c(u, T)$, describing the response of the local pseudospin to a "magnetic field" $h \equiv eu$ at $x = 0$.

The original problem has thus been replaced by that of calculating the susceptibility of a (pseudo)spin-1/2 impurity coupled to a Luttinger liquid H_{el} [Eq. (5)] by an anisotropic Kondo interaction H_K [Eq. (6)]. The presence of backscattering in H_K still makes this a hard problem, however. A perturbative renormalization group (RG) analysis [14] reveals that the backscattering terms become relevant for interacting electrons, taking the theory to a nontrivial fixed point. Here we approach the problem via a nonperturbative route, exploiting boundary

conformal field theory (BCFT) [15] to trade the Kondo interaction H_K for a scale invariant boundary condition on the bulk theory H_{el} in (5). One can then use BCFT to extract the critical exponents that govern the scaling of $\chi_{\rm imp}$ (*alias* the differential capacitance) for small values of T and u (i.e., close to the fixed point).

The fixed point describing the *isotropic* spin-1/2 Kondo effect in a Luttinger liquid [14,16] has been shown to correspond to a particular selection rule for quantum numbers of the BCFT embedding $\mathrm{U}(1) \otimes \mathrm{U}(1) \otimes \mathrm{SU}(2)_2 \otimes \mathrm{Ising}$ [17]. Here the two U(1) factors represent the spectra of left- and right-moving charge excitations, while the $\mathrm{SU}(2)_2 \otimes$ Ising block derives from a coset construction of the $\mathrm{SU}(2)_1 \otimes \mathrm{SU}(2)_1$ left- and right-moving pseudospin excitation spectra (with the indices labeling the *levels* of the corresponding Kac-Moody algebras [7]). Given this structure, it is straightforward to verify that the anisotropy in (6) introduces irrelevant operators only (in exact analogy to the Kondo effect for noninteracting electrons [18]). Thus, the fixed point for the present problem is the same as for the isotropic model, and we can exploit the BCFT scheme developed in Ref. [17].

Knowing the fixed point allows us to identify the *leading* boundary operators that drive the finite-T scaling of $\chi_{\rm imp}$. Note that, in contrast to the isotropic case in Ref. [17], operators that break (pseudo)spin-rotational invariance are now allowed [by the anisotropy of H_K in (6)]. A systematic search [19] yields two leading operators $\mathcal{O}^{(1)} = T_s \otimes \mathbb{1}_{\rm Ising} \otimes \mathbb{1}_c$ and $\mathcal{O}^{(2)} = J^z \otimes \epsilon \otimes \mathcal{O}_c$, with scaling dimensions $\Delta^{(1)} = 2$ and $\Delta^{(2)} = 3/2 + 1/2K_c$, respectively. K_c is the usual Luttinger liquid "charge parameter" with perturbative expression $K_c = (1 + 4g/v_F)^{-1/2}$ (here allowed to take values in the interval $1/2 \leq K_c \leq 1$), T_s is the $\mathrm{SU}(2)_2$ energy-momentum tensor, $\mathbb{1}$ is the identity operator in the indexed sector, J^z is the z component of the $\mathrm{SU}(2)_2$ pseudospin current, ϵ is the Ising energy density, and $\mathcal{O}_c$ is a symmetrized product of U(1) vertex operators (for details, see Ref. [17]).

Given the operators $\mathcal{O}^{(1)}$ and $\mathcal{O}^{(2)}$, the scaling behavior of $\chi_{\rm imp}(T, h = 0)$ can be calculated via an expansion in their conjugate scaling fields λ_1 and λ_2. Passing to a Lagrangian formalism, we write the partition function as a path integral, treating the (inverse) temperature as an imaginary time. To simplify the calculation, we also replace the local field h in the definition of $\chi_{\rm imp}$ by a uniform field coupling to the pseudospins of all electrons. This will change the amplitude of the impurity susceptibility [20] but, since we shall be interested in the scaling exponents only, this change is immaterial. Using a linked cluster expansion, we can then write

$$\chi_{\rm imp}(T, 0) = \lambda_1 I[\mathcal{O}_3^{(1)}] + \frac{1}{2} \sum_{i=1,2} \lambda_i^2 I[\mathcal{O}_3^{(i)}, \mathcal{O}_4^{(i)}] + \cdots, \tag{7}$$

where

$$I[\mathcal{O}_3, \ldots, \mathcal{O}_j] \equiv \int_{-\infty}^{\infty} \frac{dx_1 dx_2}{4\pi^2 \beta} \times \int_{-\beta/2}^{\beta/2} d\tau_1 \cdots d\tau_j \langle J_1^z J_2^z \mathcal{O}_3 \cdots \mathcal{O}_j \rangle_c,$$

with $\langle \cdots \rangle_c$ a connected n-point function, and $J_k^z \equiv J^z(\tau_k, x_k)$, $k = 1, 2$. Given the boundary operators $\mathcal{O}_j^{(1,2)} \equiv \mathcal{O}^{(1,2)}(\tau_j)$, $j = 3, 4$, that enter (7), we use the appropriate operator product expansions (OPEs) [7] to collapse the integrands to products of two-point functions. This allows us to easily calculate the integrals and we obtain [using $c(T, u = 0) = \chi_{\rm imp}(T, h = 0)$]

$$c(T, u = 0) = A + B[K_c] T^{1/K_c} + CT^2 + \cdots, \tag{8}$$

with A, $B[K_c]$, and C constants (where $B[K_c] = \mathrm{const}\{1/K_c - 1\}$), and where "$\cdots$" indicates subleading corrections. The short-range electron-electron interaction, encoded by the parameter K_c, is thus seen to induce a *nonanalytic term in the differential capacitance*, scaling as T^{1/K_c}, while vanishing in the noninteracting limit ($K_c = 1$).

Our result in (8) predicts a distinct signal of Luttinger liquid correlations in the proposed setup. For what temperatures should one expect to see it? Taking the 1D quantum box to have a length $\ell' \sim 1\ \mu$m and choosing parameters assuming an experiment using a GaAs heterostructure [2], the energy spacing δE close to the Fermi level corresponds to roughly 0.5 K. The temperature that sets the upper limit for the validity of our theory is the effective Kondo temperature T_K, with expression $T_K = E_C^* \exp(-1/2t\nu)$ in the limit $g\ell < 2t$ [14]. Here $E_C^* = E_C[1 - 4(t\nu)^2 + \cdots]$ is the renormalized charging energy [21], and ν is the density of states at the Fermi level. With $t \sim 0.2/\nu$ and $E_C \sim e^2/2C_\Sigma$, where $C_\Sigma \sim 30$ aF in a typical device, we obtain $T_K \sim 2$ K. With these estimates, our prediction in (8) applies for temperatures in the interval $0.5\ \mathrm{K} < T < 2\ \mathrm{K}$.

Considering the narrowness of the estimated temperature interval, it may experimentally be easier to study the scaling of the capacitance with gate voltage at a fixed temperature. Approximating the window $0.5\ \mathrm{K} < T < 2\ \mathrm{K}$ by the $T \to 0$ limit, the scaling can be obtained via a *Wegner expansion* [22] of the effective ("Kondo language") impurity free energy. Close to the critical point $T = 0, h = 0$, we thus write

$$F_{\rm imp} = \mathrm{const} + Tf\left(\frac{h}{T^\Delta}\right) + g' T^{1-\Delta'} f'\left(\frac{h}{T^\Delta}\right) + \cdots. \tag{9}$$

Here f is a scaling function, $\Delta = 1/2$ is the boundary dimension acquired by the *local* magnetic field h, and f' is the gradient of f with respect to the leading irrelevant scaling field g'. The corresponding operator $\epsilon \otimes \mathcal{O}_c$ is generated from the OPE of J^z with $J^z \otimes \epsilon \otimes \mathcal{O}_c$, and g' is thus proportional to h and carries RG eigenvalue $\Delta' = -(1/K_c - 1)/2 < 0$. In the limit $s \to \infty$, $f(s) \sim s^{1/\Delta}$. Thus, when $T \to 0$, the second term in Eq. (9) gives

an analytic contribution $\sim h^2$. Inspection of the third term in (10) reveals that it can contribute a *finite* correction $\delta F_{\rm imp}$ only via a term $\sim s^{(1-\Delta')/\Delta}$ in the expansion of f', implying that $\delta F_{\rm imp} \sim h^{1+(1-\Delta')/\Delta} = h^{2+1/K_c}$. Contributions from higher order terms in Eq. (9) are of $O[h^4]$. Summarizing, we obtain

$$c(T=0,u) = D + E[K_c]u^{1/K_c} + Fu^2 + \cdots. \qquad (10)$$

Here D, $E[K_c]$, and F are constants, with $E[K_c] \to 0$ as $K_c \to 1$.

Before concluding, we must address the question how the boundaries of the box, as well as the finite range and the anisotropy of the screened Coulomb interaction, influence the physics. Although these features must be accounted for in a faithful modeling of an experimental sample, they will not *qualitatively* change the charge fluctuation effects derived in Eqs. (8) and (10): As for the boundary effects from the quantum box, these will suppress the spectral weight at the Fermi level, at low energies reducing the effective value of K_c [9]. The finite range R of the screened Coulomb interaction further depresses K_c by a factor $[\ln(R/d)]^{-1/2}$, where d is the (common) transverse width of the wire and the box [10] (with $3 < R/d < 15$ in typical experiments on gated GaAs heterostructures [2]). Both effects are moderate, though, and as long as the renormalized K_c is larger than $1/2$ the nonanalytic terms in (8) and (10) will remain the leading ones. Turning to the expected anisotropy $\hat{U}_{01}(0) \equiv g' < \hat{U}_{00}(0) = g$, this will generate an exactly marginal term proportional to $(g - g')J_L^z J_R^z$, in addition to shift the velocities in (5). While the boundary operators identified above will still be present {with K_c renormalized upwards, with a new perturbative expression $K_c = (1 + 2[g + g']/2)^{-1/2}$}, it is conceivable that the spin sector may now contribute additional boundary operators with noninteger dimensions. However, if there results an exponent *smaller* than $1/K_c$, this implies only that the nonanalytic scaling of the capacitance gets enhanced. Conversely, the $1/K_c$ scaling remains the leading one. In either case, the picture that we have uncovered by using an SU(2) invariant description in (5) will remain valid.

In summary, we predict, under conditions specified above, that the differential capacitance of a quantum box side coupled to a quantum wire exhibits a nonanalytic scaling in temperature and gate voltage, with *the same scaling exponent in both cases*. We have traced the effect to the strong electron correlations inherent in one-dimensional systems, and we expect that high-precision charge measurements [4] should be able to detect it. An experimental verification may shed new light on the elusive Luttinger liquid behavior of electrons in one dimension.

We thank S. Eggert, J. Kinaret, and X. Wang for helpful discussions. This work was supported by the Swedish Research Council under Grant No. 621-2002-4947.

[1] F. D. M. Haldane, J. Phys. C **14**, 2585 (1981).
[2] A. R. Goñi *et al.*, Phys. Rev. Lett. **70**, 1151 (1993); S. Tarucha, T. Honda, and T. Saku, Solid State Commun. **94**, 413 (1995); A. Yacoby *et al.*, Phys. Rev. Lett. **77**, 4612 (1996); M. Rother *et al.*, Physica (Amsterdam) **6E**, 551 (2000); O. M. Auslaender *et al.*, Science **295**, 825 (2002).
[3] M. Bockrath *et al.*, Science **275**, 1922 (1997); S. J. Tans *et al.*, Nature (London) **386**, 474 (1997).
[4] R. J. Schoelkopf *et al.*, Science **280**, 1238 (1998); W. Lu *et al.*, Nature (London) **423**, 422 (2003).
[5] D.V. Averin and K. K. Likharev, *Mesoscopic Phenomena in Solids*, edited by B. L. Altshuler, P. A. Lee, and R. A. Webb (Elsevier Science, New York, 1991).
[6] The case of a small quantum dot (with level spacing larger than the temperature) is also experimentally relevant but requires a different modeling from the one presented here for a large box.
[7] A. O. Gogolin, A. A. Nersesyan, and A. M. Tsvelik, *Bosonization and Strongly Correlated Systems* (Cambridge University Press, Cambridge, England, 1998).
[8] Note that, given $\hat{U}_{00}(0) = \hat{U}_{11}(0) = \hat{U}_{01}(0) = g$, the absence of renormalization of the pseudospin velocity in (5) reflects the fact that there is no exchange of electrons between wire and box away from the point contact.
[9] A. E. Mattsson, S. Eggert, and H. Johannesson, Phys. Rev. B **56**, 15 615 (1997); F. Anfuso and S. Eggert, cond-mat/0302625.
[10] H. J. Schulz, Phys. Rev. Lett. **71**, 1864 (1993); W. Häusler, L. Kecke, and A. H. MacDonald, Phys. Rev. B **65**, 085104 (2002).
[11] K. A. Matveev, Sov. Phys. JETP **72**, 892 (1991).
[12] E. Lebanon, A. Schiller, and V. Zevin, Phys. Rev. B **64**, 245338 (2001); K. Le Hur and G. Seelig, Phys. Rev. B **65**, 165338 (2002).
[13] A. Furusaki and K. A. Matveev, Phys. Rev. Lett. **88**, 226404 (2002); E. B. Kolomeisky, R. M. Konik, and X. Qi, Phys. Rev. B **66**, 075318 (2002); E. H. Kim, Y. B. Kim, and C. Kallin, cond-mat/0205054.
[14] A. Furusaki and N. Nagaosa, Phys. Rev. Lett. **72**, 892 (1994).
[15] I. Affleck and A.W.W. Ludwig, Nucl. Phys. **B360**, 641 (1991).
[16] R. Egger and A. Komnik, Phys. Rev. B **57**, 10620 (1998).
[17] P. Fröjdh and H. Johannesson, Phys. Rev. Lett. **75**, 300 (1995); Phys. Rev. B **53**, 3211 (1996).
[18] I. Affleck, A.W.W. Ludwig, H.-B. Pang, and D. L. Cox, Phys. Rev. B **45**, 7918 (1992); P. Schlottmann, Phys. Rev. Lett. **84**, 1559 (2000).
[19] P. Kakashvili and H. Johannesson (unpublished).
[20] G. Zaránd, T. Costi, A. Jerez, and N. Andrei, Phys. Rev. B **65**, 134416 (2002).
[21] X. Wang, R. Egger, and H. Grabert, Europhys. Lett. **38**, 545 (1997).
[22] F. J. Wegner, Phys. Rev. B **5**, 4529 (1972).

Paper II

P. Kakashvili and H. Johannesson,
"Enhanced Two-Channel Kondo Physics in a Quantum Box Device",
preprint (2006), ArXiv cond-mat/0602218, submitted for publication.

Enhanced Two-Channel Kondo Physics in a Quantum Box Device

Paata Kakashvili[1] and Henrik Johannesson[2]
[1]*Department of Applied Physics, Chalmers University of Technology, SE-412 96 Göteborg, Sweden and*
[2]*Department of Physics, Göteborg University, SE-412 96 Göteborg, Sweden*

We propose a design for a one-dimensional quantum box device where the charge fluctuations are described by an anisotropic two-channel Kondo model. The device consists of a quantum box in the Coulomb blockade regime, weakly coupled to a quantum wire by a single-mode point contact. The electron correlations in the wire produce strong back scattering at the contact, significantly increasing the Kondo temperature as compared to the case of non-interacting electrons. By employing boundary conformal field theory techniques we show that the differential capacitance of the box exhibits manifest two-channel Kondo scaling with temperature and gate voltage, uncontaminated by the one-dimensional electron correlations. We discuss the prospect to experimentally access the Kondo regime with this type of device.

PACS numbers: 71.10.Pm, 73.21.-b, 73.23.Hk

The study of the Kondo effect has been at the forefront of condensed matter research ever since its inception forty years ago [1]. While the simplest case studied by Kondo − a spin-1/2 impurity coupled to a single band of conduction electrons − is by now well understood, a variety of variations of the original problem continue to challenge the experimentalist as well as the theorist.

A particularly intriguing question is how to realize the (overscreened) *two-channel Kondo effect* in an experiment. Ideally, two-channel Kondo physics emerges when there are two competing channels in which the conduction electrons can screen a spin-1/2 impurity. As a result, the impurity spin becomes overscreened below some characteristic temperature T_K, and various thermodynamic and transport properties show non-Fermi liquid (NFL) behavior [2, 3, 4]. Being the simplest example of NFL behavior driven by a localized degree of freedom, the model that encapsulates the effect − the two-channel Kondo model [5] − has attracted enormous interest. Many experimental realizations have been suggested over the years, including more recent proposals for quantum dot devices where a small spinful dot (the "impurity") is coupled to two larger dots playing the role of the two screening channels [6]. Still, the two-channel effect has remained elusive in the laboratory. The main difficulty is that the screening channels must be symmetrically coupled to the impurity and also be independent (with no mixing via cotunneling of electrons). While these requirements may be part of the specification of a quantum dot device, the extreme sensitivity of the effect against perturbations still makes it hard to observe.

A different approach is to search for realizations of two-channel Kondo physics in systems where the channel symmetry and independence are protected by some conservation law. A case in point is a quantum box (a large semiconducting quantum dot or a metallic grain) weakly connected by a point contact to a conducting lead. As shown by Matveev [7], near a degeneracy point of the average charge of the box the charge fluctuations can be modeled by an anisotropic two-channel Kondo Hamiltonian. The two available charge states in the box (corresponding to $n-1$ and n electrons) take the role of the two spin states of the impurity, while the physical spin of the conduction electrons provide for the two independent channels. In the absence of a magnetic field, this guarantees that the channel symmetry is robust. Unfortunately, the Kondo temperature T_K of this device is very small, $T_K \sim E_C e^{-1/2t\nu}$, E_C being the single-electron charging energy of the box, and t the tunneling rate through the contact. Trying to increase T_K by increasing E_C requires that the box is made smaller, which in turn threatens to kill the effect since T_K must still be larger than the level spacing in the box. Although fingerprints of two-channel Kondo charge-fluctuations may have been identified in the capacitance of a semiconducting quantum box connected to a lead [8], the difficulties to satisfy the conflicting constraints above make it unlikely that a fully developed effect can be observed in such a device [9].

In this Letter we consider a novel design for a quantum box device with an enhanced Kondo temperature, allowing for a possible experimental entry to two-channel Kondo physics. Our scheme, inspired by that of Matveev [7], adds to several recent proposals for realizing the two-channel Kondo effect in a nanoscale structure [10, 11, 12, 13, 14, 15, 16, 17, 18, 19]. With our effort we also wish to address an issue that has been notably absent from the discussion of this problem: the possible influence from *dynamic* electron interactions on a two-channel charge Kondo effect.

Our design, which is most easily implemented in a gated semiconductor heterostructure or cleaved edge overgrowth structure [20], is sketched in Fig. 1: A one-dimensional (1D) quantum box is side-coupled to a quantum wire via a low-transmission single-mode point contact, putting the box in the Coulomb blockade regime. The box is biased by a gate voltage V, initially tuned to a value where the charging energy for $n-1$ and n electrons are the same *(degeneracy point)*: $V = -ne/2C_\Sigma$ with n

an odd integer, e the electron charge, and C_Σ the capacitance of the box. The box should be made sufficiently large so that its level spacing Δ is much smaller than any other energy scale in the problem, allowing for the discrete levels to be represented by a quasi-continuum.

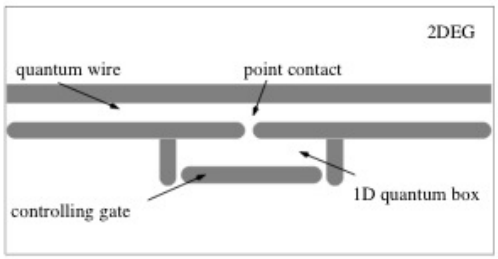

FIG. 1: Schematic picture of the proposed setup. A 1D quantum box side-coupled to a quantum wire via a point contact.

Introducing second-quantized operators $a_{k\mu\alpha}$ for electrons in the wire ($\alpha=0$) and the box ($\alpha=1$) with momentum k and spin $\mu=\uparrow,\downarrow$, we model the set-up by the Hamiltonian

$$H = H_0 + H_I + H_C + H_T, \tag{1}$$

where

$$\begin{aligned} H_0 &= \sum_{k,\mu,\alpha} \epsilon_k a^\dagger_{k\mu\alpha} a_{k\mu\alpha} \\ H_I &= \frac{1}{2}\sum_{\substack{\alpha,\alpha'\\ \mu,\mu'}} \sum_{k,k',q} V_{\alpha\alpha'}(q) a^\dagger_{k+q\,\mu\alpha} a^\dagger_{k'-q\,\mu'\alpha'} a_{k'\mu'\alpha'} a_{k\mu\alpha} \\ H_C &= \frac{Q^2}{2C_\Sigma} + VQ, \\ H_T &= t\sum_{k,k',\mu} (a^\dagger_{k\mu 0} a_{k'\mu 1} + h.c.), \end{aligned}$$

The term H_C encodes the charging energy of the box with Q the surplus charge with respect to the zero bias Fermi level, and H_T governs the tunneling through the point contact, t being a constant tunneling matrix element. By construction we have split the electron interaction in two pieces: The *mean-field* capacitive part H_C that is effective only in the finite box (assuming that the capacitance of the wire can be neglected), and a part H_I which builds dynamic electron correlations into the model [21]. H_I is most easily specified in the relevant low-energy limit where all scattering processes are confined to the neighborhood of the Fermi points $\pm k_F$. Assuming that the electron density is incommensurate with the lattice of the underlying substrate, the allowed low-energy processes can be classified into dispersive, forward and backward scattering (with the latter taking place only inside the wire or box since there is no exchange of wire and box electrons away from the point contact). Passing to a continuum description and decomposing the electron fields $\Psi_{\mu\alpha}(x) \sim \int dk e^{ikx} a_{k\mu\alpha}$ in left- and right-moving parts, $\psi_{-\mu\alpha}(x)$ and $\psi_{+\mu\alpha}(x)$, respectively, these processes are conveniently expressed via the currents

$$\begin{aligned} J_\pm &= \mathrm{sh}\vartheta :\psi^\dagger_{\pm\mu\alpha}\psi_{\pm\mu\alpha}: + \mathrm{ch}\vartheta :\psi^\dagger_{\mp\mu\alpha}\psi_{\mp\mu\alpha}: \\ \boldsymbol{J}^{[\mu]}_\pm &= \frac{1}{2} :\psi^\dagger_{\pm\mu\alpha}\boldsymbol{\sigma}_{\mu\mu'}\psi_{\pm\mu'\alpha}: \\ \boldsymbol{J}^{[\alpha]}_\pm &= \frac{1}{2} :\psi^\dagger_{\pm\mu\alpha}\boldsymbol{\sigma}_{\alpha\alpha'}\psi_{\pm\mu\alpha'}: . \end{aligned} \tag{2}$$

The normal ordering is taken w.r.t. the filled Dirac sea (obtained after linearizing the spectrum around $\pm k_F$), $\boldsymbol{\sigma}$ is the vector of Pauli matrices, and the indices $\alpha, \alpha', \sigma, \sigma'$ are summed over. The parameter ϑ is given by $2\vartheta = \mathrm{arctanh}(3g/(v_F+3g))$, with v_F the Fermi velocity and with g the strength of the screened Coulomb interaction, here approximated by its dominating component at zero-momentum transfer. For simplicity we take this interaction to be the same *between* wire and box ($\sim V_{01}(q)$) as *in* the wire and the box ($\sim V_{00}(q) = V_{11}(q)$): $V_{01}(0) = V_{00}(0) \equiv g$. In a real device one expects that $V_{01}(0) < V_{00}(0)$. However, as will be seen below, the value of the ratio $V_{01}(0)/V_{00}(0)$ at most influences subleading corrections to the charge fluctuations in the box, and for the purpose of extracting the leading behavior we may put it to unity, yielding a more transparent formalism. Given the currents in (2) we can now cast the low-energy limit of $H_0 + H_I$ on the form [22]

$$\begin{aligned} H_0 + H_I = \frac{1}{2\pi} \sum_{\substack{\ell=\pm\\ \eta=\alpha,\mu}} \int (\frac{v_c}{8} :J_\ell(x)J_\ell(x): \\ + \frac{v_{[\eta]}}{4} :\boldsymbol{J}^{[\eta]}_\ell(x)\cdot\boldsymbol{J}^{[\eta]}_\ell(x):) dx, \end{aligned} \tag{3}$$

with $v_c = v_F(1+6g/v_F)^{1/2}, v_{[\mu]} = v_{[\alpha]} = v_F - g$. We have here removed two marginally irrelevant interactions, including an unphysical exchange process between wire and dot electrons away from the point contact [23]. The U(1) charge, SU(2)$_2$ spin and SU(2)$_2$ *pesudospin* currents $J_\ell, \boldsymbol{J}^{[\mu]}_\ell$ and $\boldsymbol{J}^{[\alpha]}_\ell$, respectively, are decoupled in (3), and one recognizes $H_0 + H_I$ as the Hamiltonian for a spinful Luttinger liquid (written on "Sugawara form" [22]) with an extra pseudospin channel. Having thus coded the dynamic part of the theory we turn to its effect on the charge fluctuations in the box.

In the vicinity of the degeneracy point and with $k_BT \ll e^2/2C_\Sigma$, only the $Q=0$ and $Q=e$ states are accessible and higher charge states can be removed from the theory. Following Matveev [7], the resulting two-level system $H_C + H_T$ in (1) can then be mapped onto an anisotropic two-channel Kondo interaction H_K:

$$H_K = \frac{J_\perp}{2}\psi^\dagger_{\ell\mu\alpha}(0)\boldsymbol{\sigma}^j_{\alpha\alpha'}\psi_{\ell'\mu\alpha'}(0)S^j - hS^z. \tag{4}$$

Here $\boldsymbol{S}$ is a pseudospin-1/2 operator that implements the constraint on the allowed charge states in the box. The coupling $J_\perp$ and the field h are given by $J_\perp = 2t$ and $h = eu$ respectively, with u a small voltage bias away from the degeneracy point. Note that *all* indices in (4), $(\ell, \ell' = \pm;\, \alpha, \alpha' = 0, 1; \mu, \mu' = \uparrow, \downarrow, j = x, y)$, are summed over. To complete the mapping to a Kondo pseudospin formulation one uses that $\langle Q(u)\rangle = e[1/2 - \langle S^z\rangle(h, J_\perp)]$, implying that the differential capacitance $c(u, T)$ of the box gets modeled by an impurity pseudospin susceptibility $\chi_{imp}(h, T) \equiv -(1/e^2)\partial\langle Q\rangle/\partial u = c(u, T)$. Having translated the original problem into Kondo language, the task has thus become that of calculating the susceptibility of a pesudospin-1/2 impurity (Eq. (4)) coupled to a two-channel Lutttinger liquid $H_0 + H_I$ (Eq. (3)), with the two channels provided by the physical spin of the electrons.

It is important to realize that the backscattering of electrons off the impurity in (4) is due to the side-coupling of the box to the wire, see Fig. 1. As it turns out, it is precisely this novel feature that yields the desired properties of our set-up. As shown by Le Hur, the amplitude for two-channel electron-impurity backscattering renormalizes to a strong coupling fixed point as the temperature is lowered [24]. This is in exact analogy with the single-channel Kondo problem in a Luttinger liquid, where this effect was first noted [25]. The flow to strong coupling produces a crossover from an exponentially suppressed Kondo temperature $T_K \sim E_c \mathrm{e}^{-1/2t\nu}$ for $g \ll J_\perp$ to a power law $T_K \sim E_C(2t\nu)^{2/(1-K_c)}$ for $g \gg J_\perp$, with K_c the Luttinger liquid charge parameter. Using the crossover formula from Ref. 25 with input parameters chosen for a GaAs based device [26] and with $t\nu \lesssim 0.2$, one finds that while T_K in the noninteracting limit ($K_c = 1$) is comparable to or below the level spacing in the box, T_K becomes almost an order of magnitude larger as K_c approaches 0.6 (which is easily reached in a low-density quantum wire [27]). Although the temperature window that opens is probably too narrow for a full-fledged two-channel Kondo scaling to develop, it should at least allow for a controlled experimental study of its transient behavior. Using a *metallic* quantum wire/box with its much larger effective electron mass would stretch the window by another order of magnitude (provided that the electron density is suppressed by proper gating of the device). We here point to the recent observation that electron-shell effects can stabilize arbitrarily long metallic quantum wires, making the fabrication of a metallic device a viable and realistic prospect [28].

Suppose that the limitations set by current semiconductor based technology can indeed be overcome, allowing for the capacitance to be measured in the critical region $T \ll T_K$ using a metallic device. Would a logarithmic scaling with temperature and gate voltage emerge – as predicted for noninteracting electrons [7] – or will the strong dynamic electron correlations in the wire and the box cause a new type of behavior? In the case of spin polarized electrons it has been shown that 1D correlations strongly influence charge fluctuations [29], and one may anticipate a similar outcome also in the present case. To find out, we have employed the tools of boundary conformal field theory (BCFT) [30], building on earlier results for the isotropic two-channel Kondo effect in a Luttinger liquid [31]. The required analysis is fairly technical, and we here only sketch the key ideas together with the result.

Let us first recall that the fixed point of the *isotropic* two-channel Kondo effect in a Luttinger liquid corresponds to a particular selection rule for quantum numbers of the BCFT embedding $\otimes_{i=1,2}[\mathrm{U}(1)\otimes\mathrm{SU}(2)_2\otimes\mathrm{SU}(2)_2]^i$ implied by the Hamiltonian in (3) [31]. Here the U(1) factor represents charge, while the $\mathrm{SU}(2)_2$ factors represent spin and pseudospin, with i labelling left and right moving fields. The Kondo interaction couples left and right movers, and therefore the symmetries above are broken down to their diagonal subgroups. For the charge sector this implies that any U(1) operator with dimension $\Delta_c = \frac{1}{4}n^2 e^{\pm 2\theta} + N$ ($n, N \in \mathbb{N}$) is allowed [31]. Factorizing the diagonal subgroups in the spin and pseudospin sectors amounts to a coset construction at the level of conformal towers: The two $\mathrm{SU}(2)_2$ towers in the spin and pseudospin sectors are decomposed into $\mathrm{SU}(2)_4$ and a coset which is generated by the N=1 superconformal algebra (SCA) of central charge c=1. Primary states of the spin (pseudospin) $\mathrm{SU}(2)_4$ sectors have conformal dimensions $j(j+1)/6$ with $j \in \{0, 1/2, 1, 3/2, 2\}$. The SCA in turn is divided into two sectors: the Ramond (R) and Neveu-Schwartz (NS) algebras with primary dimensions $\{1/24, 1/16, 3/8, 9/16\}$ and $\{0, 1/16, 1/6, 1\}$ respectively.

Given this structure, it is in principle straightforward to pinpoint the effect from the exchange anisotropy (broken pseudospin rotational symmetry) and the magnetic field (broken time reversal symmetry) in (4). In contrast to the $\mathrm{SU}(2)_4$ invariant case above where only operators that transform as singlets are allowed, more operators now appear in the pseudospin sector. By inspection we find that the only relevant operator produced is the $j = 1$ primary field ϕ^z, with conformal dimension $\Delta_{\phi^z} = 1/3$. This operator is present only if pseudospin rotational *and* time reversal symmetries are simultaneously broken. In the limit of vanishing magnetic field the anisotropy is irrelevant, implying that the magnetic field is a relevant perturbation, as for the two-channel Kondo model for non-interacting electrons [32].

There are two more operators appearing because of the broken pseudospin symmetry: The first descendant J^z of the $j = 0$ identity operator, and the $j = 2$ primary field ϕ^{zz}, both being exactly marginal of dimension $\Delta = 1$. Both operators may be combined with others from charge, spin, and SCA sectors to form new composite operators provided that these (i) respect all remaining symmetries of the theory and (ii) do not vio-

late the known critical scaling of observables in the non-interacting limit $g \to 0$. For the *isotropic* problem the leading behavior of the impurity susceptibility $\chi(T,h)$ is driven by the same operator (of dimension $\Delta = 3/2$) as for noninteracting electrons, giving rise to a logarithmic divergence as $T \to 0$ or $h \to 0$ [31]. To explore whether a faster divergence may result from any of the new composite operators generated from the broken pseudospin symmetry, we have to identify those of scaling dimension $\Delta < 3/2$ and then test them against criteria (i) and (ii) above.

The outcome of the analysis (with details to be published elsewhere) is that *the breaking of the pseudospin symmetry in* (4) *produces no new operators of dimension* $\Delta < 3/2$. This result holds also in the presence of pseudospin symmetry breaking in the Luttinger liquid interaction (3), provided that this breaking only generates at most an exactly marginal term, as is the case for $V_{01} < V_{00}$. It follows that the leading behavior of the differential capacitance $c(T,u)$ of our proposed setup (*alias* the impurity susceptibility $\chi(T, h = eu)$) exhibits the same logarithmic scaling as in the two-channel Kondo effect for noninteracting electrons:

$$c(T, u{=}0) = A \ln\left(\frac{T_K}{T}\right) + ..., \quad T \ll T_K \qquad (5)$$

and

$$c(T{=}0, u) = B \ln\left(\frac{T_H}{eu}\right) + ..., \quad eu \ll T_H \qquad (6)$$

but *with significantly larger Kondo temperatures* T_K *and* $T_H \approx T_K$. Here A and B are constants, and "...." indicate subleading terms.

In conclusion, we have shown that charge fluctuations close to a degeneracy point of a 1D Coulomb blockaded quantum box side-coupled to a quantum wire exhibit logarithmic two-channel Kondo divergences with temperature T [voltage u] for $T \ll T_K$ [$eu \ll T_H$]. This leading behavior is *not* modified by the strong 1D electron correlations in the wire and the box. The Kondo temperature T_K [or T_H in the case of voltage scaling] can be significantly larger compared to a device with non-interacting electrons. While design constraints for a semiconductor implementation probably only allows for crossover effects to be observed, the fabrication of a metallic device should yield access to the full two-channel charge Kondo effect.

We thank S. Eggert and M. Granath for helpful discussions. This work was supported by the Swedish Research Council under grant number 621-2002-4947.

[1] For a review, see the special topics section of J. Phys. Soc. Jpn. **74**, 1 (2005).
[2] N. Andrei and C. Destri, Phys. Rev. Lett. **52**, 364 (1984).
[3] A. Tsvelik and P. B. Wiegman, Z. Phys. B **48**, 9887 (1984).
[4] I. Affleck and A. A. Ludwig, Nucl. Phys. B **352**, 849 (1991).
[5] P. Noziéres and A. Blandin, J. Phys. (France) **41**, 193 (1980).
[6] Y. Oreg and D. Goldhaber-Gordon, Phys. Rev. Lett. **90**, 136602 (2003).
[7] K. A. Matveev, Zh. Éksp. Teor. Fiz. **98**, 1834 (1990) [Sov. Phys. JETP **72**, 892 (1991).
[8] D. Berman, N. B. Zhitenev, R. C. Ashoori, and M. Shayegan, Phys. Rev. Lett. **82**, 161 (1999).
[9] G. Zaránd, G. T. Zimányi, and F. Wilhelm, Phys. Rev. B **62**, 8137 (2000).
[10] T. Gramespacher and K. A. Matveev, Phys. Rev. Lett. **85**, 4582 (2000).
[11] K. Le Hur and G. Seelig, Phys. Rev. B **65**, 165338 (2002).
[12] E. H. Kim, Y. B Kim and C. Kallin, J. Phys. Cond. Matt. **15**, 7047 (2003).
[13] E. Lebanon, A. Schiller, and F. B. Anders, Phys. Rev. B **68**, 041311(R) (2003); Phys. Rev. B **68**, 155301 (2003).
[14] N. Shah and A. J. Millis, Phys. Rev. Lett. **91**, 147204 (2003).
[15] K. Le Hur and P. Simon, Phys. Rev. B **67**, 201308(R) (2003).
[16] S. Florens and A. Rosch, Phys. Rev. Lett. **92**, 216601 (2004).
[17] F. B. Anders, E. Lebanon, and A. Schiller, Phys. Rev. B **70**, 201306(R) (2004).
[18] M. Pustilnik, L. Borda, L. I. Glazman and J. von Delft, Phys. Rev. B **69**, 115316 (2004).
[19] C. J. Bolech and N. Shah, Phys. Rev. Lett. **95**, 036801 (2005).
[20] O. M. Auslaender *et al.*, Science **295**, 825, (2002).
[21] For simplicity, in H_0 and H_I we take the length of the box to be equal to that of the wire, putting all finite-size effects into H_C.
[22] For an easily accessible review, see D. Sénéchal, *An Introduction to Bosonization*, cond-mat/9908262.
[23] The excluded interactions can be written in terms of $SU(4)_1$ Kac-Moody currents as $H_{excl} = -2gJ_L^{\mathcal{A}}J_R^{\mathcal{A}}$ ($\mathcal{A} = 1, ..., 15$), which is marginally irrelevant for $g > 0$.
[24] K. Le Hur, Phys. Rev. B **61**, 1853 (2000).
[25] D. H. Lee and J. Toner, Phys. Rev. Lett. **69**, 3378 (1992).
[26] A. R. Goñi *et al.*, Phys. Rev. Lett. **67**, 3298 (1991).
[27] W. Häusler, L. Kecke, and A. H. MacDonald, Phys. Rev. B **65**, 085104 (2002).
[28] For a review, see J. Bürki and C. A. Stafford, Applied Physics A **81**, 1519 (2005).
[29] P. Kakashvili and H. Johannesson, Phys. Rev. Lett. **91**, 186403 (2003).
[30] For a review, see P. Di Francesco, P. Mathieu, and D. Sénéchal, *Conformal Field Theory*, (Springer, New York, 1997).
[31] M. Granath and H. Johannesson, Z. Phys. B **103**, 225 (1997); Phys. Rev. B **57**, 987 (1998).
[32] I. Affleck, A. W. W. Ludwig, H. B. Pang, and D. L. Cox, Phys. Rev. B **45**, 7918 (1992).

Paper III

P. Kakashvili, H. Johannesson and S. Eggert,
"Local Spectral Weight of a Luttinger Liquid: Effects from Edges and Impurities",
preprint (2006), submitted for publication.

Local Spectral Weight of a Luttinger Liquid: Effects from Edges and Impurities

Paata Kakashvili,[1] Henrik Johannesson,[2] and Sebastian Eggert[1,3]

[1]*Department of Applied Physics, Chalmers University of Technology, SE 412 96 Göteborg, Sweden*

[2]*Department of Physics, Göteborg University, SE 412 96 Göteborg, Sweden*

[3]*Department of Physics, University of Kaiserslautern, D-67663 Kaiserslautern, Germany*

Abstract

We calculate the finite-temperature local spectral weight (LSW) of a Luttinger liquid with an "open" (hard wall) boundary. Close to the boundary the LSW exhibits characteristic oscillations indicative of spin-charge separation. The line shape of the LSW is also found to have a Fano-like asymmetry, a feature originating from the interplay between electron-electron interaction and scattering off the boundary. Our results can be used to predict how edges and impurities influence scanning tunneling microscopy (STM) of one-dimensional electron systems at low temperatures and voltage bias. Applications to STM on single-walled carbon nanotubes are discussed.

PACS numbers: 71.10.Pm, 68.37.Ef, 71.27.+a, 73.40.Gk

I. INTRODUCTION

Metallic electrons confined to one dimension exhibit a plethora of intriguing effects, driven by interactions and the coupling to impurities and defects [1]. At low energies a clean system is described by the concept of a spinful *Luttinger liquid* (LL) [2], with properties very different from those of a Fermi liquid: the quasiparticle pole vanishes identically and only collective modes remain, separately carrying spin and charge. The response of an LL to the addition of a local potential scatterer also differs dramatically from that of a Fermi liquid: The repulsive electron-electron interaction produces long-range density oscillations that get tangled up with the impurity potential in such a way as to suppress the single-electron spectral weight close to the impurity, as well as the conductance through it [3, 4]: In the zero-temperature limit and with a spin-rotational invariant interaction the impurity effectively cuts the system in two parts, with "open" boundaries (hard walls) replacing the impurity. The case of a magnetic impurity − which interacts dynamically with the conduction electrons − is similar: In the zero-temperature limit the physics is that of two LLs separated by open boundaries, with the finite-T response governed by a scaling operator that tunnels electrons through the boundaries [5]. The pictures that emerge in both cases are universal in the sense that all response functions depend only on the electron-electron interaction, with critical exponents which for a spin-rotational interaction is coded by the single LL *charge parameter* K_c. Details of the coupling of the electrons to the impurity, or the structure of the impurity potential, are irrelevant.

The fact that an impurity in an LL drives the system to an *open boundary fixed point* [6] has spurred considerable theoretical work on properties of LLs with an open boundary condition (OBC) [7, 8, 9, 10, 11, 12, 13, 14]. Added interest comes from the fact that many measurements on one-dimensional electron structures − such as the single-wall carbon nanotubes (SWCNTs) [15], or quantum wires, realized in gated semiconductor heterostructures [16] or grown on metallic substrates [17] − are expected to be significantly influenced by electron scattering from the edges, where the confining potential to a first approximation can be treated as an OBC.

Most work to date has focused on the *local spectral weight* (LSW) of an LL with an OBC, yielding predictions for single-electron tunneling and photoemission measurements close to an edge [18] or close to an impurity at sufficiently low temperatures [19]. Measuring the

energy ω (with $\hbar=1$) with respect to the Fermi level, the low-temperature LSW $A(\omega)$ close to an open boundary scales as [3, 7, 8]

$$A(\omega) \sim \omega^{(K_c^{-1}-1)/2} \tag{1}$$

where $K_c < 1$ for a repulsive electron-electron interaction [20]. This is to be compared with that of a clean system probed away from its edges, where $A(\omega) \sim \omega^{(K_c+K_c^{-1})/4-1/2}$ [2]. Experiments on SWCNTs seem to agree with the theoretical prediction that the tunneling rate of electrons should follow a characteristic power law with temperature [15], with a significant reduction of tunneling into the end of a tube as compared to tunneling into its interior ("bulk" regime) [21]. Oscillation patterns that suggest spin-charge separation have also been seen in the tunneling conductance between two quantum wires produced by cleaved edge overgrowth[22], in qualitative agreement with theoretical results. In another line of research, photoemission spectroscopy measurements on quasi-one-dimensional organic conductors have been interpreted within a picture where the one-dimensional chains in the samples are cut by impurities into disconnected pieces, each modeled as an LL with OBCs. Again using results for the LSW, it has been argued [8, 9, 10, 17, 23] that this approach gives better agreement with experiments than conventional theory where photoemission spectra are compared to predictions from ordinary "bulk" LL theory [24]. However, this alternative interpretation remains controversial and the issue has been difficult to settle, much due to the fact that photoemission measurements on these materials are subject to a variety of subtle effects.

The most direct way to probe an LSW is via scanning tunneling microscopy (STM) [18]. These experiments are delicate, as the STM tip must be positioned at a very small distance from the sample for electrons to tunnel [25]. While this is feasible for SWCNTs, the high-precision STM experiments that have been carried out have probed tubes deposited on metallic substrates. This leads to a suppression of the electron-electron interaction from screening charges, and early results were successfully interpreted within a free electron model [26, 27]. In another effort STM measurements were performed on SWCNTs freely suspended over a trench [28], thus bypassing the problem with screening charges. However, the resolution achieved in this experiment was not sufficient to test for the expected LL scaling at small energies. In more recent experiments SWCNTs deposited on atomically clean Au(111) surfaces were studied by high-resolution STM spectroscopy [29], revealing that the electronic

standing waves close to the end of a tube have en enhanced charge velocity which may imply spin-charge separation, and *a fortiori* LL behavior [30].

Turning to theory, the spectral properties of LLs with OBCs are by now fairly well understood, although some open problems remain. Maybe most pressing is the question about the very applicability of LL theory: What is the energy scale Δ below which the power law in Eq. (1) becomes visible? Obviously, an answer to this question is essential for making sensible predictions for experiments. From numerical and other studies of the one-dimensional Hubbard model [31] it is known that the decrease of the LSW − as predicted by LL theory − is often preceded by a sharp increase, and that this effect is particularly pronounced near an edge [13, 14] or close to an impurity [32]. The effect is expected to be generic for any one-dimensional metallic system where the amplitude for back-scattering is larger than for forward scattering. For some systems with a (weakly screened) long-range interaction, such as the carbon nanotubes, back-scattering gets suppressed above a threshold temperature, and one expects the asymptotic LL scaling in Eq. (1) to be visible at accessible energy scales, as is also suggested by experiments [15]. More work is needed, though, to obtain a reliable estimate of the crossover scale Δ, given data from the underlying microscopic physics.

We shall not address this issue here, but rather revisit the problem of determining the full coordinate- and temperature dependence of the LSW of one-dimensional interacting electrons with an OBC, assuming that the energy scale is sufficiently low for LL theory to be applicable. Knowing the detailed structure of the LSW is important for making predictions of future high-precision STM measurements of LL systems, of which the SWCNTs are presently the prime candidates [33]. In earlier works the zero-temperature properties of the LSW [18], as well as the finite temperature properties of the uniform part of the LSW (neglecting Friedel oscillations) [9], have been reported. Here we treat the full problem at a finite temperature and exhibit the LSW for different choices of interaction strength and band filling. We shall find that close to an open boundary the line shape of the LSW has a marked asymmetry as a function of energy with respect to the Fermi level, a property that arises from the phases that appear in the single-electron Green's function, and which has not been examined before. The form of the asymmetry in the neighborhood of the Fermi level resembles a Fano line shape, a feature expected universally whenever a resonant state (like that induced by a magnetic impurity in an electron system) interferes with a non-resonant

one [34]. As we shall see, the origin of the asymmetric line shape in the present case is very different, and is formed by an interplay between electron-electron interaction and scattering off the open boundary. The asymmetry is fairly robust against thermal effects, suggesting that Fano-like line shapes produced by the reflection of interacting electrons off boundaries can be observed at temperatures higher than those originating from their interference with a resonating level. Having access to the full LSW we will also be able to give a systematic description of how charge- and spin separation shows up as an oscillation pattern when being close to an edge (or, an impurity, at low temperatures). This information, which we extract for different temperatures, can be directly translated into a prediction of the measured differential conductance when probing an LL system by STM. Also, given the full LSW we derive its crossover from boundary to thermal scaling near the Fermi level. The thermal effects soften the power law singularities of the LSW, since the non-chiral terms in the electron Greens's function produce a leading scaling term that is linear in energy at higher temperatures. This softening should not be confused with the averaging effects that always occur when the experimental tunneling currents are calculated by integrating over the Fermi-Dirac distribution.

Our paper is organized as follows: In Sec. II we review some basics about temperature-dependent local spectral weights and STM currents. In Sec. III we derive an exact representation of the local spectral weight for a Luttinger liquid with an open boundary, paying due attention to the phase dependence that has not been examined in earlier studies. In this section we also show how to adapt the theory for applications to scanning tunneling microscopy of SWCNTs. Sec. IV contains our results, and in Sec. V we summarize the most important points. A reader mostly interested in the physics of the problem is advised to go directly to Sec. IV. Unless otherwise stated we use units where $\hbar = k_B = c = 1$.

II. PRELIMINARIES

In order to calculate tunneling currents e.g. from an STM tip we will consider the transition rate of adding electrons to an LL system at a position x and with energy ω,

$$\Gamma^{+}(\omega, x; \beta) = 2\pi g^2 Z^{-1} \sum_{m,n} \exp(-\beta E_m) \left|\langle n|\Psi_\sigma^\dagger(x)|m\rangle\right|^2 \delta(\omega - E_n + E_m). \tag{2}$$

This expression follows from Fermi's golden rule assuming a tunneling Hamiltonian of the form $-g\Psi^\dagger_\sigma\psi_{\sigma,\mathrm{tip}} + h.c.$, and treating the tip as a reservoir with unit probability that an electron is available for tunneling. Here Z is the partition function of the N-particle system, $\Psi^\dagger_\sigma(x)$ creates an electron in the sample with spin σ at x, and $\psi_{\sigma,\mathrm{tip}}$ removes an electron of the same spin from the tip. Equation (2) represents the probability that the N-particle states $|\,m\rangle$ of energy E_m are connected to the $(N+1)$-particle states $|\,n\rangle$ of energy $E_n = E_m + \omega$ by the addition of an extra electron of energy ω and coordinate x. The transition rate Γ^- of removing an electron is given by Eq. (2) by simply replacing the index m by n in the Boltzmann weight, assuming that a "hole" is available in the tip with unit probability.

In order to calculate the transition rates it is useful to define the single-electron local spectral weight (LSW) $A(\omega, x; \beta)$ which is directly related to the transition rates by

$$\begin{aligned} A(\omega, x; \beta) &= Z^{-1}(1 + \exp(-\beta\omega)) \sum_{m,n} \exp(-\beta E_m)\, |\langle n|\Psi^\dagger_\sigma(x)|m\rangle|^2\, \delta(\omega - E_n + E_m) \\ &= (1 + \exp(-\beta\omega))\Gamma^+(\omega, x; \beta)/2\pi\lambda^2 \\ &= (1 + \exp(\beta\omega))\Gamma^-(\omega, x; \beta)/2\pi\lambda^2. \end{aligned} \tag{3}$$

It is well-known that the LSW defined in this way can be extracted from the spectral representation of the single-electron retarded Green's function

$$G^R(t, x, \beta) = -i\Theta(t)\langle\{\Psi_\sigma(t, x), \Psi^\dagger_\sigma(0, x)\}\rangle_\beta, \tag{4}$$

by using that [36]

$$A(\omega, x; \beta) = -\frac{1}{\pi}\mathrm{Im}\int_0^\infty G^R(t, x; \beta)\mathrm{e}^{i\omega t}dt. \tag{5}$$

At zero temperature this quantity is known to be the single-electron local density of states $N(\omega, x)$ in agreement with the definition in Eq. (3).

We shall extract the LSW in the standard way by first calculating the single-electron retarded Green's function. The calculation of $A(\omega, x; \beta)$ for the present problem requires some care in order to analyze the analytic structure and phase dependence in detail. In fact, the result which we derive in the next section, using bosonization, reveals a surprising asymmetric energy dependence of the LSW close to the Fermi level for a semi-infinite LL with an open boundary condition (OBC).

Before taking on this task, let us recall how scanning tunneling microscopy (STM) is used to experimentally probe the LSW close to edges and impurities. In the simplest approach,

when the STM tip is assumed to couple only to the conduction electrons (thus neglecting tunneling into localized impurity levels) the tunneling current is given by the integrated difference between the transition rates Γ^+ and Γ^-, weighted by the corresponding probabilities that an electron [hole] is available in the tip for tunneling to [from] the sample. With an applied voltage V one thus has:

$$\begin{aligned} I(V,x;\beta) &= e\int_{-\infty}^{\infty} N_{STM}(\omega-eV)\left[f(\omega-eV)\Gamma^+(\omega,x;\beta)-(1-f(\omega-eV))\Gamma^-(\omega,x;\beta)\right]d\omega \\ &\approx 2\pi e g^2\rho_0\int_{-\infty}^{\infty}[f(\omega-eV)-f(\omega)]A(\omega,x;\beta)d\omega, \end{aligned} \tag{6}$$

where $f(\omega)$ is the Fermi-Dirac distribution and we have approximated the density of states $N_{STM}(\omega)$ in the tip by a constant ρ_0 in the last step. It is clear that we recover the conventional formula for tunneling at zero temperature [37]

$$I(V,x) = 2e\pi g^2\int_0^{eV} N(\omega,x)N_{STM}(\omega-eV)d\omega, \tag{7}$$

where $N(\omega,x)$ is the local single-electron density of states for a conduction electron in the sample, and $N_{STM}(\omega)$ is the density of states of the STM tip measured relative to the Fermi energy. By differentiating, the local differential tunneling conductance can then be directly related to the local density of states in Eq. (7)

$$\frac{dI(V,x)}{dV} \propto 2e^2\pi g^2\rho_0 N(V,x). \tag{8}$$

This expression remains valid at a finite temperature T, provided that the thermal length $\lambda_T \sim v_s/T$ is larger than any other characteristic length L of the experimental setup (such as the distance between the STM tip and the edge of the sample). The speed v_s that determines λ_T is that of the spin collective modes (which in a one-dimensional interacting electron system are slower than the collective charge modes). When $L > \lambda_T$ a temperature-dependent description becomes necessary, and the expression for $I(V,x)$ has to be modified according to Eq. (6). The local differential conductance at finite temperature can therefore be written as

$$\frac{dI(V,x;\beta)}{dV} = 2eg^2\pi\rho_0\int_{-\infty}^{\infty}\frac{d}{dV}f(\omega-eV)A(\omega,x;\beta)d\omega. \tag{9}$$

It follows that the line shape properties of the local tunneling conductance are directly determined by the LSW.

With these preliminaries we now turn to the calculation of the finite-temperature LSW for an LL with an open boundary.

III. DERIVING THE LOCAL SPECTRAL WEIGHT

We consider an interacting electron liquid on a semi-infinite line, $x \geq 0$, subject to an OBC at the end $x = 0$. Following standard Luttinger-liquid approach [1], we linearize the spectrum and decompose the electron field Ψ_σ into left- (L) and right- (R) moving chiral fermions at the two Fermi points $\pm k_F$,

$$\Psi_\sigma(x) = e^{-ik_F x}\psi_{L\sigma}(x) + e^{ik_F x}\psi_{R\sigma}(x). \tag{10}$$

The zero-temperature single-electron Green's function at a point x can then be expressed in terms of the propagators of the time-evolved chiral fermions

$$\begin{aligned} G(t>0,x) \;&=\; \langle \Psi_\sigma(t,x)\Psi^\dagger_\sigma(0,x)\rangle = \langle \psi_{L\sigma}(t,x)\psi^\dagger_{L\sigma}(0,x)\rangle + \langle \psi_{R\sigma}(t,x)\psi^\dagger_{R\sigma}(0,x)\rangle \\ &+\; e^{i2k_F x}\langle \psi_{R\sigma}(t,x)\psi^\dagger_{L\sigma}(0,x)\rangle + e^{-i2k_F x}\langle \psi_{L\sigma}(t,x)\psi^\dagger_{R\sigma}(0,x)\rangle. \end{aligned} \tag{11}$$

We see that there are two types of contributions to $G(t > 0, x)$: oscillatory and non-oscillatory. While the latter are always present, the former are nonzero only if the left- and right moving fermions get entangled at a boundary. Imposing an open *(Dirichlet)* boundary condition at the "phantom site" which is situated one lattice spacing a from the end of the LL at $x = -a$,

$$\Psi_\sigma(-a) = e^{ik_F a}\psi_{L\sigma}(-a) + e^{-ik_F a}\psi_{R\sigma}(-a) = 0, \tag{12}$$

and assuming that the chiral fermions are slowly varying on the scale of a, it follows that

$$\psi_{R\sigma}(0) = e^{i\gamma}\psi_{L\sigma}(0), \tag{13}$$

where

$$\gamma = \pi + 2k_F a = \pi(1 + n_e), \tag{14}$$

with n_e the filling factor ($n_e = 1$ for a half-filled band). Although not essential here, the "softening" of the boundary − implied by imposing the Dirichlet condition at $x = -a$ − is sometimes useful for modeling the dependence of the scattering phase shift γ on the shape of the edge- or impurity-potential. The value of γ may therefore depend on the details of the boundary geometry, but it is important to notice that it is in general not a multiple of π even at half-filling. Using Eq. (13) to analytically continue to negative coordinates [6], the right-movers may be represented by left-movers as

$$\psi_{R\sigma}(x) = e^{i\gamma}\psi_{L\sigma}(-x), \quad x > 0. \tag{15}$$

We can then express the Green's function in Eq. (11) in terms of left-moving fermions only, now taking values on the full line $-\infty < x < \infty$

$$\begin{aligned} G(t>0,x) &= \langle \psi_{L\sigma}(t,x)\psi^\dagger_{L\sigma}(0,x)\rangle + \langle \psi_{L\sigma}(t,-x)\psi^\dagger_{L\sigma}(0,-x)\rangle \\ &+ e^{i(2k_F x+\gamma)}\langle \psi_{L\sigma}(t,-x)\psi^\dagger_{L\sigma}(0,x)\rangle + e^{-i(2k_F x+\gamma)}\langle \psi_{L\sigma}(t,x)\psi^\dagger_{L\sigma}(0,-x)\rangle. \quad (16) \end{aligned}$$

Introducing

$$G_{LL}(t,x,x') = \langle \psi_{L\sigma}(t,x)\psi^\dagger_{L\sigma}(0,x')\rangle = \langle \psi^\dagger_{L\sigma}(t,x)\psi_{L\sigma}(0,x')\rangle, \quad (17)$$

with the second equality following from the charge conjugation symmetry of the linearized theory, Eq. (16) may be written as

$$\begin{aligned} G(t>0,x) = G_{LL}(t,x,x) + G_{LL}(t,-x,-x) \\ + e^{i(2k_F x+\gamma)}G_{LL}(t,-x,x) + e^{-i(2k_F x+\gamma)}G_{LL}(t,x,-x). \quad (18) \end{aligned}$$

With the definition in Eq. (4) the retarded Green's function can finally be cast on the compact form

$$\begin{aligned} G^R(t,x) = -i\Theta(t)(4ReG_{LL}(t,x,x) + 2e^{i(2k_F x+\gamma)}ReG_{LL}(t,-x,x) \\ + 2e^{-i(2k_F x+\gamma)}ReG_{LL}(t,x,-x)), \quad (19) \end{aligned}$$

using Eqs. (17) and (18). To obtain the LSW in Eq. (5) we thus need to calculate the chiral Green's function in (17), identify its real part, and then Fourier transform the resulting expression for $G^R(t,x)$ from (19). The first part can be done analytically by using bosonization, and we turn to this task in the next section.

A. Chiral Green's function from bosonization

Using standard bosonization [38] we write the left- and right-moving fermion fields as coherent superpositions of free bosonic charge and spin fields, $\phi_{rc} = (\phi_{r\uparrow} + \phi_{r\downarrow})/\sqrt{2}$ and $\phi_{rs} = (\phi_{r\uparrow} - \phi_{r\downarrow})/\sqrt{2}$, with $r = L, R$

$$\begin{aligned} \psi_{L\sigma}(t,x) &= \frac{\eta_{L\sigma}}{\sqrt{2\pi\alpha}} \exp\left(-i\sqrt{2\pi}(\cosh\theta\,\phi_{Lc}(x,t) + \sinh\theta\,\phi_{Rc}(x,t) + \sigma\phi_{Ls}(x,t))\right) \\ \psi_{R\sigma}(t,x) &= \frac{\eta_{R\sigma}}{\sqrt{2\pi\alpha}} \exp\left(i\sqrt{2\pi}(\cosh\theta\,\phi_{Rc}(x,t) + \sinh\theta\,\phi_{Lc}(x,t) + \sigma\phi_{Rs}(x,t))\right). \quad (20) \end{aligned}$$

Here α is a small-distance cutoff of the order of the lattice spacing of the underlying microscopic model, and $\eta_{r\sigma}$ are Klein factors obeying a diagonal Clifford algebra that ensure that fermion fields of different chirality r and/or spin σ anticommute. The parameter θ is related to the LL charge parameter K_c by $K_c = \mathrm{e}^{2\theta}$, and is parameterized by the amplitudes for the low-energy scattering processes. For a system with long-range interaction these amplitudes become momentum dependent, but since we shall only be interested in the asymptotic low-energy behavior of the Green's functions we can restrict them to zero momentum and treat K_c as a constant (taking a value <1 for repulsive interaction). Note that this shortcut assumes a finite-range interaction, whereas an unscreened Coulomb interaction which diverges at vanishing momentum leads to very different physics [39]. Away from a half filling umklapp scattering vanishes, and standard RG arguments show that backscattering processes become irrelevant (again assuming a repulsive electron-electron interaction). As is well-known, for this case the remaining dispersive and forward scattering vertices can be written as quadratic forms in bosonic operators, leading to two free boson theories, one for charge, and one for spin

$$\mathcal{H} = \sum_{j=c,s} \frac{v_j}{2} \left((\partial_x \phi_{Lj})^2 + (\partial_x \phi_{Rj})^2 \right). \tag{21}$$

This defines the LL Hamiltonian density, here expressed in the chiral fields, with $v_{c\,(s)}$ the speed of the charge (spin) bosonic modes.

The logic of the construction just sketched is strictly valid only for a translational invariant system where all interaction processes can be classified into dispersive, forward, backward, or umklapp scattering [1]. For a system with an open boundary, translational invariance is broken and a two-particle interaction leads to additional scattering processes. As shown by Meden *et al.* [14], however, the theory in Eq. (21) still captures the universal low-energy physics. Perturbative arguments suggest that the energy range where it applies increases with the range of the interaction of the original microscopic theory.

To make progress we analytically continue the charge ϕ_{Lc} and spin ϕ_{Ls} boson fields in (20) to $x < 0$ such that the boundary condition in Eq. (13) is satisfied

$$\begin{aligned} \phi_{Lc}(t,-x) &= -\phi_{Rc}(t,x) + \frac{\gamma}{\sqrt{2\pi K_c}} \\ \phi_{Ls}(t,-x) &= -\phi_{Rs}(t,x), \quad x > 0. \end{aligned} \tag{22}$$

Using (22) we can write

$$\psi_{L\sigma}(t,x) = \frac{e^{i\gamma(1-K_c)/2K_c}\eta_{L\sigma}}{\sqrt{2\pi\alpha}} \times \exp\left(-i\sqrt{2\pi}(\cosh\theta\,\phi_{Lc}(t,x) - \sinh\theta\,\phi_{Lc}(t,-x) + \sigma\phi_{Ls}(t,x))\right). \quad (23)$$

Given (23) the chiral Green's functions in (19) are now easily calculated, using that $\phi_{Lc/s}$ are chiral bosons governed by the free theory in (21) [38]

$$G_{LL}(t,x,x) = \left[\frac{1}{\alpha+iv_st}\right]^{1/2}\left[\frac{1}{\alpha+iv_ct}\right]^{k_1+k_2}\left[\frac{4x^2}{(\alpha+iv_ct)^2+4x^2}\right]^{k_3}, \quad (24)$$

$$G_{LL}(t,x,-x) = \left[\frac{1}{\alpha+i(v_st+2x)}\right]^{1/2}\left[\frac{1}{\alpha+i(v_ct+2x)}\right]^{k_1}\left[\frac{1}{\alpha+i(v_ct-2x)}\right]^{k_2}\left[\frac{4x^2}{(\alpha+iv_ct)^2}\right]^{k_3} \quad (25)$$

with $G_{LL}(t,-x,-x)$ and $G_{LL}(t,-x,x)$ obtained from (24) and (25) respectively by taking $x \to -x$. The exponents are given by

$$\begin{aligned} k_1 &= (K_c + 1/K_c + 2)/8 \\ k_2 &= (K_c + 1/K_c - 2)/8 \\ k_3 &= (1/K_c - K_c)/8 \end{aligned} \quad (26)$$

To obtain the finite-temperature Green's function we use conformal field theory techniques [40] and map the complex planes $\{z_j = v_j\tau + ix\}$ on which the zero-temperature chiral theory is defined (with $\tau = it$ the Euclidean time, and $j = c, s$) onto two infinite cylinders $\Gamma_j = \{w = v_j\tau' + ix'\}$ of circumference $\beta = 1/T$

$$w_j = \frac{v_j\beta}{\pi}\arctan\left(\frac{\pi}{\beta v_j}z_j\right). \quad (27)$$

Employing the transformation rule

$$\langle e^{i\alpha_1\phi(w_1)}...e^{i\alpha_n\phi(w_n)}\rangle = \prod_{i=1}^{n}\left(\frac{dw}{dz}\right)^{-\alpha_i^2/8\pi}_{w=w_i}\langle e^{i\alpha_1\phi(z_1)}...e^{i\alpha_n\phi(z_n)}\rangle \quad (28)$$

we obtain for the finite-temperature versions of the Green's functions

$$G_{LL}(t,x,x;\beta) = \left(\frac{\pi}{\beta v_c}\right)^{k_1+k_2}\left(\frac{\pi}{\beta v_s}\right)^{1/2}\left[\frac{1}{\sin(\frac{\pi}{\beta}(\alpha+it))}\right]^{1/2}\left[\frac{1}{\sin(\frac{\pi}{\beta}(\alpha+it))}\right]^{k_1+k_2} \times \left[\frac{\sinh^2(\frac{\pi}{\beta}\frac{2x}{v_c})}{\sin(\frac{\pi}{\beta}(\alpha+i(t+2x/v_c)))\sin(\frac{\pi}{\beta}(\alpha+i(t-2x/v_c)))}\right]^{k_3}, \quad (29)$$

$$G_{LL}(t,x,-x;\beta)=\left(\frac{\pi}{\beta v_c}\right)^{k_1+k_2}\left(\frac{\pi}{\beta v_s}\right)^{1/2}\left[\frac{1}{\sin(\frac{\pi}{\beta}(\alpha+i(t+2x/v_s)))}\right]^{1/2}\left[\frac{1}{\sin(\frac{\pi}{\beta}(\alpha+i(t+2x/v_c)))}\right]^{k_1}$$
$$\times\left[\frac{1}{\sin(\frac{\pi}{\beta}(\alpha+i(t-2x/v_c)))}\right]^{k_2}\left[\frac{\sinh^2(\frac{\pi}{\beta}\frac{2x}{v_c})}{\sin^2(\frac{\pi}{\beta}(\alpha+it))}\right]^{k_3}. \quad (30)$$

We have here dropped the primes on the transformed coordinates and reinserted the real time variable.

B. An exact representation of the LSW

Having obtained the chiral Green's functions we next calculate their real parts, which, according to Eq. (19), define the LSW. It is essential here to consistently identify the phases of the Green's functions that appear in (19). This is most easily done by exponentiating the expressions in (29) and (30) and choosing the negative real axis as branch cut of the logarithm [41]. Treating t as a complex variable, this amounts to choosing the branch cuts for $G_{LL}(t,x,x;\beta)$ as shown on Fig. 1. Functions $G_{LL}(t,x,x;\beta)$ and $G_{LL}(t,x,-x;\beta)$ have

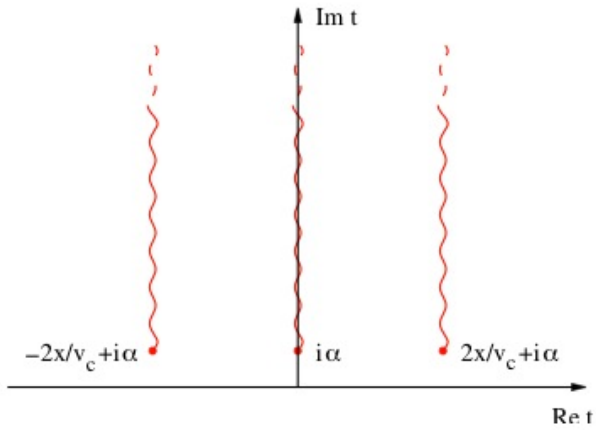

FIG. 1: [color online] Branch points and branch cuts for $G_{LL}(t,x,x;\beta)$. The phases are different in different regions defined by branch points.

different phases in different regions defined by branch points, since the phases differ by 2π

on opposite sides of the cuts. Taking the cutoff $\alpha \to 0$ we get

$$\begin{aligned} Re\, G_{LL}(t,x,x;\beta) &= \left(\frac{\pi}{\beta v_c}\right)^{k_1+k_2}\left(\frac{\pi}{\beta v_s}\right)^{1/2}\cos\zeta(t)\left|\sinh(\frac{\pi}{\beta}t)\right|^{-(1/2+k_1+k_2)} \\ &\left|\frac{\sinh(\frac{\pi}{\beta}(t+2x/v_c))\sinh(\frac{\pi}{\beta}(t-2x/v_c))}{\sinh^2(\frac{\pi}{\beta}\frac{2x}{v_c})}\right|^{-k_3}, \\ Re\, G_{LL}(t,x,-x;\beta) &= \left(\frac{\pi}{\beta v_c}\right)^{k_1+k_2}\left(\frac{\pi}{\beta v_s}\right)^{1/2}\cos\zeta'(t)\left|\sinh(\frac{\pi}{\beta}(t+2x/v_s))\right|^{-1/2} \\ &\left|\sinh(\frac{\pi}{\beta}(t+2x/v_c))\right|^{-k_1}\left|\sinh(\frac{\pi}{\beta}(t-2x/v_c))\right|^{-k_2}\left|\frac{\sinh(\frac{\pi}{\beta}t)}{\sinh(\frac{\pi}{\beta}\frac{2x}{v_c})}\right|^{-2k_3}, \end{aligned} \quad (31)$$

where

$$\zeta(t) = \begin{cases} \frac{\pi}{4}+\frac{\pi k_1}{2}+\frac{\pi k_2}{2} & 0<t<\frac{2x}{v_c} \\ \frac{\pi}{4}+\frac{\pi k_1}{2}+\frac{\pi k_2}{2}+\pi k_3 & t>\frac{2x}{v_c} \end{cases}$$

$$\zeta'(t) = \begin{cases} \frac{\pi}{4}+\frac{\pi k_1}{2}+\frac{\pi k_2}{2}+\pi k_3 & t<-\frac{2x}{v_s} \\ -\frac{\pi}{4}+\frac{\pi k_1}{2}+\frac{\pi k_2}{2}+\pi k_3 & -\frac{2x}{v_s}<t<-\frac{2x}{v_c} \\ -\frac{\pi}{4}-\frac{\pi k_1}{2}+\frac{\pi k_2}{2}+\pi k_3 & -\frac{2x}{v_c}<t<0 \\ -\frac{\pi}{4}-\frac{\pi k_1}{2}+\frac{\pi k_2}{2}-\pi k_3 & 0<t<\frac{2x}{v_c} \\ -\frac{\pi}{4}-\frac{\pi k_1}{2}-\frac{\pi k_2}{2}-\pi k_3 & t>\frac{2x}{v_c} \end{cases} \quad (32)$$

We see that the phases that appear in the real parts of the Green's functions take different values in different domains, consistent with the fact that the end points of the domains are branch points (see Fig. 1). Given the results in Eq. (31) we can finally write down an exact representation of the LSW for an LL with an open boundary. Combining (5) and (19) we find that

$$\begin{aligned} A(\omega,x,\beta) &= \frac{4}{\pi}\int_0^\infty dt\cos\omega t Re G_{LL}(t,x,x;\beta) \\ &+ \frac{2}{\pi}\int_{-\infty}^\infty dt\cos(2k_F x+\gamma-\omega t) Re\, G_{LL}(t,x,-x;\beta). \end{aligned} \quad (33)$$

This expression reveals that $A(\omega,x,\beta)$ has a nontrivial dependence on the interaction strength (via k_1,k_2,k_3 and the velocities v_c and v_s that parameterize the chiral Green's functions), in addition to an oscillation in the second term that is shifted by a phase controlled by the band filling via k_F and γ in Eq. (14) and the distance x to the boundary. This leads to an interesting asymmetric dependence of the LSW on energy as will be discussed in Sec. IV.

One of the most promising candidates for LL behavior are single-walled carbon nanotubes (SWCNT), which however require some modification to the Green's functions in Eqs. (29)-(31) due to the presence of two electronic channels. Depending on the substrate the interaction constant K_c may be very small ≈ 0.25 and strongly k-dependent for isolating substrates or closer to unity $\approx 0.6 - 1$ for metallic substrates. Especially in the latter case backscattering processes may also play an important role at very low temperatures. Following [42, 43] the low energy expression for the electron field is written in terms of Bloch functions on the two graphite sublattices in order to arrive at two spinful channels of 1D Fermion operators $\psi_{L\alpha\sigma}$ and $\psi_{R\alpha\sigma}$ where $\sigma = \uparrow, \downarrow$ is the spin and $\alpha = \pm$ labels the two distinct channels. In order to bosonize the problem it is then possible to introduce bosonic fields of total and relative ($\delta = \pm$) charge and spin chiral bosons $\phi_{rj\delta}\,(r = L, R, \quad j = c, s)$ and write the bosonization formula

$$\psi_{L\alpha\sigma} = \frac{\eta_{L\alpha\sigma}}{\sqrt{2\pi\alpha}} \exp(-i\sqrt{\pi}[\cosh\theta\phi_{Lc+}(x) + \sinh\theta\phi_{Rc+}(x) + \alpha\phi_{Lc-}(x) + \sigma\phi_{Ls+}(x) + \alpha\sigma\phi_{Ls-}(x)]), \quad (34)$$

where $\psi_{R\alpha\sigma}$ is obtained by taking the complex conjugate of the right-hand-side of Eq. (34) and switching $L \leftrightarrow R$.

An open end or an impurity will in general mix the two channels so the effective "open" boundary condition will in most cases not be a simple reflection. The analytic continuation analogous to Eq. (22) may therefore turn out to be more complicated for the four bosons. In the simplest symmetric cases we see that the boundary Green's functions have again a structure as given in Eqs. (29-31), however with the exponent 1/2 replaced by 3/4 and $k_1 = (K_{c+} + 1/K_{c+} + 2)/16$, $k_2 = (K_{c+} + 1/K_{c+} - 2)/16$ and $k_3 = (1/K_{c+} - K_{c+})/16$. Accordingly $\zeta(t)$ and $\zeta'(t)$ are given by Eq. (32) with each occurrence of the term $\pi/4$ in (32) replaced by $3\pi/8$. The oscillating Friedel-like terms in the LSW in the second term of Eq. (33) turn out to have the opposite sign on the two sublattices [44].

IV. RESULTS

In order to extract the physics from the LSWs derived in the previous section we have numerically carried out the Fourier transforms in Eq. (33). The results reveal a rich structure in the LSW of a Luttinger liquid when an edge or an impurity is present. We here focus

on three aspects of the LSW of particular interest for STM experiments: Its asymmetric line shape as a function of energy, oscillation patterns revealing spin-charge separation, and thermal effects.

A. Properties of the LSW

One of the most striking feature of the LSW of an LL is the well-known power law suppression at low energies proportional to $\omega^{(K_c+K_c^{-1})/4-1/2}$. For the special case of zero temperature and commensurate oscillations (i.e. setting $2k_F na + \gamma = \pi m\,(m \in \mathbb{Z})$) the LSW of Eq. (33) near a boundary at $x = na$ has been analyzed before [8, 18]. In that case the first term of Eq. (33) takes on a scaling form with the variable ωx that shows a crossover from bulk scaling to boundary scaling in Eq. (1) with slow oscillations proportional to $\sin(2\omega x/v_c)\omega^{k_3-1}x^{k_3-k_1-k_2-1/2}$ [8]. If the phase is neglected or set to $2k_F na + \gamma = m\pi$ the second Friedel-like term in Eq. (33) also takes on a scaling form, but shows both spin and charge modulations that decay with $\omega^{k_1-1}x^{-k_2-1/2}$. We will now focus on the energy dependence at both small and large temperatures together with the effect of the phase γ.

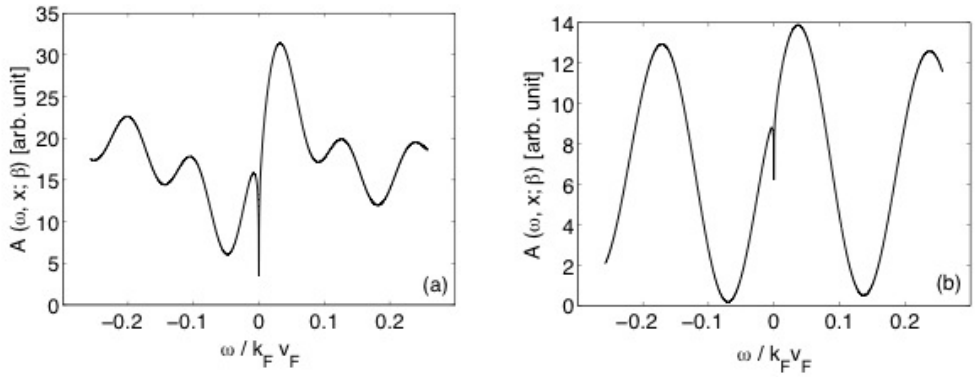

FIG. 2: Local spectral weight $A(\omega, x; \beta)$ for $K = 0.7$, $v_c/v_F \approx 1.43$, $v_c/v_s \approx 3$ (a), $K = 0.9$, $v_c/v_F \approx 1.11$, $v_c/v_s \approx 1.26$ (b) with $T/k_F v_F = 2.6 \times 10^{-6}$, $x = 10a$, $n_e = 0.97$.

1. Asymmetric line-shape

At small energies, the most striking feature of the LSW is the asymmetry of its line shape, as seen in Fig. 2. From Eq. (33) it is apparent that this property is due to the phase $2k_F x + \gamma$ appearing in the second term of $A(\omega, x; \beta)$. Here the distance from the boundary $x = na$ has to be measured in integer units of the lattice spacing a, since the original Fermion operators typically correspond to orbitals in the crystal lattice. The phase causes a shift of the periodic structure of $A(\omega, x; \beta)$ with respect to the Fermi level, and accordingly determines how the spectral weight suppression close to the Fermi level affects the line shape. The shift depends upon the filling factor n_e since, for fixed x, n_e determines the values of k_F

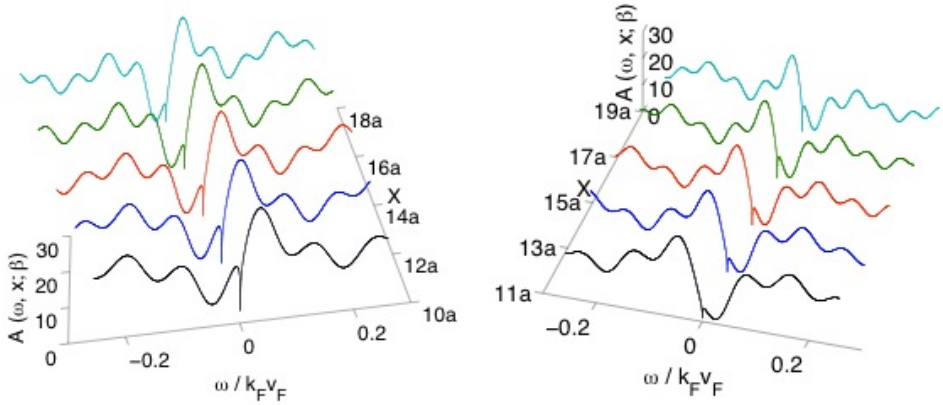

FIG. 3: [color online] $A(\omega, x; \beta)$ for $K = 0.7$, $v_c/v_F \approx 1.43$, $v_c/v_s \approx 3$, $T/k_F v_F = 2.6 \times 10^{-6}$, $n_e = 0.97$, shown for even and odd sublattices.

and γ in Eq. (14). The LSW is asymmetric in general, but for particular fillings for which $2k_F na + \gamma = \pi m \, (m \in \mathbb{Z})$ it becomes a symmetric function of ω. By inspection of Eqs. (31) and (33) one finds that for a given interaction strength the asymmetry tends to zero very close to the boundary ($2\omega x/v_s \ll 1$) and very far from the boundary ($2\omega x/v_c \gg 1$, "bulk" regime) and reaches a maximum in the intermediate region. It is important to realize that the shift of the periodic structure with respect to the Fermi level is present also for the non-interacting case when the LSW takes the simple form $A(\omega, x; \beta) \sim \cos(2k_F x + \gamma - 2\omega x/v_F)$. We conclude that the shift is a pure boundary effect, and is due to the interference of the incoming and reflected electrons at the boundary. In contrast, the dip of the spectral weight

at the Fermi level is an interaction effect.

In Fig. 3 we show the energy and coordinate dependence of the LSW for even and odd sublattices. The Friedel oscillations on the scale of the lattice spacing a are easily visible as a flip of the asymmetry when going from one graph to the other. The spin and charge modulations of the amplitude are also present over longer wavelengths in real space, but are not clearly visible due to the relatively narrow coordinate range in Fig. 3. Note that the asymmetry with energy varies with the distance to the boundary since the phase $2k_F x + \gamma$ also varies with distance.

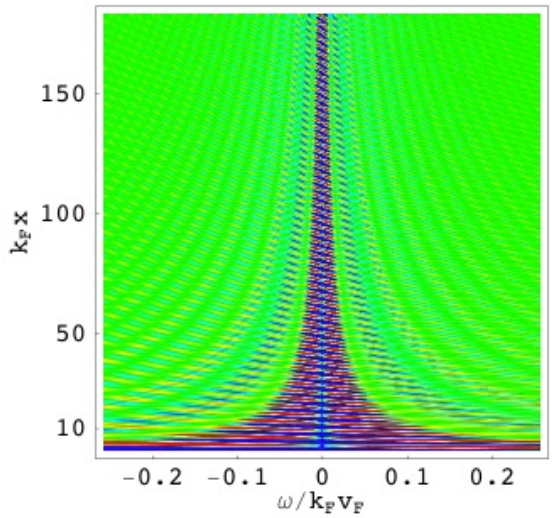

FIG. 4: [color online] $A(\omega, x; \beta)$ for $K = 0.7$, $v_c/v_F \approx 1.43$, $v_c/v_s \approx 3$, $T/k_F v_F = 2.6 \times 10^{-4}$, $n_e = 0.97$.

It is interesting to note the similarity of the typical asymmetric line shapes in Figs. 2 and 3 with that of a Fano resonance [34] when ω is close to the Fermi level. A Fano resonance is known to develop in the LSW for non-interacting electrons when coupled e.g. to a magnetic impurity, the effect being produced by the interference between resonating and nonresonating electron paths through the impurity [35]. As we have seen, the asymmetry in the present case instead comes from the combined effect of electron interactions (causing a dip in the LSW at the Fermi level) and the reflection of electrons off the boundary (causing a phase shifted oscillation in the LSW). As one expects the Fano line shape to survive for

interacting electrons coupled to a magnetic impurity it is indeed satisfying to see this feature reproduced by the open boundary for which the impurity gets traded at low temperatures.

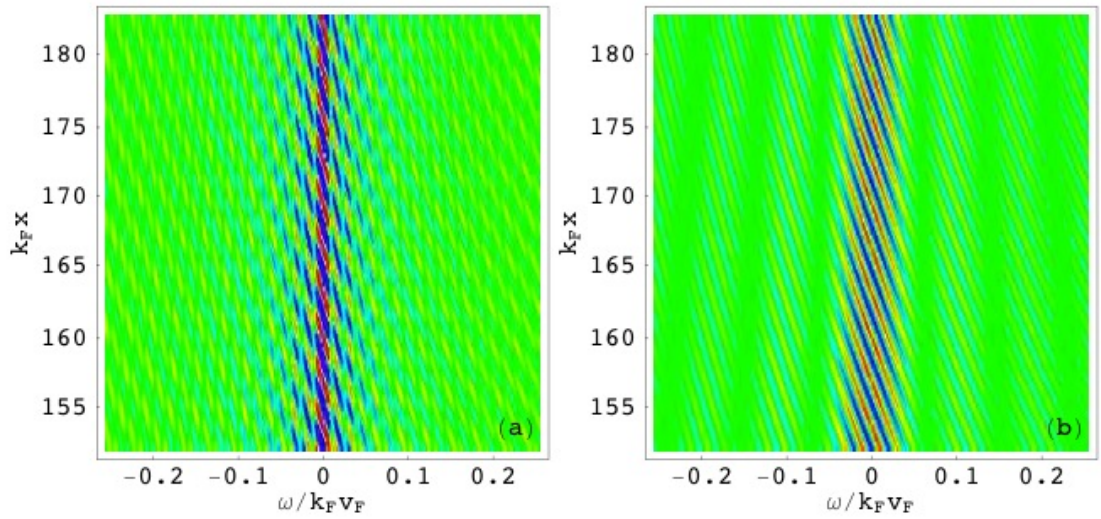

FIG. 5: [color online] $A(\omega, x; \beta)$ for $T/k_F v_F = 2.6 \times 10^{-6}$, $n_e = 0.97$, with $K = 0.7$, $v_c/v_F \approx 1.43$, $v_c/v_s \approx 3$ (a) and $K = 0.9$, $v_c/v_F \approx 1.11$, $v_c/v_s \approx 1.26$ (b). The color coding is the same as in Fig. 4.

2. *Spin-charge separation*

The proximity to an open boundary reveals a key property of interacting electrons in one dimension − spin-charge separation − i.e. the fact that the collective spin and charge excitations (induced e.g. by inserting an extra electron into the system), propagate with different speeds, and hence "separate" [2]. The effect shows up in the LSW as a characteristic peak structure at intermediate distances from the boundary. Very far from the boundary ($\omega x_s \gg 1$) $A(r, \omega; \beta)$ is a monotone function scaling as ω^α near the Fermi level, with bulk exponent $\alpha = (K_c + K_c^{-1})/4 - 1/2$ at low temperatures [2]. Extremely close to the boundary ($\omega x_s \ll 1$) $A(r, \omega; \beta)$ has a similar structure, but with an enhanced suppression near the Fermi level, $A(r, \omega; \beta) \sim \omega^{\alpha_B}$, with boundary exponent $\alpha_B = (K_c^{-1} - 1)/2$ at low temperatures [3, 7, 8] (see Fig. 4, with color coding in arbitrary units). As one moves away from the immediate vicinity of the boundary an oscillation pattern emerges, which becomes most

pronounced when $\omega x_s \sim \mathcal{O}(1)$. This oscillatory feature (see Fig. 5) which is a superposition of spin and charge waves is due to the two types of branch points in Eqs. (29) and (30) which define the propagating collective spin and charge modes. The two panels correspond to two different choices of K_c, with two different values of the ratio v_c/v_s, leading to the two different peak structures. By close inspection of the graphs one can easily read off the corresponding velocity ratios. To see how, let us make a "cut" of the two panels in Fig. 5 at a distance $x = 100a$ from the boundary, yielding the panels in Fig. 6.

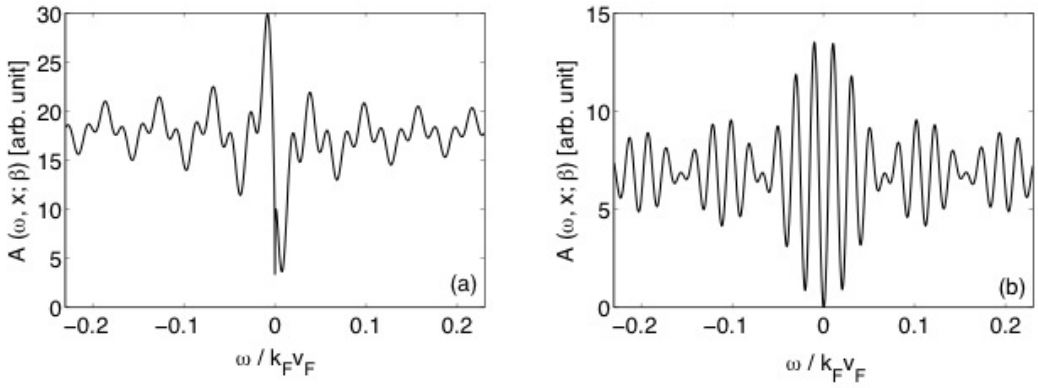

FIG. 6: $A(\omega, x; \beta)$ for $T/k_F v_F = 2.6 \times 10^{-6}$, $n_e = 0.97$, with $x = 50a$, $K = 0.7$, $v_c/v_F \approx 1.43$, $v_c/v_s = \lambda_c/\lambda_s \approx 3$ (a) and $x = 100a$, $K = 0.9$, $v_c/v_F \approx 1.11$, $v_c/v_s = \lambda_c/\lambda_s \approx 1.26$ (b).

When $K_c = 0.7$ (panel (a)) the spin and charge velocities differ significantly. For this case the short wavelength ($\lambda_s = \pi v_s/x$) spin oscillations are modulated by long wavelength charge oscillations ($\lambda_c = \pi v_c/x$). We note that there are three spin oscillations per one charge oscillation which is in agreement with the fact that in this case $\lambda_c/\lambda_s = v_c/v_s \approx 3$ (see Fig. 6 (a)). When K_c gets closer to unity (non-interacting limit) the spin and charge velocities approach each other and the spin-charge separation manifests itself as a beating pattern, provided that K_c is not identical to unity (see Fig. 6 (b) where $K_c = 0.9$). The short wavelength ($\lambda = 2\pi v_s v_c/x(v_s + v_c)$) oscillations are now amplitude modulated by long wavelength oscillations ($\lambda' = 2\pi v_s v_c/x(v_c - v_s)$). We see that there are about six short wavelength oscillations per "bubble" of the long wavelength amplitude modulations, which is in agreement with the fact $\lambda'/\lambda \approx 12$ in this case, corresponding to $\lambda_c/\lambda_s = v_c/v_s \approx 1.26$.

The spin-charge oscillations in the LSW are also present in real space as discussed before

[18]. The oscillations as a function of energy might be easier to observe, however, since here there are no superimposed Friedel oscillations. We also remark that the existence of the beating pattern for values of K_c close to unity was proposed in Ref. [45] as a diagnostic tool for spin-charge separation in possible tunneling experiments of an LL where a scanning probe microscopy tip would be used as an impurity.

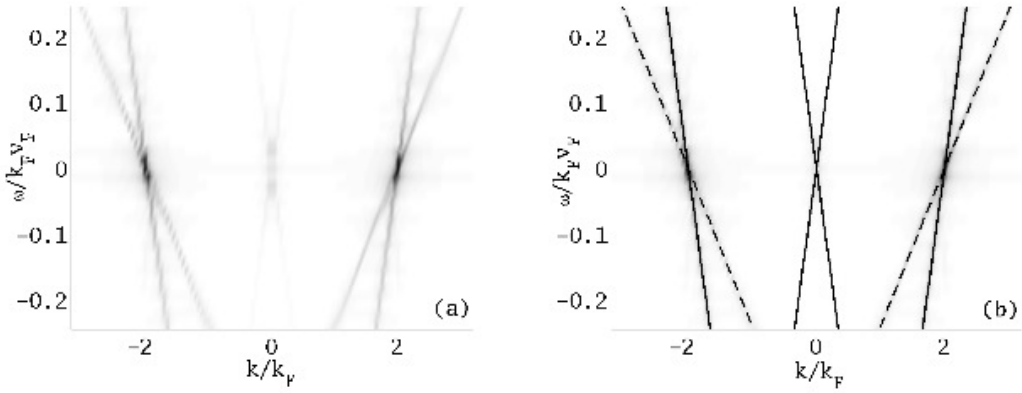

FIG. 7: Fourier transform of the LSW for $K = 0.7$, $v_c/v_F \approx 1.43$, $v_c/v_s \approx 3$, $T/k_F v_F = 2.6 \times 10^{-4}$, $n_e = 0.97$ (a) and the same graph with charge (solid lines) and spin (dashed lines) wave dispersions superimposed (b).

One can map the dispersion of the spin and charge waves by taking a Fourier transform of the LSW (see Fig. 7 (a)). This Fourier transform should not be confused with the momentum or angle resolved spectral weight, which is measured in photoemission experiments, although it shows similar features of spin charge separation. The dominant weights in the transform correspond to the $\omega(k)$ dependence of the excitations. The dispersion lines at $k = 0$ come from the non-oscillatory part of the LSW and represent the charge excitations, since the non-oscillatory part contains only charge oscillations. This feature at $k = 0$ is also a clear indication of interaction effects and disappears as $K_c \to 1$. The dispersion lines at $k \neq 0$ come from the Friedel terms, and contain spin and charge branches shifted from $k = 0$ by $\pm 2k_F$. The mirror symmetry about $k = 0$ reflects the standing wave nature of the oscillations. In Fig. 7 (b) the dispersion relations $\omega(k) = \pm k v_c/2$ at $k \approx 0$ and $\omega(k) = (\pm k - 2k_F)v_{c/s}/2$ at $k \approx \pm 2k_F$ are plotted on top of the Fourier transform and agree with the location of the maxima.

3. Thermal effects

On general grounds one expects that thermal effects become visible only for energies $\omega \lesssim T$ and distances $x \gtrsim \lambda_T = v_s/T$. Choosing e.g. $T \lesssim 10\text{K}$ and $v_F \approx 10^5\text{m/s}$ (a typical value for a quasi-1D organic metal for which LL theory should be applicable [1]) this implies that the spin-charge peak structure as seen in Fig. 5 will remain intact for distances not too far from the edge ($2x/\beta v_s \ll 1$). We should caution the reader that the energy range for which the LL theory is applicable to a specific experiment may sometimes be smaller than the range depicted in Fig. 5 (cf. our discussion in Sec. I). For $2x/\beta v_c \gtrsim 1$ the spin and charge waves loose their coherence before reaching the edge and therefore spin-charge separation is destroyed (see Fig. 9(a)).

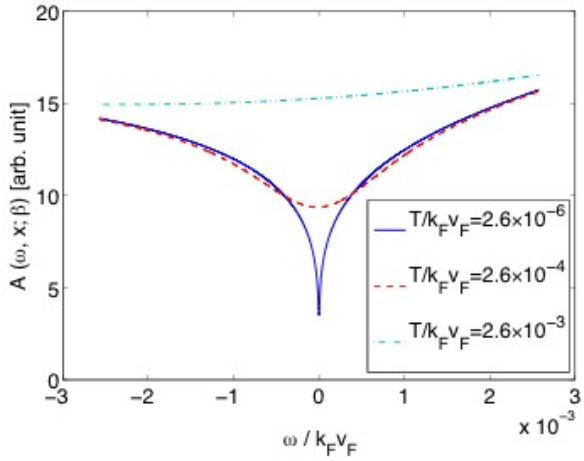

FIG. 8: [color online] $A(\omega, x; \beta)$ for $K = 0.7$, $v_c/v_F \approx 1.43$, $v_c/v_s \approx 3$, $x = 10a$, $n_e = 0.97$ at different temperatures.

A more interesting issue is the fate of the asymptotic scaling behavior of the LSW near the Fermi level as the temperature increases. In earlier work it was found that the "uniform part" of the LSW (corresponding to the first term in (33) crosses over to ω^2 scaling in both boundary ($2\omega x/v_s \ll 1$) and bulk regimes ($2\omega x/v_c \gg 1$) when $\omega\beta < 1$ [9]. The effect was found to originate in the exponential damping of the density correlations for unequal times due to thermal fluctuations. By performing an expansion of the *full* LSW in Eq. (33) with

the small parameter $\omega\beta$ we find that the power law is now modified to

$$A(\omega, x; \beta) \sim A + B\omega + C\omega^2, \quad \omega\beta \ll 1 \tag{35}$$

where A, B and C depend on the temperature and the distance from the boundary. We

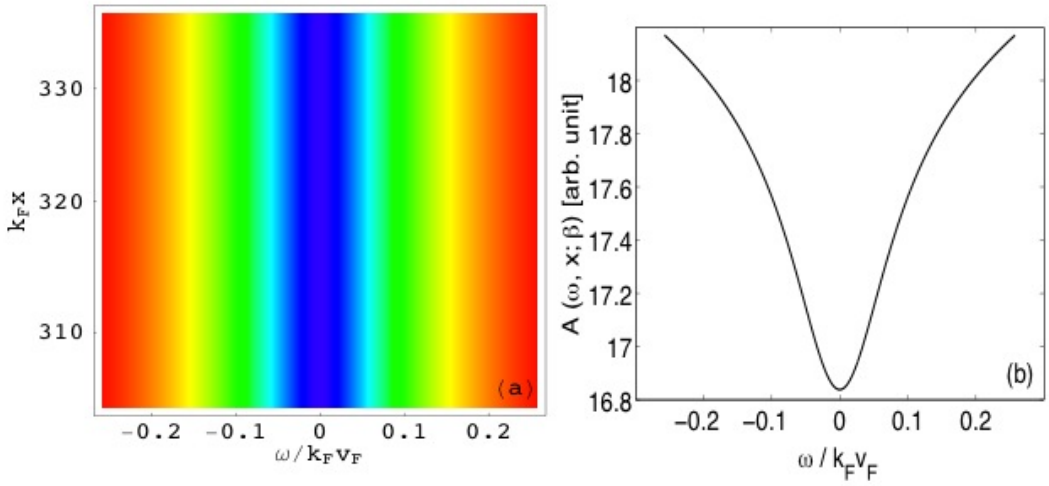

FIG. 9: [color online] $A(\omega, x; \beta)$ for $T/k_F v_F = 2.6 \times 10^{-2}$, $K = 0.7$, $v_c/v_F \approx 1.43$, $v_c/v_s \approx 3$, $n_e = 0.97$ (a) and cut at $x = 200a$ (b).

depict the crossover from boundary scaling $\sim \omega^{(K_c^{-1}-1)/2}$ for $\omega\beta \gg 1$ to thermal scaling $\sim A + B\omega + C\omega^2$ for $\omega\beta \ll 1$ in Fig. 8. Note that one is able to observe this crossover for $2x/\beta v_s \ll 1$. For $2x/\beta v_c \gtrsim 1$ the boundary scaling is completely washed out. Since in this regime $G_{LL}(t, x, -x; \beta)$ in Eq. (30) is exponentially suppressed compared to $G_{LL}(t, x, x; \beta)$ in (29), it follows that $A(\omega, x; \beta) \sim A + C\omega^2$, and the line shape becomes symmetric (see Fig. 9b).

B. Properties of the Local Tunneling Conductance

The *local differential tunneling conductance*, defined in Eq. (9), exhibits the very same features as the LSW. The only difference is that the fine structure of the differential conductance is thermally smeared via the temperature dependence of the Fermi-Dirac distribution. This can clearly be seen by examining the energy dependence at some fixed distance from the boundary, as done in Fig. 10, and then comparing to the corresponding graphs for the

LSW in Fig. 6. As the smearing occurs on the scale of T, spin-charge separation is wiped out for temperatures $T \gtrsim \lambda_s$. The distance x from the boundary determines the wavelength of the oscillations in energy space, so in most cases it should be possible to find a range for x which shows many waves in the energy interval where LL theory applies that are not washed out by temperature, i.e. $1/\Delta \ll x/v_c \ll 1/T$, where Δ is the bandwidth. Note that the inequality above coincides with the criterion for observing spin-charge separation in the LSW, discussed in the previous subsection.

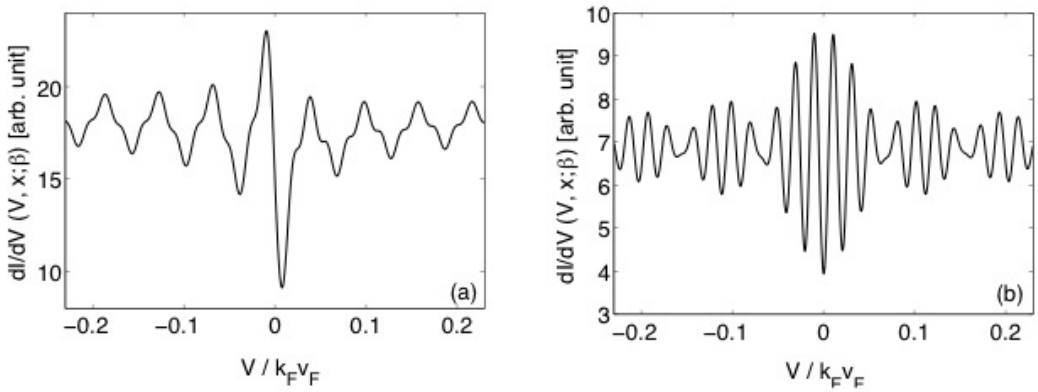

FIG. 10: $dI/dV(V, x; \beta)$ for $T/k_F v_F = 2.6 \times 10^{-3}$, $n_e = 0.97$, with $x = 50a$, $K = 0.7$, $v_c/v_F \approx 1.43$, $v_c/v_s = \lambda_c/\lambda_s \approx 3$ (a) and $x = 100a$, $K = 0.9$, $v_c/v_F \approx 1.11$, $v_c/v_s = \lambda_c/\lambda_s \approx 1.26$ (b).

When applying the results to SWCNTs similar features can be expected as has already been partially confirmed experimentally [30]. The dominant effect is the complicated interference pattern of the Bloch waves, which strongly depends on the geometry of the boundary condition and the chirality of the tubes [44]. Nonetheless, an enhanced velocity, a suppressed spectral weight and a characteristic power law of decaying oscillations are clear signatures of interaction effects which all have been seen in experiments [30]. A more complete theoretical analysis would also have to include the effects of backscattering, band structure, longer-range interactions and the mixing of the channels near the boundary which we defer to a future publication.

V. SUMMARY

We have derived the full finite-temperature LSW for a Luttinger liquid with an edge or impurity (modeled as an open boundary condition), relevant to high-precision STM measurements. We have also generalized our approach to the "two-channel" case that describes SWCNTs in the Luttinger liquid regime, which is qualitatively similar to the single-channel case.

The LSW (determining the local differential tunneling conductance in STM measurements) exhibits a very rich structure as a function of temperature, distance from the impurity, and the strength of the electron interaction. Depending on the choice of parameters one is able to see *asymmetric Fano-like line shapes* and *spin and charge oscillations*. The Fano-like asymmetries are caused by an interplay of boundary and interaction effects, and, as we have shown, are closely linked to the Friedel oscillations in real space. Spin and charge oscillations appear due to the interference of propagating spin and charge waves reflected from the boundary.

We have discussed how to consistently determine the key parameters of a Luttinger liquid (the interaction parameter K_c, and the spin and charge velocities) from experimental measurements of the tunneling conductance. We have also extensively discussed various thermal effects with focus on their influence on the Fano-like asymmetries and spin-charge oscillations in the LSW as a function of energy. The thermal suppression of the coherence of spin and charge waves makes it hard to detect interaction effects in the LSW and even more so in the local differential tunneling conductance (where the finite-temperature LSW gets weighted by the Fermi-Dirac distribution): For temperatures $T \gtrsim v_s/x$ (where v_s is the speed of the spin excitations, and x is the distance to the edge or the impurity) the characteristic power law behavior near the Fermi level is completely washed out and replaced by an interaction-independent analytic scaling. For these temperatures spin-charge separation also becomes virtually impossible to detect.

In conclusion, our results provide guidelines for identifying and interpreting signals of electron correlations in STM data on SWCNTs and other one-dimensional systems, and as such should be useful in the search for realizations of Luttinger liquid physics.

Acknowledgments

It is a pleasure to thank Reinhold Egger for valuable input at the early stages of this project. We are also indebted to Andrew Green for helpful discussions. Financial support from the Swedish Research Council is acknowledged.

[1] T. Giamarchi, *Quantum Physics in One Dimension* (Oxford University Press, Oxford, 2004).

[2] J. Voit, Rep. Prog. Phys. **58**, 977 (1995).

[3] C. L. Kane and M. P. A. Fisher, Phys. Rev. B **46**, 15233 (1992).

[4] A. Furusaki and N. Nagaosa, Phys. Rev. B **47**, 4631 (1993).

[5] A. Furusaki and N. Nagaosa, Phys. Rev. Lett. **72**, 892 (1994).

[6] S. Eggert and I. Affleck, Phys. Rev. B **46**, 10866 (1992).

[7] M. Fabrizio and A.O. Gogolin, Phys. Rev. B **51**, 17827 (1995).

[8] S. Eggert, H. Johannesson, and A. Mattsson, Phys. Rev. Lett. **76**, 1505 (1996).

[9] A. E. Mattsson, S. Eggert, and H. Johannesson, Phys. Rev. B **56**, 15615 (1997).

[10] J. Voit, Y. Wang, and M. Grioni, Phys. Rev. B **61**, 7930 (2000).

[11] Y. Wang, J. Voit, and F.-C. Pu, Phys. Rev. B **54**, 8491 (1996).

[12] F. Anfuso and S. Eggert, Phys. Rev. B **68**, 241301(R) (2003).

[13] K. Schönhammer, V. Meden, W. Metzner, U. Schollwöck, and O. Gunnarsson, Phys. rev. B **61**, 4393 (2000).

[14] V. Meden, W. Metzner, U. Schollwöck, O. Schneider, T. Stauber, and K. Schönhammer, Eur. Phys. J. B **16**, 631 (2000).

[15] M. Bockrath, D. H. Cobden, H. Lu, A. G. Rinzler, R. E. Smalley, L. Balents, and P. L. McEuen, Nature **397**, 598 (1999).

[16] A. Yacoby, H. L. Stormer, N. S. Wingreen, L. N. Pfeiffer, K. W. Baldwin, and K. W. West, Phys. Rev. Lett. **77**, 4612 (1996).

[17] P. Segovia, D. Purdie, M. Hengsberger, and Y. Baer, Nature **402**, 504 (1999).

[18] S. Eggert, Phys. Rev. Lett. **84**, 4413 (2000).

[19] S. A. Kivelson, I. P. Bindloss, E. Fradkin, V. Oganesyan, J. M. Tranquada, A. Kapitulnik, and C. Howald, Rev. Mod. Phys. **75**, 1201 (2003).

[20] Note that the boundary exponent in Ref. [8] is expressed via a non-standard parameterization of the LL interaction.

[21] Z. Yao, H. W. Ch. Postma, L. Balents, and C. Dekker, Nature **402**, 273 (1999).

[22] O. M. Auslaender, A. Yacoby, R. de Picciotto, K. W. Baldwin, L. N. Pfeiffer, and K. W. West, Science **295**, 825 (2002).

[23] F. Zwick, S. Brown, G. Margaritondo, C. Merlic, M. Onellion, J. Voit, and M. Grioni, Phys. Rev. Lett. **79**, 3982 (1997).

[24] For a review, see O. Gunnarsson, K. Schönhammer, J. W. Allen, K. Karlsson, and O. Jepsen, J. Electr. Spectr. **117**, 1 (2001).

[25] An alternative setup which avoids this problem is to use the scanning tip to create a local potential with a scanning probe microscopy tip which scatters electrons, and then measure how the tunneling into the system from a fixed tunnel junction depends on the distance from the tip position as suggested by Ref. [45].

[26] L. C. Venema, J. W. G. Wildoer, J. W. Janssen, S. J. Tans, H. L. J. T. Tuinstra, L. P. Kouwenhoven, and C. Dekker, Science **283**, 52 (1998).

[27] S. G. Lemay, J. W. Janssen, M. van den Hout, M. Mooij, M. J. Bronikowski, P. A. Willis, R. E. Smalley, L. P. Kouwenhoven, and C. Dekker, Nature **412**, 617 (2001).

[28] B. J. LeRoy, S. G. Lemay, J. Kong, and C. Dekker, Appl. Phys. Lett. **84**, 4280 (2004)

[29] J. Lee, H. Kim, S.-J. Kahng, G. Kim, Y.-W. Son, J. Ihm, H. Kato, Z. W. Wang, T. Okazaki, H. Shinohara, and Y. Kuk, Nature (London) **415**, 1005 (2002).

[30] J. Lee, S. Eggert, H. Kim, S. J. Kahng, H. Shinohara, and Y. Kuk, Phys. Rev. Lett. **93**, 166403 (2004).

[31] K. Penc, K. Hallberg, F. Mila, and H. Shiba, Phys. Rev. Lett. **77**, 1390 (1996); Phys. Rev. B **55**, 15475 81997).

[32] V. Meden, W. Metzner, U. Schollwöck, and K. Schönhammer, Phys. Rev. B **65**, 045318 (2002).

[33] R. Egger and A. O. Gogolin, Eur. Phys. J. B **3**, 281 (1998).

[34] U. Fano, Nuovo Cimento **12**, 156 (1935); Phys. Rev. **124**, 1866 (1961).

[35] O. Újsághy, J. Kroha, L. Szunyogh, and A. Zawadowski, Phys. Rev. Lett. **85**, 2557 (2000).

[36] G. Rickayzen, *Green's Functions and Condensed Matter* (Academic Press, London, 1980).

[37] J. Tersoff and D. R. Hamann, Phys. Rev. B **31**, 805 (1985).

[38] A. O. Gogolin, A. A. Nersesyan, and A. M. Tsvelik, *Bosonization and Strongly Correlated Systems* (Cambridge University Press, Cambridge, 1998).

[39] H. J. Schulz, Phys. Rev. Lett. **71**, 1864 (1993).

[40] P. Di Fransesco, P. Mathieu, and D. Senechal, *Conformal Field Theory* (Springer Verlag, New York, 1997).

[41] G. Mahan, *Many-Particle Physics* (Plenum, New York, 1981).

[42] R. Egger and A. O. Gogolin, Phys. Rev. Lett. **79**, 5082 (1997).

[43] L. Balents and M. P. A. Fisher, Phys. Rev. B **55**, R11973 (1997).

[44] C.L. Kane and E.J. Mele, Phys. Rev. B **59**, R12759 (1999).

[45] I. Ussishkin and L. I. Glazman, Phys. Rev. Lett. **93**, 196403 (2004).

Paper IV

P. Kakashvili and H. Johannesson,
"Boundary Green's function for Spin-Incoherent Interacting Electrons in 1D",
preprint (2006), submitted for publication.

Boundary Green's Function for Spin-Incoherent Interacting Electrons in 1D

Paata Kakashvili[1] and Henrik Johannesson[2]

[1]*Department of Applied Physics, Chalmers University of Technology, SE-412 96 Göteborg, Sweden and*

[2]*Department of Physics, Göteborg University, SE-412 96 Göteborg, Sweden*

Abstract

Recently the properties of one-dimensional (1D) strongly interacting, very low-density electrons in the spin-incoherent regime have been under intense study. For sufficiently low densities the potential energy dominates the kinetic energy, making the electrons form a Wigner crystal with an exponentially small spin exchange energy. One can then easily reach the spin-incoherent regime where the exchange energy is much smaller than the temperature. The physics of the spin-incoherent regime has been addressed using Bethe's Ansatz and a bosonized path integral approach, revealing that the spin incoherence dramatically influences the correlations of charge excitations. We here introduce a bosonization scheme for strongly interacting electrons, allowing us to generalize the description to account for the presence of a boundary. By calculating the exact single-electron Green's function we find that the charge sector power-law scaling is highly sensitive to the boundary, strongly modifying the tunneling of electrons close to it. Our approach also allows for a detailed description of the crossover between boundary and bulk regimes.

PACS numbers: 71.10.Pm, 71.27.+a, 73.21.-b

I. INTRODUCTION

The spin-incoherent regime of one-dimensional strongly interacting, very low-density electrons has recently attracted a lot of interest [1, 2, 3, 4, 5, 6]. For zero temperature the kinetic energy of an electron can be estimated by the Fermi energy $E_F = (\pi\hbar n)^2/8m$. For low densities, $n \ll a_B^{-1}$, this energy is small compared to the Coulomb potential energy $e^2 n/\epsilon$ (with ϵ being the dielectric constant and $a_B = \epsilon\hbar^2/me^2$ the effective Bohr radius of the material). In the limit of low densities the system turns into a *Wigner crystal* [7], which − in a classical picture − can be viewed as a system of electrons placed equidistantly so as to minimize the potential energy. Quantum fluctuations induce an exponentially small antiferromagnetic spin exchange $J > 0$ between the electrons. In the case when J is the smallest energy scale, $J \ll T \ll E_F$, the spin exchange can no longer support collective spin excitations, and the system is driven to a *spin incoherent* regime [1, 2, 3]. The physics of the spin-incoherent regime has been addressed using Bethe's Ansatz [1, 2] and a bosonized path integral approach [3]. Surprisingly, it was found that the spin incoherence dramatically influences the correlations of charge excitations, leading to a power-law decay in the charge sector with an interaction-dependent non-unitary exponent.

In this paper we generalize the description in Ref. 3 to account for the presence of an open boundary. For this purpose we introduce a new bosonization scheme, valid for strongly interacting electrons, and presented in Sec. II. In Sec. III we then derive the single-electron Green's function in the presence of an open boundary condition (OBC). The last section contains a brief summary of our results.

II. BOSONIZATION IN THE STRONG COUPLING REGIME

We here introduce a bosonization scheme for strongly interacting electrons, for which the applicability of ordinary bosonization [8] becomes questionable. In the strong-coupling regime, the electrons are localized at the lattice sites of the Wigner crystal, and the usual procedure of linearizing the spectrum around the Fermi points $\pm k_F$ and then expanding the electron fields in left- and right-movers is no longer justified. In what follows we show that one can nonetheless perform an "effective" bosonization, valid for low energies and large distances.

To begin with, it can be shown that a bosonic Hamiltonian correctly describes the low-energy properties of a 1D Wigner crystal [9]. To justify this statement we turn to the classical picture and describe a 1D Wigner crystal as a system of electrons vibrating around their equilibrium positions. This is very similar to the classical description of phonons as lattice vibrations. For low energies (long-wavelength limit) the vibrations can be described by elasticity theory, with the energy of the system expressed by the Hamiltonian

$$H = \int dx \left[\frac{p^2}{2mn} + \frac{1}{2} mns^2 (\partial_x u)^2 \right]. \tag{1}$$

Here $u(x)$ is the displacement of the medium and $p(x)$ is the momentum density. Density fluctuations are given by $\delta n = -n\partial_x u$, and s plays the role of the speed of density waves.

The classical Hamiltonian in Eq. (1) can be straightforwardly quantized by imposing a canonical commutation relation between $u(x)$ and $p(x)$,

$$[u(x), p(x')] = i\delta(x - x'). \tag{2}$$

The resulting quantum Hamiltonian describes the propagation of density fluctuation in the Wigner crystal, and can be written in terms of a bosonic field $\varphi_c(x)$ and its conjugate momentum $\Pi_c(x)$, connected to $u(x)$ and $p(x)$ by

$$u(x) = -\frac{\sqrt{2}}{\sqrt{\pi} n} \varphi_c(x), \qquad p(x) = -\frac{\sqrt{\pi} n}{\sqrt{2}} \Pi_c(x). \tag{3}$$

It follows that

$$H = \frac{v_c}{2} \int dx \left[K_c \Pi_c^2 + \frac{1}{K_c} (\partial_x \varphi_c)^2 \right], \tag{4}$$

where

$$v_c = s \qquad K_c = \frac{v_F}{s}, \tag{5}$$

with $v_F = \pi n / 2m$ the Fermi velocity for non-interacting spinful electrons, and with $v_c = s$ the speed of the propagating charge density fluctuations.

We have thus managed to write the Hamiltonian for a 1D Wigner crystal in bosonized form although we did not know the bosonization formula which connects electron and boson fields. We next derive such a formula, applying a kind of "reverse engineering" to the bosonic description of the Wigner crystal above. First we observe that in the $J \to 0$ limit, electrons behave like *spinless* fermionic particles, i.e. only charge degrees of freedom survive and spin

degrees of freedom simply define the huge degeneracy of the ground state. We may thus omit the spin index and write

$$\Psi(x) = \psi_-(x) + \psi_+(x), \tag{6}$$

where $\psi_-(x)$ [$\psi_+(x)$] is the part of the electron operator which contains negative [positive] momenta. In analogy with ordinary bosonization of spinless fermions [8] we introduce two chiral boson fields ϕ_{c-} and ϕ_{c+}, connected to φ_c by $\varphi_c = \phi_{c-} + \phi_{c+}$. We can then write an "effective" bosonization formula, valid for low energies,

$$\psi_\ell(x) \approx \frac{1}{\sqrt{2\pi\alpha}} e^{i\ell\tilde{k}_F x} e^{\ell i\sqrt{\lambda}\phi_{c\ell}(x)}, \quad \ell = \pm \tag{7}$$

with α a short-distance cutoff, and where $\tilde{k}_F$ and λ are to be determined. Using that the density operator is given by

$$\rho = \Psi^\dagger(x)\Psi(x) = n + \sqrt{\frac{2}{\pi}}\partial_x\varphi_c, \tag{8}$$

with the product of electron fields defined by point splitting [8], and where n is the average density and $(\sqrt{2/\pi})\partial_x\varphi_c$ a fluctuation term (cf. Eqs. (1) and (3)), we find that

$$\tilde{k}_F = \pi n, \qquad \lambda = 8\pi. \tag{9}$$

We have here used that the fast oscillating non-chiral terms $\psi_\pm^\dagger\psi_\mp$ contained in $\Psi^\dagger\Psi$ effectively average out to zero over large distances, and hence can be neglected in the long-wavelength limit. Also note that the doubling of the Fermi momentum in (9) is in agreement with our description of spinless fermions, since now only a single fermion can occupy a given momentum state. As can be easily verified, the case of noninteracting spinless fermions corresponds to $K_c = 1/2$. It follows that in this bosonization scheme interactions are absorbed in two stages: Local interactions among the spinful electrons are incorporated in a free Hamiltonian for spinless fermions (with $K_c = 1/2$), while long-range interactions renormalize the value of K_c (away from $K_c = 1/2$). To see this explicitly, note that for a delta function interaction among the electrons – corresponding to the low-energy, long-wavelength limit of the infinite-U 1D Hubbard model [7] – the description as noninteracting spinless fermions becomes exact (with $K_c = 1/2$).

To obtain a more conventional parameterization (where a unit value of an effective "charge parameter" K corresponds to the case of noninteracting spinless fermions) we define a

bosonic field $\varphi \equiv \sqrt{2}\varphi_c$ with conjugate momentum $\Pi \equiv \Pi_c/\sqrt{2}$. Then the bosonization formula in (7) and the Hamiltonian in (4) take the forms

$$\psi_\ell(x) \approx \frac{1}{\sqrt{2\pi\alpha}} e^{i\ell\tilde{k}_F x} e^{\ell i\sqrt{4\pi}\phi_\ell(x)}, \quad \ell = \pm \tag{10}$$

and

$$H = \frac{v_c}{2}\int dx \left[K\Pi^2 + \frac{1}{K}(\partial_x\varphi)^2\right], \tag{11}$$

respectively, with $K \equiv 2K_c = 2v_F/s = \tilde{v}_F/s$ (in agreement with the doubling of the Fermi momentum $\tilde{k}_F$).

III. BOUNDARY GREEN'S FUNCTION

The bosonization procedure presented in the previous section can easily be adapted to the case when a boundary is present. Imposing an open boundary condition (OBC) at the end, $x = 0$, of a semi-infinite system with $x \geq 0$, we have that

$$\Psi(0) = \psi_-(0) + \psi_+(0) = 0. \tag{12}$$

Analytically continuing the chiral fermion operators to negative coordinates,

$$\psi_+(x) = -\psi_-(-x), \tag{13}$$

and then following the standard procedure for an OBC [10] – using our Eq. (10) – we obtain a bosonization formula for strongly interacting spin-incoherent electrons with an OBC,

$$\psi_-(x) \approx \frac{1}{\sqrt{2\pi\alpha}} e^{-i\tilde{k}_F x} e^{-i\sqrt{4\pi}(\cosh(\vartheta)\tilde{\phi}_-(x) - \sinh(\vartheta)\tilde{\phi}_-(-x))}. \tag{14}$$

Here $e^{2\vartheta} = K$, with $\tilde{\phi}_- = \cosh(\vartheta)\phi_- + \sinh(\vartheta)\phi_+$ governed by the free chiral boson Hamiltonian

$$H = \frac{v_c}{2}\int dx\, (\partial_x\tilde{\phi}_-(x))2. \tag{15}$$

To calculate the zero-temperature single-electron Green's function in the presence of the OBC we follow the path integral approach introduced in Ref. 3. The averaging over spin introduces a factor $2^{-N(x,x',\tau)}$ in the expression for the Green's function, where $N(x, x', \tau)$ samples the number of electrons, or equivalently, the number of non-crossing world lines in the interval $x - x'$. In the spin-incoherent regime, here realized by first taking $J \to 0$ and then

$T \to 0$, the spin configurations all carry the same weight, and the probability that the world lines in the interval $x - x'$ all have the same spin (as required for a non-zero contribution to the low-energy Green's function) becomes equal to 2^{-N}. Given this, the calculation of the Green's function $G(x, x', \tau)$ translates into the calculation of four correlators for spinless time-boosted fermions, with the spin averaging factor $2^{-N(x,x',\tau)}$ properly inserted [11]:

$$\begin{aligned} G(x,x',\tau) &= \langle 2^{-N(x,x',\tau)} \Psi(x,\tau)\Psi^\dagger(x',0)\rangle \\ &= \langle 2^{-N(x,x',\tau)} \psi_-(x,\tau)\psi_-^\dagger(x',0)\rangle + \langle 2^{-N(x,x'\tau)} \psi_+(x,\tau)\psi_+^\dagger(x',0)\rangle \\ &+ \langle 2^{-N(x,x',\tau)} \psi_-(x,\tau)\psi_+^\dagger(x',0)\rangle + \langle 2^{-N(x,x',\tau)} \psi_+(x,\tau)\psi_-^\dagger(x',0)\rangle. \end{aligned} \tag{16}$$

The operator $N(x, x', \tau)$ can be expressed as

$$N(x,x',\tau) = n|x-x'| + \frac{1}{\sqrt{\pi}}(\varphi(x,\tau) - \varphi(x',0)), \tag{17}$$

where n is the average electron (or world line) density, and with $(1/\sqrt{\pi})(\varphi(x,\tau) - \varphi(x',0)) = (\cosh(\vartheta) + \sinh(\vartheta))(\tilde{\phi}_-(x,\tau) - \tilde{\phi}_-(-x,\tau) - \tilde{\phi}_-(x',0) + \tilde{\phi}_-(-x',0)/\sqrt{2}$ the fluctuation term.

The correlators in Eq. (16) are straightforwardly calculated by first using Eq. (13) to replace all occurrences of right-moving fermion fields by left-movers, and then applying the bosonization formula (14). Introducing relative and center-of-mass coordinates, $r = x - x'$ and $R = (x + x')/2$, respectively, we obtain for the G_{--} piece of the Green's function:

$$\begin{aligned} G_{--}(x,x',\tau) &\equiv \langle 2^{-N(x,x',\tau)} \psi_-(x,\tau)\psi_-^\dagger(x',0)\rangle \\ &= \frac{1}{2\pi\alpha} e^{-\frac{\ln 2}{\pi} k_F |r|} e^{-ik_F r} e^{i\zeta_{--}} \frac{1}{(\alpha\ \mathrm{sign}\tau + v_c\tau + ir)} \frac{1}{((\alpha\ \mathrm{sign}\tau + v_c\tau)^2 + r^2)^{-2\Delta_1+2\Delta_2}} \\ &\times \left(\frac{\sqrt{(\alpha^2 + (2R+r)^2)(\alpha^2 + (2R-r)^2)}}{(\alpha\ \mathrm{sign}\tau + v_c\tau)^2 + 4R^2} \right)^{2\Delta_1+2\Delta_3}, \end{aligned} \tag{18}$$

where

$$\begin{aligned} \zeta_{--} &= \frac{\ln 2}{4\pi} K \left(\ln \frac{(\alpha^2 + (2R+r)^2)(\alpha^2 + (2R-r)^2)}{((\alpha\ \mathrm{sign}\tau + v_c\tau)^2 + 4R^2)^2} + 2\ln \frac{(\alpha\ \mathrm{sign}\tau + v_c\tau)^2 + r^2}{\alpha^2} \right) \\ &+ \frac{\ln 2}{4\pi} \left(\ln \frac{(\alpha - i(r+2R))(\alpha - i(r-2R))}{(\alpha + i(r+2R))(\alpha + i(r-2R))} + 2\ln \frac{\alpha\ \mathrm{sign}\tau + v_c\tau + ir}{\alpha\ \mathrm{sign}\tau + v_c\tau - ir} \right), \end{aligned} \tag{19}$$

and with the exponents given by

$$\begin{aligned} \Delta_1 &= \frac{K}{8}\left(\frac{\ln 2}{\pi}\right)^2 \\ \Delta_2 &= \frac{1}{8}\left(\frac{1}{K} + K - 2\right) \\ \Delta_3 &= \frac{1}{8}\left(\frac{1}{K} - K\right) \end{aligned} \tag{20}$$

The G_{-+} part of the Green's function reads

$$\begin{aligned} G_{-+}(x,x',\tau) &\equiv \langle 2^{-N(x,x',\tau)}\psi_-(x,\tau)\psi_+^\dagger(x',0)\rangle \\ &= e^{-\frac{\ln 2}{\pi}\tilde{k}_F|r|}e^{-i2\tilde{k}_F R}e^{i\zeta_{-+}}\frac{1}{(\alpha\ \mathrm{sign}\tau + v_c\tau + i2R)}\frac{1}{((\alpha\ \mathrm{sign}\tau + v_c\tau)^2 + 4R^2)^{2\Delta_1+2\Delta_2}} \\ &\times \left(\sqrt{(\alpha^2+(2R+r)^2)(\alpha^2+(2R-r)^2)}((\alpha\ \mathrm{sign}\tau + v_c\tau)^2 + r^2)\right)^{2\Delta_1} \\ &\times \left(\frac{\sqrt{(\alpha^2+(2R+r)^2)(\alpha^2+(2R-r)^2)}}{(\alpha\ \mathrm{sign}\tau + v_c\tau)^2 + r^2}\right)^{2\Delta_3}, \end{aligned} \tag{21}$$

where

$$\begin{aligned} \zeta_{-+} &= \frac{\ln 2}{4\pi}K\ln\frac{\alpha^2+(2R+r)^2}{\alpha^2+(2R-r)^2} \\ &+ \frac{\ln 2}{4\pi}\left(\ln\frac{(\alpha-i(r+2R))(\alpha-i(r-2R))}{(\alpha+i(r+2R))(\alpha+i(r-2R))} + 2\ln\frac{\alpha\ \mathrm{sign}\tau + v_c\tau + ir}{\alpha\ \mathrm{sign}\tau + v_c\tau - ir}\right), \end{aligned} \tag{22}$$

and with the same exponents as in Eq. (20). The expressions for the G_{++} and G_{+-} pieces of the Green's function are immediately obtained from Eqs. (18) - (21) by using that

$$\begin{aligned} G_{++}(x,x',\tau) &= G_{--}^*(x,x',\tau) \\ G_{+-}(x,x',\tau) &= G_{-+}^*(x,x',\tau) \end{aligned} \tag{23}$$

Having derived the full expression for the boundary Green's function we can study boundary and bulk regimes by taking the proper limits. The bulk regime is defined by the limit $R \to \infty$. For the chiral G_{--} piece we obtain

$$\begin{aligned} G_{--}(x,x',\tau) &= \langle 2^{-N(x,x'\tau)}\psi_-(x,\tau)\psi_-^\dagger(x',0)\rangle \\ &= \frac{1}{2\pi\alpha}e^{-\frac{\ln 2}{\pi}\tilde{k}_F|r|}e^{-i\tilde{k}_F r}e^{i\zeta_{LL}} \\ &\times \frac{1}{(\alpha\ \mathrm{sign}\tau + v_c\tau + ir)}\frac{1}{((\alpha\ \mathrm{sign}\tau + v_c\tau)^2 + r^2)^{-2\Delta_1+2\Delta_2}}\ , \end{aligned} \tag{24}$$

in agreement with the result for the bulk Green's function derived in Refs. 1 and 3. In contrast to the chiral part G_{--} (G_{++}) of the Green's function, G_{-+} (G_{+-}) decays with a power law and vanishes in the bulk limit, as it must:

$$G_{-+}(x,x',\tau) \sim \frac{1}{R^K} \tag{25}$$

For the boundary case, defined by $v_c\tau >> r, R$, the chiral and nonchiral parts of the Green's function show the same behavior, with the asymptotic scaling

$$G_{--}(x,x',\tau) \sim G_{-+}(x,x',\tau) \sim \frac{1}{\tau^{1/K}}. \tag{26}$$

This agrees with the result in Ref. 5 (see also 6). Importantly, our general result allows for a study of the crossover between boundary and bulk regimes.

IV. CONCLUSIONS

We have calculated the exact single-electron boundary Green's function for one-dimensional spin-incoherent electrons in the low-energy, long-wavelength limit, using a bosonization scheme valid in the strong-coupling regime. The Green's function thus obtained correctly reproduces known results in the bulk and extreme boundary regimes. As revealed by the expressions in Eqs. (18) and (21), the charge sector power-law scaling of the Green's function is highly sensitive to the presence of the boundary also at "intermediate" distances away from it, where the center-of-mass coordinate $R \sim \mathcal{O}(v_c\tau)$. This feature will strongly influence the local tunneling density of states, and may be probed experimentally by scanning tunneling microscopy of one-dimensional conductors of spin-incoherent electrons, or by using quantum interference devices built from such conductors [6].

Acknowledgments

It is a pleasure to thank M. Zvonarev for an inspiring discussion on spin-incoherent electrons, and G. Fiete for helpful communication. This research was supported by a grant from the Swedish Research Council.

[1] V. V. Cheianov and M. B. Zvonarev, Phys. Rev. Lett. **92**, 176401 (2004).

[2] V. V. Cheianov and M. B. Zvonarev, J. Phys. A: Math. Gen. **37**, 2261-2297 (2004).

[3] G. A. Fiete and L. Balents, Phys. Rev. Lett. **93**, 226401 (2004).

[4] G. A. Fiete, J. Qian, Y. Tserkovnyak and B. I. Halperin, Phys. Rev. B **72**, 045315 (2005).

[5] G. A. Fiete, K. Le Hur and L. Balents, Phys. Rev. B **72**, 125416 (2005).

[6] M. Kindermann, P. W. Brouwer, and A. J. Millis, cond-mat/0603604.

[7] H. J. Schulz, G. Cuniberti, and P. Pieri, in *Field Theories for Low-Dimensional Condensed Matter Systems*, edited by G. Morandi *et al.* (Springer, 2000).

[8] A. O. Gogolin, A. A. Nersesyan, and A. M. Tsvelik, *Bosonization and Strongly Correlated Systems*, (Cambridge University Press, 1998).

[9] K. A. Matveev, Phys. Rev. B **70**, 245319 (2004).

[10] S. Eggert and I. Affleck, Phys. Rev. B **46**, 10866 (1992).

[11] In contrast to Ref. 3 we do not include the permutation factor $(-1)^N$ in the expression for the Green's function since it is automatically taken into account in our spinless fermion formulation. In Ref. 3, averages are carried out for spinless bosons, requiring the permutation factor to be explicitly inserted (cf. the discussion after Eq. (41) in Ref. 4).